Spring 2023

Impact Resistance of Hybrid Metal-Organic Frameworks/Carbon Fibers Composites

Derek Isaac Espinosa Ramirez
Embry-Riddle Aeronautical University, espinod5@my.erau.edu

By

A Thesis Submitted to the Faculty of Embry-Riddle Aeronautical University

In Partial Fulfillment of the Requirements for the Degree of

Master of Science in Aerospace Engineering

Embry-Riddle Aeronautical University

Daytona Beach, Florida

By

THESIS COMMITTEE

Marwan Al-Haik
Digitally signed by Marwan Al-Haik
DN: cn=Marwan Al-Haik, o=Kennesaw State Univeristy, ou=Mechanical Engineering, email=malhaik@kennesaw.edu, c=US
Date: 2023.04.17 16:00:43 -04'00'

Ali Tamijani
Digitally signed by Ali Tamijani
Date: 2023.04.19 09:23:10 -04'00'

Sirish Namilae
Digitally signed by Sirish Namilae
Date: 2023.04.17 18:49:00 -04'00'

Hever Moncayo
Digitally signed by Hever Moncayo
Date: 2023.04.19 14:15:00 -04'00'

Graduate Program Coordinator,
Dr. Hever Moncayo

Date

Dean of the College of Engineering,
Dr. James W. Gregory

Date

Associate Provost of Academic Support,
Dr. Christopher Grant

Date

ACKNOWLEDGEMENTS

I would like to acknowledge all the coworkers, faculty members, friends, and family that helped me throughout my project and provided me with the support and motivation needed to be able to complete this thesis.

I would like to thank Dr. Marwan Al-Haik for being my advisor and providing guidance and support throughout any questions or obstacles in the project. Furthermore, the stress-free and respectful environment that he follows allowed for successful progress in the thesis.

I would like to thank Dr. Ali Tamijani and Dr. Sirish Namilae for being members of my thesis committee, answering any doubts that I had, and reviewing my work. Furthermore, I would like to thank Dr. David Sypeck for the guidance and help using the impact testing machine.

I would like to thank my family for supporting me in every decision and loving me unconditionally through this journey. I want to show my gratitude to my parents, Carlos, and Maria Elena; my siblings, Juan Carlos, and Tatiana; and my wife, Abbigail; their patience and moral support help me stay on track and taking the right decisions.

Finally, I would like to thank Embry-Riddle Aeronautical University for the knowledge provided through their faculty members, the proper equipment and work environment that they possess, and the financial support. These factors helped me perform better and finish my thesis.

ABSTRACT

The increase in the use of carbon fiber-reinforced polymers (CFRPs) composites in the aerospace industry generated the need of improving the properties and capabilities of these composites by adding nano-reinforcements to the carbon fibers, also called hybrid fiber reinforced polymer composites. In this study, the energy absorption due to impact at low speed will be tested and simulated in four configurations of CFRPs utilizing the same $[0/90]_S$ layout throughout them.

The carbon fiber configurations used during this study are de-sized, acid-activated, metal-organic frameworks (MOF), and carbon nanotubes (CNTs). Nickel (II) Nitrate, Methylimidazole, and Methanol were used to grow the MOF nano-reinforcement on the carbon fibers; On the other hand, CNTs were grown by reducing the MOF on the carbon fibers and using Ethylene (C_2H_4), Nitrogen (N_2), and Hydrogen (H_2) to grow CNTs on the carbon fibers.

To evaluate the composites' mechanical properties, such as tensile tests and impact tests were performed; Furthermore, a dynamic mechanical analysis (DMA) was performed to assess the dynamic properties of the composites manufactured. Lastly, an impact simulation was performed on LS-Dyna utilizing the properties obtained in the mechanical testing performed. The results obtained proposed that an appropriate combination and recipe of MOF growth could potentially increase the energy absorption of carbon fiber-reinforced polymers.

TABLE OF CONTENTS

LIST OF FIGURES

LIST OF TABLES

ABBREVIATIONS

CF	Carbon Fiber
CFRP	Carbon Fiber Reinforced Composites
CNTs	Carbon Nanotubes
CCVD	Chemical Vapor Deposition
CVD	Chemical Vapor Deposition
C_2H_4	Ethylene
DI	Distilled
DIC	Digital Image Correlation
DMA	Dynamic Mechanical Analysis
FEM	Finite Element Method
FRPs	Fiber Reinforced Composites
H_2	Hydrogen
ILSS	Inter-Laminar Shear Strength
MAT	Material
MOF	Metal Organic Frameworks
MTS	Material Testing System
N_2	Nitrogen
PVD	Physical Vapor Deposition
RPM	Revolutions per Minute
SEM	Scanning Electron Microscope

1 Introduction

Composite materials are composed of two or more materials combined at the macroscopic scale to form a third material that exhibits the best qualities of their constituents and displays qualities that neither constituent possesses [1]. Composite materials have been part of human evolution since ancient times, from the use of straws on bricks or mud to the modern-day fiber reinforced polymer composites (FRPs) that propel the development of different technologies. The main constituents of these composites are continuous fibers that supply the needs for strength and stiffness and polymeric matrix that protects the fiber and permits load transfer. The morphologies of FRPs are represented in Figure 1.1.

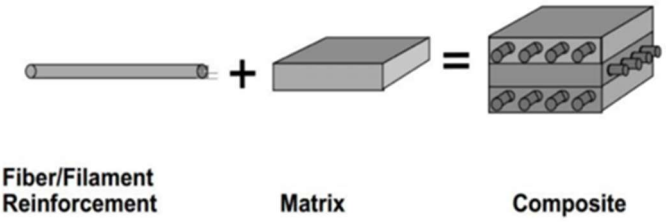

Figure 1.1 FRP composite morphology [62]

One of the most widely used composites in aerospace structures is carbon fiber reinforced polymers (CFRP). The CFRP have many advantages, they are lighter, stiffer, and stronger than common metallic structural materials, making them ideal for usage in different industries such as automotive, sports equipment, civil engineering, robotics, and aerospace structures, among many others. Due to their advancements in the aerospace industry, CFRPs constitute up to 50% of modern commercial airplane structures. Although CFRPs possess numerous advantages, they have several drawbacks that must be considered, such as: lack of multi-functionality, weak off-axis performance, insufficient damping capacity, and poor out-of-plane mechanical properties that lead

to the root cause of failure in laminated composites; delamination. These shortcomings are generally introduced in CFRP by static bending, compression, or tension, cyclic fatigue, and impact (of low-to-high-energies). Consequently, generating severe reductions in the in-plane strength and stiffness, leading to possible catastrophic failure of the whole structure.

1.1 Techniques Applied for Improving CFRPs Mechanical Performance

Different techniques have been adopted to resolve some of the drawbacks of CFRPs. These techniques include stitching, fiber surface treatments, and interleaving with toughened polymer [2–4]. Although some of these techniques overcome some of the drawbacks of CFRPs, they generally reduce other properties including strength and stiffness. A novel technique was introduced that entails integrating nano-sized reinforcement into CFRPs. This technique yielded what is denominated as hybrid fiber reinforced polymer composite (HFRP). This technique provides a larger surface area that increases the interface adhesion between the fibers and the matrix. Furthermore, it could contribute other beneficial properties depending on the nature of the nano-reinforcement added to HFRP.

The next sections outline some of the methods utilized for treating the surface of carbon fibers toward enhancing the properties of their derived CFRPs.

1.1.1 Surface Area Modification by Acid Oxidation Treatment

Acid oxidation is a treatment that consists in exposing carbon fibers to acid solutions under different temperatures and different durations to clean any impurity or imperfection that the carbon fibers could had encounter during the manufacturing processes. Furthermore, this process usually

roughens the surface of the carbon fibers, increasing the surface area of the fibers [5]. The typical acid used for this process is nitric acid (HNO_3), where -COOH and -OH particles get attached to the surface of the carbon fibers as shown on Figure 1.2.

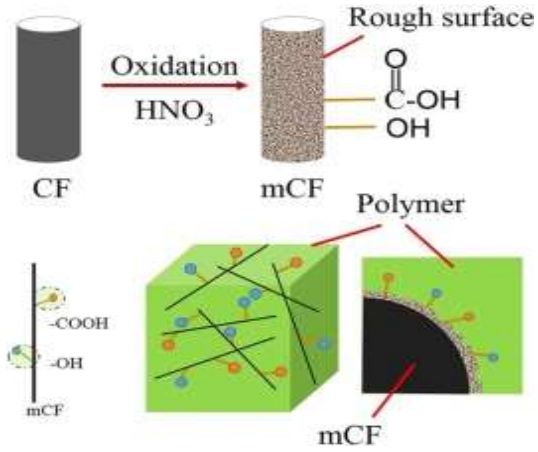

Figure 1.2: Morphology of nitric acid oxidation on carbon fibers [63]

The removal of impurities and roughening of the surface caused by the acid treatment benefits the interface adhesion of the fibers with the epoxy. However, this technique tends to cause significant damage to the carbon fibers outer surface, reducing its thickness, and weakening its mechanical properties. The temperature, acid concentration, and duration of the process needs to be properly set to avoid major damage on the fibers that will significantly decrease the properties of the CFRPs.

1.1.2 Surface Area Modification by Growing Carbon Nanotubes (CNTs)

Carbon nanotubes (CNTs) are one of the many allotropes of carbon, which can be envisioned by a 2-D single layer graphene sheet rolled into a tube. CNTs can be single walled (SWCNTs) or

multi-walled (MWCNTs) as shown in Figure 1.3. CNTs can be synthetized by different techniques such as laser ablation, arc discharged, catalytic chemical vapor deposition, among other [6].

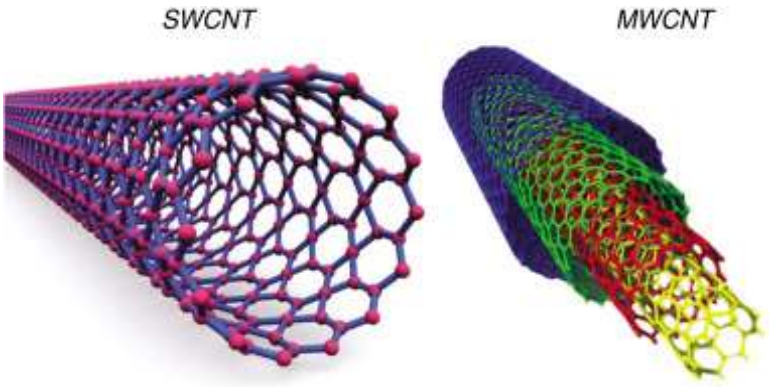

Figure 1.3: Schematic structure of SWCNTs and MWCNTs [6]

CNTs are a novel structure due to their superior mechanical and electrical properties, depending on their geometry. Although growing CNTs on carbon fibers could improve the interlaminar shear strength (ILSS) of CFRPs, it can significantly deteriorate other mechanical properties when they are grown in carbon fibers. The significant degradation of the fiber dominated properties is a result of the exposure to elevated temperatures, needed to grow CNTs, for extended periods of time. For Example, Sager et al. Reported a 30% decrease in the tensile strength of carbon fibers when CNTs are growth on them [7].

1.1.3 Surface Area Modification by Growing Zinc-Oxide (ZnO) Nanorods

Zinc Oxide (ZnO) is an inorganic compound that crystallizes into hexagonal wurtzite and cubic zincblende structures that can be synthesized in nanoscale such as nanowires, nanorods, nanoparticles, therapods, among others [8]. Some of these nanostructures are represented in Figure

1.4. To synthesize ZnO nanostructures various methods are utilized including physical and thermal evaporation, electrodeposition, sputtering, among others [8].

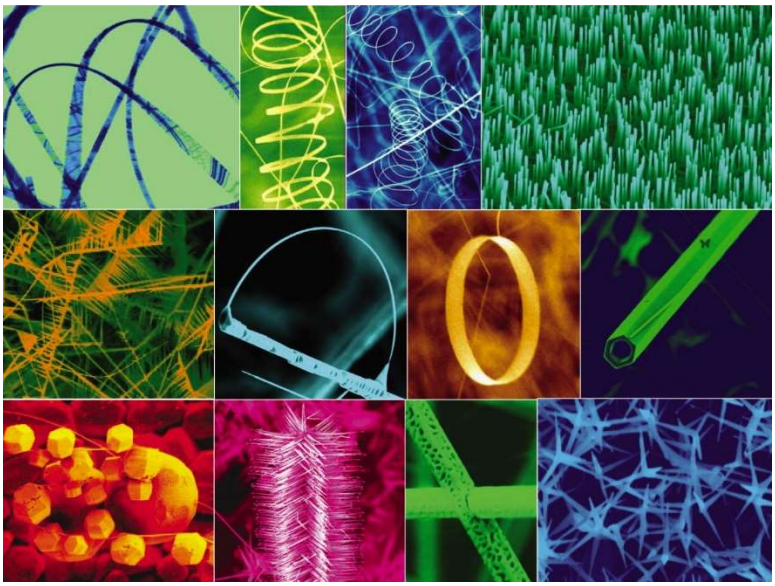

Figure 1.4: Different nanostructures of Zinc Oxide [64]

The ZnO nanostructures are attractive due to their semiconducting, piezoelectric, and pyroelectric characteristics. ZnO belongs to the II-VI semiconductor group; furthermore, the high electromechanical coupling, heat capacity, and heat conductivity helps ZnO to have many piezoelectrical applications for smart materials such as sensors and transducers [8]. This material has also been grown on carbon fibers to take advantage of its unique properties. However, it was reported that ZnO NWs would not increase the impact resistivity of CFRPs significantly. The ZnO growth on Carbon fiber can also negatively affect the fibers strength and stiffness due to the moisture absorption during the hydrothermal synthesis technique [9].

1.1.4 Surface Area Modification by Growing Metal Organic Frameworks (MOFs)

Metal organic frameworks (MOFs) are organic-inorganic hybrid crystalline porous materials; it is formed by an array of positively charged metal ions surrounded by organic linker molecules [10]. The metal ions form nodes that bind the arms of the linkers together to form a repeating cage-like structure as shown on Figure 1.5. Due to this hollow structure, MOFs have an extraordinarily large internal surface area that would significantly benefit the interface adhesion of fibers and matrix. Due to their high porosities and extended surface areas, MOFs are usually applied for gas storage and separation, liquid separation and purification, electrochemical energy storage, catalysis, and sensing [10].

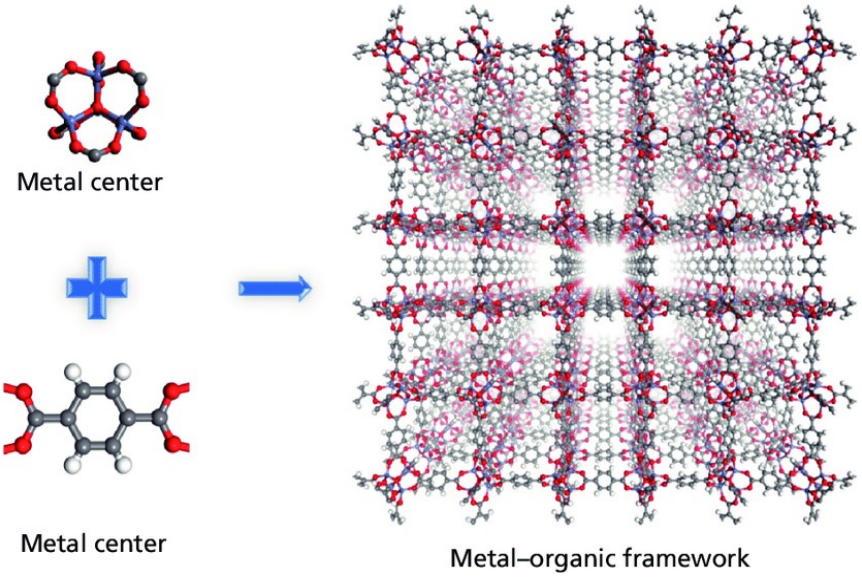

Figure 1.5: Metal-organic frameworks(MOFs) structure [65]

The biggest drawbacks from the previously discussed techniques are the damage to the carbon fibers due to the nanomaterial synthesis environment, stringent growth environment (elevated temperature, inert, vacuum, etc.), and lack of scalability. MOFs growth technique overcomes most of those disadvantages. For this thesis, a nickel-metal ion-based MOF is grown on the surface of the carbon fibers to increase their surface area. The MOF growth is envisioned to benefit HFRP

by increasing the ILSS and tensile strength, as well as the impact resistivity of the composites. Furthermore, MOF can be used as a catalyst to grow CNTs on the surface of the carbon fibers.

1.2 Impact Resistance

The impact resistance of a material refers to the energy required to break a sample. CFRPs have weak off-axis performance and poor out-of-plane mechanical properties that minimize their impact resistance. The previously mentioned techniques to modify the surface area of carbon fibers could potentially enhance the impact resistance of CFRPs.

1.2.1 Impact Modeling

Modeling of CFRPs is challenging due to the interlaminar adhesion of the fibers and the matrix. Software like ABAQUS, NASTRAN, and ANSYS offer materials and options that could simulate the behavior of CFRPs during different scenarios. Furthermore, impact modeling has been difficult to perform due to the dynamic finite element analysis required. LS-DYNA is a software capable of executing dynamic finite element analysis, which is owned by ANSYS. This software can be used for drop tests, impact and penetration, crashes, among other dynamic evaluations.

1.3 Thesis Objectives

The goal of this thesis is to enhance the impact resistance of CFRPs by the modification of the surface of the fibers. The enlarged surface area will enhance the adhesion, and thus, the mechanical properties of CFRPs. These properties will be obtained experimentally to validate an impact

simulation model to the data obtained from the drop weight impact experiment. Three different surface area modification techniques will be investigated: acid oxidation, MOFs growth, and CNTs growth. The thesis will probe which surface modifications could yield more impact resistance without causing a major reduction of other static mechanical properties.

1.4 Thesis Outline

This thesis is composed of seven chapters that will describe the reasoning of this study, the experimental and simulation procedures carried out, and the results obtained from the different hybrid composites evaluated. Chapter 1 introduces CFRPs and the different surface area modifications that can be performed to alter the properties of CFRPs. Furthermore, the impact resistance of a material is presented with current modeling software to evaluate the impact resistance. Chapter 2 provides a more thorough literature review of the fibers modification techniques from Chapter 1 and showcases different applications. This chapter describes different recipes used to perform fiber modifications, and the results from the different recipes and techniques used. Chapter 3 describes the experimental procedures used to perform the different surface modifications, and the technique to manufacture HFRPs. Chapter 4 discusses the testing techniques implemented to obtain microstructural and mechanical properties of the different CFRPs, together with a non-destructive inspection method. Chapter 5 presents the results obtained for the different tests performed together with discussion of the effects of the surface treatments on the CFRPs properties. Chapter 6 outlines the finite element model applied for drop-weight impact simulations and compares the simulation results with the experimental results. Chapter 7 concludes the thesis with a summary of the overall results and techniques applied to evaluate which

configuration stood out over the others. Furthermore, future work is suggested to further improve the performance of the HFRPs.

2 Review of the Relevant Literature

Much research has been performed over the years to increase the strength and stiffness of carbon fibers reinforced polymers (CFRPs) and lessen some of the disadvantages they have. To overcome the CFRP insufficient out-of-plane properties, different ideas had been proposed; however, not many of those procedures had been applied in woven carbon fibers based CFRP. Trabelsi et al. [2] showed how a chain stitching technique adapted to thin composite laminates would improve the interlaminar fracture toughness and the impact damage tolerance under experimental test on mode I and mode II. However, they stated that depending on the modal ratios, there is a possibility to obtain large crack propagation without failure of the stitching. This situation would compromise the composite structures due to the liability of stitching techniques; especially in the aerospace industry, where no propagation of the delamination is allowed at limit loads of the structure. Chung [3] suggested that fiber surface treatments along with a viscoelastic interlayer could increase the damping performance of the composite. The fibers' surface treatment was performed by exposure to ozone gas at 160 ºC, introducing surface oxidation. Aksoy & Carlsson [4] evaluated interleaved toughened polymer composites, consisting of sandwiching thin discrete layers of ductile resin in-between the plies in the laminate. This method yielded an enhancement in the interlaminar fracture toughness, energy absorption capability, and a reduction on size and number of internal delamination. However, interleaving can generate cohesive failures, microcracking, plastic deformation, and material yield. Although these techniques are attractive due to the improvement in specific performances or characteristics of the CFRP, their substantial disadvantage is the loss in in-plane properties of the material.

CFRP has two constituents (carbon fibers and epoxy resin) that are formed by establishing bonding or adhesion between these components. Due to the chemically inert and smooth surface of carbon fibers, the adhesion to the matrix is not adequate, opening the pathway for vast research to improve the fiber/matrix interfacial adhesion. Inadequate interfacial adhesion produces an ineffective load transfer from the matrix to the fibers, and hence, catastrophic failure of the CFRPs. Surface treatments suggest a solution to this problem in two different approaches. The first approach depends on improving the physical adhesion by roughening the fibers; this would increase the fibers surface area allowing larger number of contact points with the matrix [11]. The second approach is based on establishing chemical reactions that would improve the chemical bonding between the fibers and the matrix [11]. Figure 2.1 shows a classification of different surface treatments on carbon fibers; oxidative and non-oxidative being the two main categories [12]. Rahmani et al. [13], performed a chemical modification on carbon fibers using di-amines; providing an improvement in the adhesion of the carbon fiber filaments to the epoxy resin used, these results led to tensile and flexural properties enhancement on the CFRP. Although these surface treatment techniques can improve the fiber-matrix adhesion, they affect the fiber strength negatively, reducing some mechanical properties of the carbon fibers and the CFRPs.

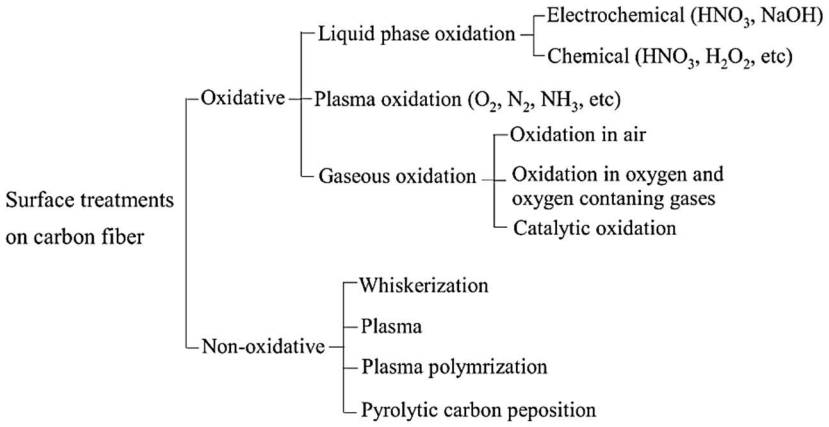

Figure 2.1 Surface treatment methods on carbon fibers [12]

2.1 Oxidation Treatment of Carbon Fibers

The oxidation treatment is effectively a chemical etching process that produces functional groups on the surface of a material. This treatment could be performed with gases (air, oxygen, ozone, etc.) or liquids (sulfuric acid, nitric acid, etc.) [12]. The effectiveness of the treatment depends on the chemical concentration of the oxidizing agent applied to the material, treatment time, temperature, and the material to be applied to [11]. Typically, the chemical oxidation treatment is performed in aquas environment, such as: water, wastewater, contaminated water, and oil, to remove color, odor, organic compounds, and inorganic compounds that would be in the substances where its being applied [14]. Research has been developed to expand the use of this technique to different materials. Due to the requirement of sufficient bonding of the fibers to the matrix on CFRP, this method emerged as a feasible technique to increase the interfacial bonding of the two components.

2.1.1 Acid Activation Treatment of Carbon Fibers

One of the most common types of oxidation treatments on carbon fibers are acid treatments. Numerous research investigations had been carried out to evaluate the effects of the different acids (sulfuric acid, hydrochloric acid, nitric acid, etc.) activation treatments. For example, Zhang et al. [5] in an attempt to develop an understanding of the oxidation process of carbon fibers, used a sulfuric/nitric acid oxidation treatment; they found a complex and rapid interplay of the H_2SO_4/HNO_3 solution, preparing sites for subsequent oxidation on the fibers. The acid activation treatment is based primarily on etching the surface of a material, removing any excess or anomality in the surface and roughening the material.

Rand & Robinson [15] oxidized carbon fibers for periods of time of 9, 12, 25, and 50 hours by refluxing with 68% fuming nitric acid. The treatment led to a slight increase in Young's modulus and a decrease in strength with the increase in oxidation time. Furthermore, after 50 hr treatment, the external surface area increased by a factor of 3.7. Wu et al. [16] performed a nitric acid oxidation on carbon fibers at 115 °C for periods of time from 0 to 90 minutes, followed by treating the fibers in refluxing aqueous sodium hydroxide (NaOH). The surface area of carbon fibers increased with nitric acid oxidation time. However, nitric acid oxidation decreased the tensile strength of the fiber and the fiber weight. The aqueous NaOH treatment did not affect the tensile strength after oxidation but produced a further weight loss on the fibers. Su et al. [17] modified carbon fibers with strong HNO_3 etching, plasma bombardment, and anodic oxidation. These treatments improved the tribological and mechanical properties of composites manufactured with the modified carbon fibers, the adhesion strength of the carbon fibers and the matrix was also increased. An X-ray photoelectron spectroscopy (XPS) analysis showed that the nitric acid-treated fibers resulted in a reduction in C and N concentration, while the O concentration increased on the carbon fibers surface. Nohara et al. [18] treated carbon fibers with hydrochloric acid (HCl) and nitric acid, as well as argon and oxygen cold plasmas. The acid treatments were performed at 103 °C for durations of 5, 10 and 20 minutes. The HCl treatment had a smoothening effect on the surface of the carbon fibers, while the other treatments showed a roughening effect. Furthermore, the HNO_3 treatment resulted in a higher level of oxidation compared to the other treatments performed. All treatments resulted in a reduction of the tensile strength, except for the argon plasma treatment for 10 minutes. Tran et al. [19] oxidized carbon fibers by boiling them in HNO_3 under reflux temperature of 120 °C for 5 hr. By increasing the severity of oxidation, the oxygen and nitrogen contents increased on the surface, leading to an increase in overall surface energy of

the carbon fibers. Li [20] performed a nitric acid oxidation on carbon fibers under reflux temperature of 120 ºC for 5 hours. Nitric acid oxidation modified the nature of the chemical functions converting hydroxy-type oxygen into carboxyl functions; furthermore, it modified the element constituent the fiber increasing the nitrogen concentration by 1.2. Nitric acid treatment improves the interfacial adhesion of fibers and matrix, hence, improving the tensile strength of the composite. Langston & Granata [21] oxidized carbon fibers by immersing them in refluxing HNO_3 at 120 ºC for periods of time from 0 to 160 minutes. The properties changes were evaluated as a function of oxidation time and two stages were identified. The first staged was characterized by surface modification, where the tensile strength, degree of surface oxidation and surface energy increased; the second stage was characterized by carbon material loss; where the tensile strength, surface oxidation, surface morphology and energy stabilized but the fiber diameter experienced a rapid decrease.

Different oxidation techniques have been evaluated, but the gained advantages from the process do not compensate for the drawbacks after the treatments are performed. Alternatively, integrating nano-sized reinforcements into the fibers of Fiber Reinforced Polymers (FRPs) could be an approach that would benefit the development of CFRP. This nano-sized reinforcement typically entails deposition of the nano phase on the surface of the fibers prior to manufacturing the CFRPs.

2.2 Hybrid Fiber Reinforced Polymer Composites

Nano-sized reinforcements possessing inherent high aspect ratios contribute to increasing the surface area for the composite interface. Furthermore, due to the multifunctionalities of the nano materials, the reinforced composite materials would attain different physical and mechanical

properties depending on the type of nano-reinforcement utilized. Due to the weak interface of CFRPs, nano-reinforcements could strengthen the interface adhesion of the fibers and the matrix due to the enlarged surfaces of the fibers. Different nano reinforcements can be added to the carbon fibers, such as: carbon nanotubes, carbon nanofibers, zinc oxide nanowires, bucky paper, metal organic frameworks, etc. The following sections highlight the contributions of the different nanofillers to CFRPs.

2.2.1 Carbon Nanotubes Growth on Carbon Fibers

Carbon nanotubes (CNTs) have inspired many researchers to take advantage of their superior properties and incorporate them in different applications. CNTs can be exemplified by cylindrical rolled graphene sheets, where the tubular structure are rolled-up layers of interconnected carbon atoms. Many properties of CNTs depend on their geometry, mostly on the diameter and chirality. The CNTs are classified as Single-Walled (SWCNT) or Multi-Walled (MWCNTs). CNTs are fabricated by different methods, such as: arc-discharge, chemical vapor deposition (CVD), laser ablation, and others [7]. By far, the CVD technique is most utilized due to the low tooling cost. During CVD growth of CNTs, a metal catalyst is needed (Nickel, Cobalt, Iron, etc.) and a hydrocarbon gas would flow on the catalyst material forming CNTs. CNTs have unique electronic, mechanical, catalytic, adsorption, and transport properties, making them interesting for a plethora of applications [22]. Han et al. [23] investigated a CNT-BG-PEEK composite seeking to develop a suitable bone substitute material, this material showed good mechanical strength and biological activity. Wu et al. [24] fabricated a supercapacitor composed of $NiCo_2O_4$@CNTs, demonstrating potential for practical application in wearable electronic devices. Based on their superior

mechanical properties, several investigations sought to incorporate CNTs on carbon fibers to increase their surface area and improve their derived composite performance.

Sharma & Lakkad [25] grew CNTs on carbon fibers using the CVD technique by catalytic decomposition of acetylene. The morphology of CNTs was evaluated with scanning electron microscopy (SEM) and high-resolution transmission electron microscope (HRTEM). Tensile test was performed on the CFRPs elaborated. The authors concluded that the composites with CNTs growth showed 69% higher tensile strength compared to a composite where the carbon fibers experienced similar heat treatments but without CNTs growth. Lee et al. [26] reinforced woven carbon fibers with MWCNTs and carbon nanofibers (CNFs), utilizing the electrophoretic deposition (EPD) method. The composite with MWCNTs showed an increase in the through-thickness electrical conductivity by 15 times. Furthermore, the interlaminar shear strength exhibited an increase of 13% compared to the reference plain woven composite, due to the good interfacial bonding between MWCNTs and matrix. Boura et al. [27] grew CNTs on carbon fibers using the CVD method. CNTs were synthesized over FeCo bimetallic catalysts by the catalytic decomposition of acetylene at 750 ^{o}C. The CNTs improved the interlaminar shear strength of the fiber and matrix composite by approximately 10%. De Greef et al. [28] grafted CNTs on carbon fibers by using two different catalytic CVD processes; the conventional catalytic thermal decomposition of ethylene, and the oxidative dehydrogenation reaction between acetylene and carbon dioxide. The processes were executed at 500 ^{o}C maintaining the fiber intact after growth. They revealed that the strength rand strain remained unchanged; strength and strain-to-failure compared to the plain fibers received from the manufacturer. Fan et al. [29] developed an innovative technique to graft CNTs on carbon fiber with the use of CVD with nickel (Ni) as a catalyst at a temperature of 500 ^{o}C. It was determined that the tensile strength of carbon fibers

with CNTs increased 10% compared to untreated carbon fibers. Yao et al. [30] grew CNTs on the surface of carbon fibers by the CVD technique. The carbon source used was carbon monoxide (CO) and the catalyst was ferric nitrate (FE $(NO_3)_3$ $9H_2O$). The CNTs were grown on sized carbon fibers, desized carbon fibers, and oxidized carbon fibers. It was determined that the surface roughness and the large number of reactive groups on the surface of carbon fibers generated by oxidation benefited the growth of CNTs. Wang et al. [31] explored the effects of the moving speed and growth atmosphere on the morphology and mechanical properties of carbon fibers reinforced with CNTs by the CVD method. It was shown that with a moving speed of 3 cm/min and 4 cm/min, the surface graphitization degree and tensile strength of the carbon fibers reached their maximum values.

Nano scaled particles, such as CNTs, in the carbon fibers surface generate enormous surface area compared to conventional fiber. The surface area improves the interface adhesion but has a high tendency of CNTs to form agglomerates [32]. This extreme interfacial adhesion would reduce fracture toughness of a composite material, damaging the fibers and increasing the brittleness of the CFRPs.

2.2.2 Zinc Oxide Growth on Carbon Fibers

Much research has been developed to apply different inorganic nanomaterials in CFRPs. When a material is reduced to nanometer scale, its properties modify drastically; nanosized semiconductors possess structural, thermal, electrical, and optical properties that can be used in different industries. Zinc Oxide (ZnO) is a front runner among metal oxide semiconductors because of its diverse morphologies, ease and economic manufacturing, and its thermal, mechanical, and chemical stability. Due to its unique properties, ZnO has been used in rubber,

textile, electronics, smart materials (sensors, photocatalysis, energy generators, etc.), biomedicine, and other industries [8]. ZnO production can be performed with different techniques, such as: vapor deposition, precipitation in water solution, hydrothermal synthesis, sol-gel process, precipitation from microemulsions, mechanochemical, and many other processes [33–36]. Depending on the precursor, solvents, temperature, and method used, the particles obtained would have different shape, size, and spatial structure [37]. Roy et al. [33] synthesized ZnO nanoparticles in natural rubber by a polymeric sol-gel method; the natural rubber with 0.5 phr (parts per hundred parts of rubber) nano-sized ZnO was compared to natural rubber with 5 phr (conventional) micro-sized ZnO. The natural rubber with nano-sized ZnO generated an 8 times greater specific surface area, decreased the curing time, and increased the cure rate by 60.02%. The authors concluded an enhancement of the curing, mechanical and thermal properties compared to the conventional natural rubbers with 5 phr ZnO. Cherumannil Karumuthil et al. [34] fabricated a Poly(vinylidene fluoridetrifluoroethylene) (PVDF-TrFE) / 1% ZnO piezoelectric polymer nanocomposite pressure sensor. The packaged device sensed air pressure with a sensitivity of 0.175 μV/psi. Stanković et al. [35] synthetized spherical ZnO nanoparticles by a microwave synthesis method and it was examined in copolymer poly(DL-lactide-co-glycolide) (PLGA). PLGA/nano-ZnO nanoparticles were proposed for controlled drug-delivery function and prevention or elimination of possible infections. ZnO nanoparticles had also been investigated with carbon fibers, as a nano-sized reinforcement, to increase the interfacial adhesion of fibers and matrix and to enhance the properties of CFRP.

Sharma et al. [36] modified the surface of carbon fibers by uniform growth of ZnO nano-walls, the growth was performed by a radio-frequency magnetron sputtering technique. The microstructure and morphology of the modified carbon fibers were studied. It was suggested to

use the ZnO nano-walls for UV laser diode and visible violet light emitting diodes. Masghouni & Al-Haik [38] sputtered a thin layer of ZnO on the interface of woven carbon fibers to grow ZnO nano-wires (NWs). The CFRPs manufactured with the ZnO NWs exhibited improvements in the on-axis strength and stiffness by 20% and 7.5%, respectively, and the off-axis strength by 14%. Furthermore, the enhancement of interlaminar shear strength and damping capacities were 88% and 51%, respectively over the reference composite. Besides the mechanical properties improvement, the developed ZnO/CFRP beams were utilized for energy harvesting applications. Ayyagari et al. [9] employed a hydrothermal synthesis method (90 ºC) to grow ZnO on the surface of carbon fibers. The CFRPs with ZnO showed an increase in strength and stiffness by 20.14% and 2.61%, respectively. However, the damping properties were reduced by 15.86%, the result is attributed to the moisture in the structure, between the nanorods. Groo et al. [39] performed a colloidal suspension method to grow ZnO on plain woven aramid fabrics. The reinforced aramid fabric was placed in between two carbon fabrics to manufacture HFRP. Matrix failure, interfacial debonding, delamination, and fiber failure within the test specimen containing ZnO NWs was shown as spontaneous charge separation due to the piezoelectric properties from the ZnO NWs. The charge separation could be detected via voltage output and defined as voltage emission. Tunç et al. [40] performed a hydrothermal synthesis method to grow ZnO NWs on carbon fibers; different temperature, concentration, and growth time were implemented to optimize the photocatalytic degradation of methylene blue aqueous solutions. The most effective structure was obtained at 120 °C, 30 mM $Zn(NO_3)_2 \cdot {}_6H_2O$ and 4 hr of hydrothermal synthesis parameters. Albiss & Abu-Dalo [41] grew ZnO NWs on carbon fibers by a hydrothermal method to determine the photocatalytic degradation of methylene blue (MB). Adsorption and photocatalytic activities of the synthesized catalytic adsorbents were analyzed using MB under UV irradiation. The activated

fibers with ZnO nanorods showed excellent photocatalytic activity, approximately 99% degradation of MB in 2 hr. Zhong et al. [42] synthesize ZnO on the surface of carbon fibers by an efficient and simple plasma-liquid interaction strategy, improving the piezoelectric response of the ZnO/CF composite. Based on the inverse piezoelectric effect, the piezoelectric coefficient d_{33} of the composite is 5.24 p.m./V. The literature of ZnO growth on carbon fibers shows a major interest in the sensing, energy harvesting and photocatalytic activities that the ZnO can provide to carbon fibers. ZnO shows more affinity and development to applications on smart materials than in the enhancement of mechanical properties of CFRPs.

2.2.3 Metal Organic Frameworks Growth on Carbon Fibers

A novel nano-reinforcement that had been developed in recent decades is metal organic frameworks (MOF), also known as porous coordination networks. MOFs are a highly ordered crystalline materials prepared by the self-assembly of metal ions with organic linkers to yield low density network structures of diverse topology [43]. MOFs had attracted research due to their ease and inexpensive manufacturing, good magnetism, and tunable pore metrics. Due to their porosity, MOFs are useful for gas separation and storage, chemical sensors, drug delivery, catalysis, among other applications. Ni & Masel [44] presented a technique to synthesize high quality MOFs within a minute, called "microwave-assisted solvothermal synthesis". Meng et al. [45] used MOF as a nano-catalyst to grow CNTs at a relatively low temperature (as low as 430 ºC) pyrolysis process. The resultant CNTs possess large specific surface area, suitable pore size distribution, appropriate doping, interior voids, and robust frameworks, resulting in high electrochemical activity, fast mass transport and good strain accommodation. Tran et al. [46] synthetized a composite of Ni-MOF and MWCNTs for non-enzymatic urea detention. The composite showed a very high sensitivity of 685

$\mu AmM^{-1}cm^{-2}$, low detection limit of 3 µM and a response time of 10 sec. Furthermore, the sensor didn't show loss in activity after storage under ambient conditions for 30 days. Liu et al. [47] synthetized a Ni-MOF/C composite and modified the preparation temperature to optimize impedance matching to achieve strongest absorption intensity and broaden the effective frequency bandwidth. Lei et al. [48] loaded MOF on flexible cellulose aerogels (UiO-66-NH_2@CA) by using in situ growth method at room temperature. The composite material can be recycled to absorb Pb^{2+} and Cu^{2+} in water after simple cleaning, with a reusability of more than 5 cycles. The maximum decomposition temperature was increased by 62.1 ºC, and the equilibrium absorption capacity of Pb^{2+} absorbed by the composite was 89.4 mg g^{-1}. Zhang et al. [49] prepared a Ni-MOF derived hierarchically mesoporous nickel phosphate (NiPo) via a facile hydrothermal method. The obtained NiPo was mixed with wood fibers to form a composite. The composite experienced an increase in tensile and impact strength, and a 43% reduction in total smoke production when 5 wt. % ammonium polyphosphate was substituted by NiPo. Xue et al. [50] reviewed MOF composites, their synthetic methods, and their development to overcome the poor electrical conductivity and narrow micropores of MOFs. It is shown that the MOFs composites can have various electromechanical applications, such as catalysts, sensors, supercapacitors, and batteries. As the literature review suggests, MOF had been used in a variety of industries to take advantage of its characteristics. Due to the increase in surface area generated from MOF, it has become a novel treatment to be applied on carbon fibers to enhance different mechanical and electrical properties of CFRP.

Liu et al. [51] reviewed the literature and grouped reports focused on MOFs-carbon composites, the methods used for their synthesis and their applications. The combination of MOFs and carbon-based materials generate several novel functionalities, such as structure change,

enhanced stabilities, template effects, among others. The composites were synthesized with different techniques, in situ approach (one-pot synthesis and stepwise synthesis), ex situ approach, and other approaches. Furthermore, the MOFs-carbon composite can be applied as absorbents, chemical sensors, batteries and supercapacitors, catalysts, and others. Yang et al. [52] synthesized MOFs on carbon fibers, the MOFs were in situ intergrown onto the surface of the fibers by nitric acid oxidation. It was reported that the interfacial and interlaminar shear strength and tensile strength were enhanced. Furthermore, with an ultrasonic "cleaning" process, the surface area and tensile strength increased 102% and 11.6%, respectively. Fu et al. [53] activated carbon fiber cloth by a two-step procedure: homogeneous growth of MOF on the cloth and subsequent activation catalyzed by the MOFs derivatives. These treatments created a 3D interconnected hierarchical carbon network with micropores, mesopores, and macropores. Furthermore, the composite demonstrated advantages over a carbon cloth supported sulfur melt or sulfur slurry electrodes when used as a sulfur host in Lithium-Sulfur batteries. Li et al. [54] synthesized MOFs on the surface of carbon fibers in situ by a layer-by-layer approach. The composite increased the interfacial shear strength and surface energy by 70.30% and 69.75%, respectively. Furthermore, MOFs as nanocarriers have the potential to heal a failure surface, reaching 97.01% efficiency of the first healing agent. Ayyagari et al. [55] synthesized MOFs on the surface of carbon fibers to enhance the fiber/matrix interface. It was reported that the growth of MOFs on the carbon fibers enhanced the strength, and damping parameters by 11% and 500%, respectively. The glass transition temperature was increased by 20 ºC, and the shear lap joint strength was increased by 40%.

3 Carbon Fiber Reinforced Polymer Composites Preparation

As previously mentioned, this thesis will be based on the use of four different configurations of carbon fibers; these are: de-sized carbon fibers (reference) , acid activated carbon fibers, metal organic frameworks growth on carbon fibers, and carbon nanotubes growth on carbon fibers. This chapter outlines how these different configurations were developed and elaborated using a PAN based T-650/35 carbon fiber manufactured by Solvay, Inc.

3.1 Carbon Fibers De-sizing

Carbon fiber manufacturers add a protective polymeric layer to the fibers called sizing, this coating provides several benefits to the fibers as protection from moisture, UV and allows ease of handling. “Commercial carbon fibers are subjected to electrolytic surface activation after carbonization. Then, a sizing is applied by drawing the carbon fiber roving through a bath of sizing emulsion or dispersion. Moderate heat treatment results in drying of the sizing later” [56]. Due to these factors, it is necessary to remove the sizing to be able to modify the fibers.

De-sizing was executed by placing the carbon fibers in a tube furnace. Nitrogen was set to flow in the tube while the furnace was set to 550 °C. After the furnace reaches the desired temperature, it was set to follow an isothermal process for 1 hr. To finalize the de-sizing process, the carbon fibers were left to air cool by turning off the furnace before removing them from the tube furnace. The equipment setup used for de-sizing is shown in Figure 3.1.

Figure 3.1 Tube furnace utilized in carbon fiber de-sizing.

3.2 Carbon Fiber Acid Activation Treatment

To start the process of growing MOFs, the fibers need to follow a pre-step of activation to intake the metal molecules on the surface. This procedure was performed by creating a solution of nitric acid and distilled (DI) water; the nitric acid was dilluted into the DI water and these two elements were magnetically stirred at 400 rpm. The de-sized carbon fibers samples were placed inside a glass container then submerged in the solution for approximately 24 hrs. After the fibers were removed from the growth bath, they were placed inside a drying oven for approximately 24 more hours to remove excess of moisture.

3.3 Metal Organic Frameworks Growth on Carbon Fiber

After the fibers were acid activated, they were ready for the MOFs growth. The MOFs growth solution created for this research is based on a mix of nickel nitrate, methylimidazole, and methanol. This solution was magnetically stir-mixed for 5 hrs at 400 rpm to properly dissolve all the particles in the mix. Carbon fibers samples were placed in a glass container then submerged by the growth solution as shown in Figure 3.2. The fibers were left in the container for approximately 24 hours for the MOFs to grow; after the growth was completed, the carbon fibers were repeatedly washed with ethanol, followed up with 24 hours drying in the oven to remove excess moisture.

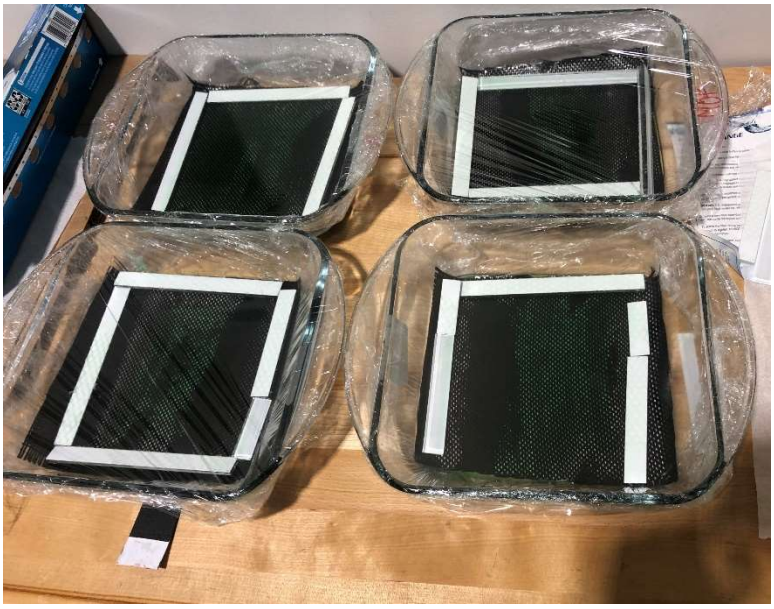

Figure 3.2 Carbon fibers fabrics submerged in MOFs growth solution

3.4 Carbon Nanotubes Growth on Carbon Fibers

Due to the need for pre-deposition of a catalyst metal to grow CNTs, the carbon fibers with MOFs growth were used to perform the CNTs growth on the carbon fibers. The CNTs growth

procedures follow the graphitic structures by design (GSD) protocol that consist of two catalytic chemical vapor deposition (CCVD) steps.

The first step is called reduction, this step implies reducing the metal particles attached in the carbon fibers to have pure metal particles for the initiation of CNTs growth. To perform the reduction, the carbon fibers were placed inside a tube furnace and a mix of nitrogen and hydrogen gases was set to flow inside the furnace at a temperature of 550 ℃, after the desired temperature was reached, an isothermal process was followed for 2 hr approximately.

The second step is called growth. After the reduction step is completed, nitrogen, hydrogen, and ethylene are set to flow in the tank for approximately 30 minutes. The growth time depends on the amount of carbon nanotubes that are desired to grow on the carbon fibers. The last step of the CNTs growth process is to let the fibers be air-cooled inside the tube furnace before removal. The equipment used for CNTs growing is the same as the equipment previously used for de-sizing shown in Figure 3.1; the glass tube had to be changed with a cleaner tube for CNT growing.

3.5 Manufacturing of Hybrid CFRPs

After all the carbon fiber plies were processed with the different nanomaterials growth, carbon fiber plates were manufactured using a Wabash MPI hydraulic composite press. The composite plates created were 60%wt. carbon fiber and 40%wt. epoxy. The epoxy consists of a mix of EPON^{TM} resin 862 and EPIKURE^{TM} curing agent W. The resin mix was prepared according to the protocol suggested by the manufacturer. Each composite sample was manufactured by vacuum assisted hand lay up using different dimensions and laminates layout, depending on the purpose of the testing that was going to be performed on them; the two layouts used were $[0/90]_S$, and $[45/-45]_S$.

An aluminum plate covered by a vacuum bag was used as mold. A vacuum bag was placed to seal the composite laminate and to allow the use of vacuum pump to extract any air and excess epoxy while the curing cycle was proceeding. The curing cycle consisted of a 2.5-hour cycle at maximum temperature of 177 ℃ and pressure of 70 psi, the hydraulic press plates took approximately 0.25 hours to reach the desired temperature and the rest of the time was an isothermal curing process. The vacuum pump was used for approximately 1 hour. After the curing cycle was completed, air cooling and water cooling were performed for 8 minutes in the hydraulic press to cool down the composite sample created to be able to remove it from the hydraulic press.

4 Composite Characterization

After the composites samples were manufactured, it was necessary to evaluate their mechanical properties to probe the effects of the four different fibers preparations on the mechanical and physical properties of the CFRPs. Furthermore, the mechanical properties obtained are needed for the impact computer simulations that will be outlined in an upcoming chapter. The main tests that were performed are: tensile testing, dynamic three-point bending testing, and low velocity drop weight impact testing.

Besides the mechanical testing, several microstructural and damage analysis techniques were implemented including scanning electron microscopy (SEM) and computerized X-ray tomography (CT Scan).

4.1 Tensile Testing

Tensile tests provide strength, strain to failure as a measure of ductility, and elastic modulus for the composites. Depending on the layout (stacking order) of the plies, the behavior of the laminate will vary showing different properties. Two layouts of composites of 6 in. × 6 in. were manufactured for the tensile testing for each of the CFPR configurations. The $[0°/90°]_4$ laminate provided the longitudinal and transverse properties due to their characteristic of being woven fibers, the second laminate was $[45°/-45°]_4$ that provided the off-axis shear properties of the composites. The tensile testing performed on the composite samples followed the ASTM - D3039/D3039M0 standards for tensile testing.

An MTS Criterion^{TM} Model 43 mechanical testing frame was used to perform the tensile testing and Correlated Solutions CSI-6MP cameras were used for digital image correlation (DIC)

to measure the strain of each of the samples under tensile loading. To prevent sample slippage in the wedge grips of the tensile matching, G-10 tabs were added to the composite plates. After the tabs were properly glued to the composites and they dry-cured, the different composite configurations plates were cut into coupons of 6 in × ½ in . These coupon samples were speckled with white paint in preparation for the DIC cameras to capture the movement of the speckles and analyze the strain in each of the samples. The tensile test was performed at 3 mm/min constant crosshead speed until the samples failed. The tensile machine software and the DIC cameras were configured to obtain data every second of the testing to further correlate all the data and analyze the results in Microsoft Excel. To examine the tensile tests results repeatability, six (6) samples of each composite configuration were tested.

4.2 Dynamic Mechanical Analysis (DMA)

The dynamic mechanical analysis (DMA) was performed to evaluate the glass transition temperature of the composites, as well as their damping (viscoelastic) and stiffness (elastic) characteristics. The test is performed at an oscillating (frequency) loading to evaluate the material behavior. The damping capacity of a material depends on its ability to absorb or dissipate kinetic energy. The stiffness and damping abilities of a material can be denoted by the storage modulus (energy stored), loss modulus (energy dissipated) and tan(δ) (ratio of loss modulus to storage modulus) obtained after performing a DMA test.

The test was performed in a PerkinElmer DMA 8000, following the ASTM D4065-20, ASTM D7028-07 and ASTM D5023-15 standards. Samples were cut into with 50.00 mm × 6.25 mm coupons. A three-point bending test fixture was used with a span of 35.00 mm. The frequency sweep test was performed at a frequency range from 1 Hz. to 55 Hz., at a temperature of 25 ºC, a

strain of 0.05 mm and a static force of 2N. The temperature sweep test was performed at a temperature range of 25 ºC to 160ºC, under a constant frequency of 1 Hz., a strain of 0.05 mm, a static force of 2N and a temperature ramp rate of increase of 2 ºC/min.

4.3 Drop Weight Impact Testing

The drop weight impact test provides the energy required to penetrate through a material using a puncture device. To perform the test, a height, energy, or velocity must be provided to the testing machine. A $[0°/90°]_4$ laminate of composite plates of 9 in. × 9 in. for each configuration were manufactured to perform the impact test. To fit the samples in the small testing area, the plates were cut into 4 pieces of 4.5 in.× 4.5 in smaller plates with the use of a diamond saw based on the recommendations of the ASTM standards D7136/D7136M [57]. Furthermore, $[0°/90°]_2$ and $[0°/90°]_8$ laminate plates of 4.5 in. × 4.5 in. were manufactured for the different configurations to evaluate the change in performance per the number of plies.

The drop weight impact tests were performed in an Instron 9250HV testing machine. The tests were performed with a cylindrical impactor bullet with a rounded tip made of stainless steel 304 with a diameter of $^5/_8$ in. and a load cell weight of approximately 6.5 kg. To evaluate the energy absorption and behavior of each composite configuration manufactured, different tests velocities were used, 3 m/s, 6 m/s, and 9 m/s. The impactor was placed at the required height to reach the final terminal velocity to hit the composite plates; if necessary, springs at the top of the machine were used to provide more initial acceleration to reach the desired initial impact velocity. The data acquisition device is placed as close to the impact location as possible to obtain accurate data; this device collects 8192 data points within 0.02 sec of impact duration.

4.4 Non-Destructive Inspection

A non-destructive inspection was performed on the impacted CFRPs samples to evaluate the crack zone generated after the impact and any other failures that could not be seen by the naked eye, such as internal delamination. A Bruker Skyscan 1275, 3D X-ray computerized tomography (CT) system was utilized to inspect the internal damage of the impacted composite plates. The composites were cut to a size of 2 in. × 2 in., focusing on the impacted area (center), Cutting was performed using a waterjet cutter to avoid any delamination or additional damage to the samples. The scan was performed at voltage of 40 kV, current of 250 μA, and with no additional filter (due to the light density of the CFRPs) to obtain the damage micrographs. The NDI was performed on composites with a layout of $[0°/90°]_4$ and $[0°/90°]_8$ at the highest velocity tested, that was 9 m/s.

5 Experimental Results and Analysis

The main objective of this thesis is to evaluate the impact resistance of different hybrid carbon fiber reinforced composites compared to the reference CFRP. Furthermore, the mechanical characterization of the different composites is important to validate the impact model. This chapter will discuss the results from the different tests performed on the four different CFRPs configurations (Reference, Acid Activated, MOF, and CNTs).

Figure 5.1 - Figure 5.4 show the surface of the reference carbon fibers, and the surface modification via acid activation, MOFs growth, and CNTs growth, respectively. These micrographs were obtained by an SEM (at three different magnifications) to evaluate how each surface treatment modifies the carbon fibers.

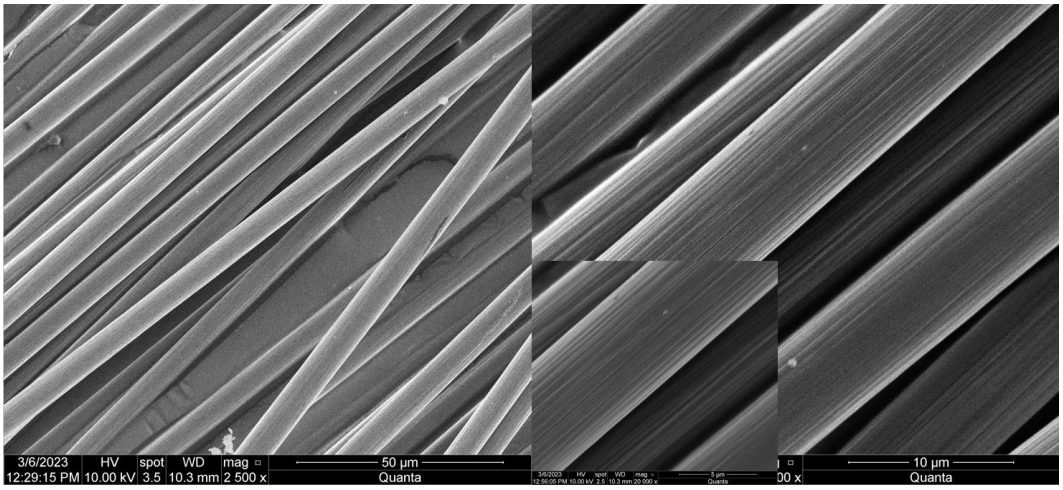

Figure 5.1: SEM micrograph of reference carbon fibers

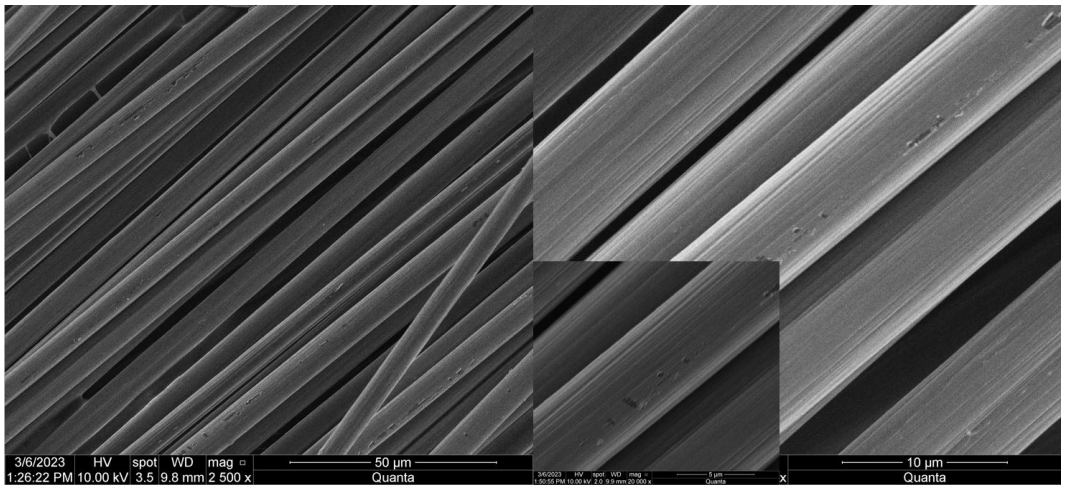

Figure 5.2: SEM micrograph of Acid Activated carbon fibers

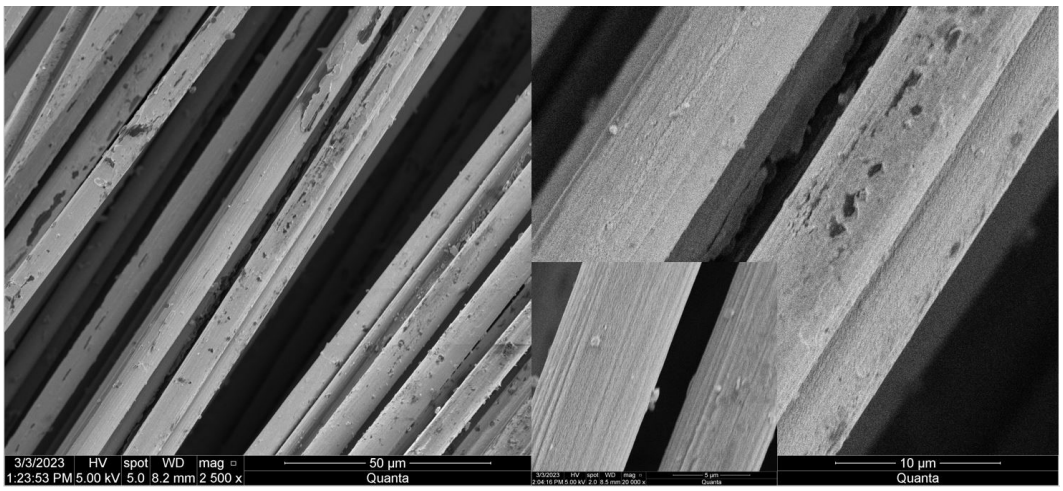

Figure 5.3: SEM micrograph of MOFs growth on carbon fibers

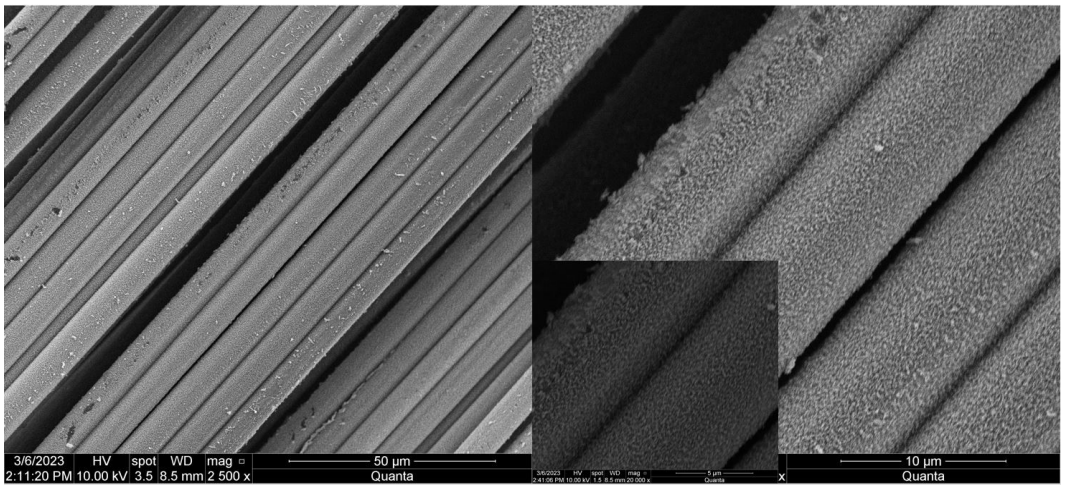

Figure 5.4: SEM micrograph of CNTs growth on carbon fibers

5.1 Tensile Test Results

The tensile tests were performed on the different CFRPs configurations at different layouts ($[0°/90°]_4$, and $[45°/-45°]_4$), to evaluate the apparent axial and shear moduli that are needed for the computational analysis. The properties of interest were the strength, stiffness, and strain to failure. The averages of these parameters were calculated and presented in Figure 5.5, Figure 5.6, Figure 5.7, and Figure 5.8., respectively.

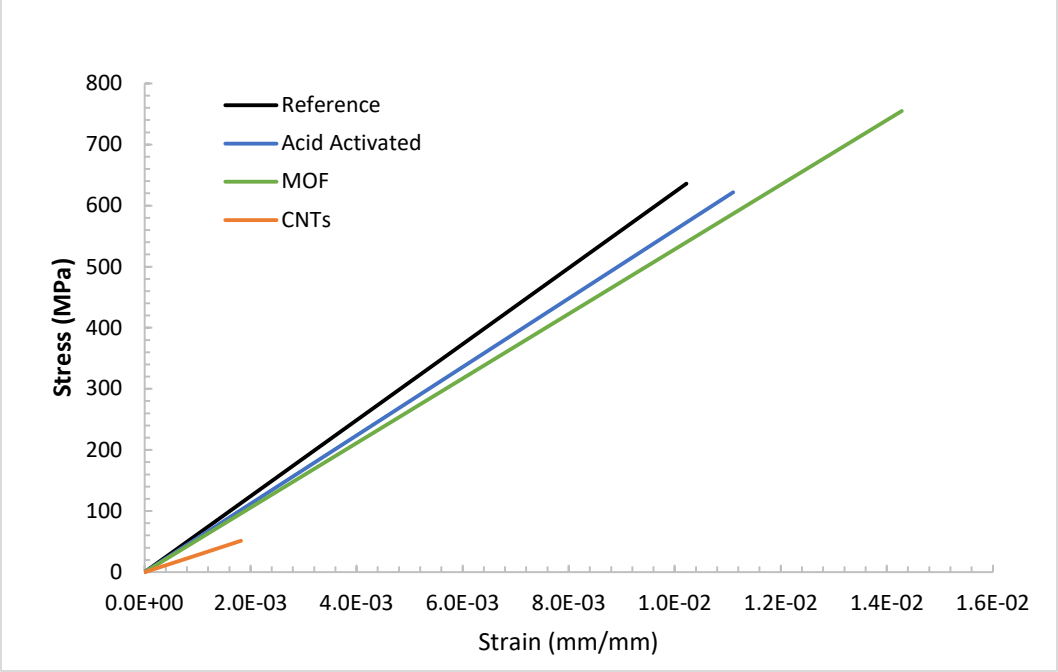

Figure 5.5: Comparison of tenstile test results for $[0°/90°]_4$ layout of the different composite configurations

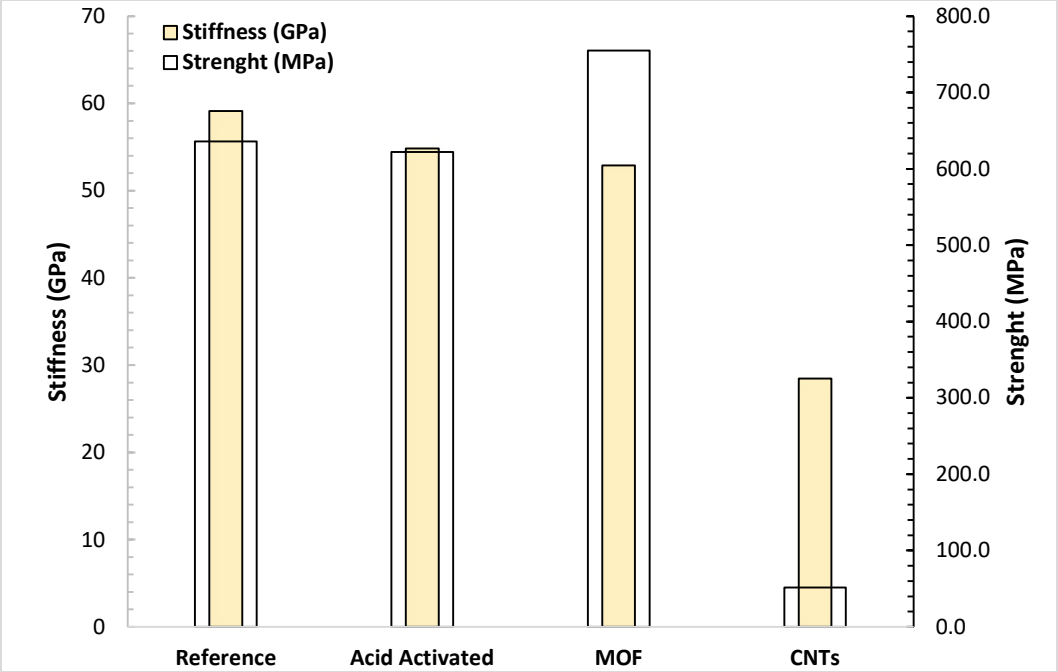

Figure 5.6: Comparison of the stiffness and strenght for [0 °/90 °]$_4$ layout for the different composites

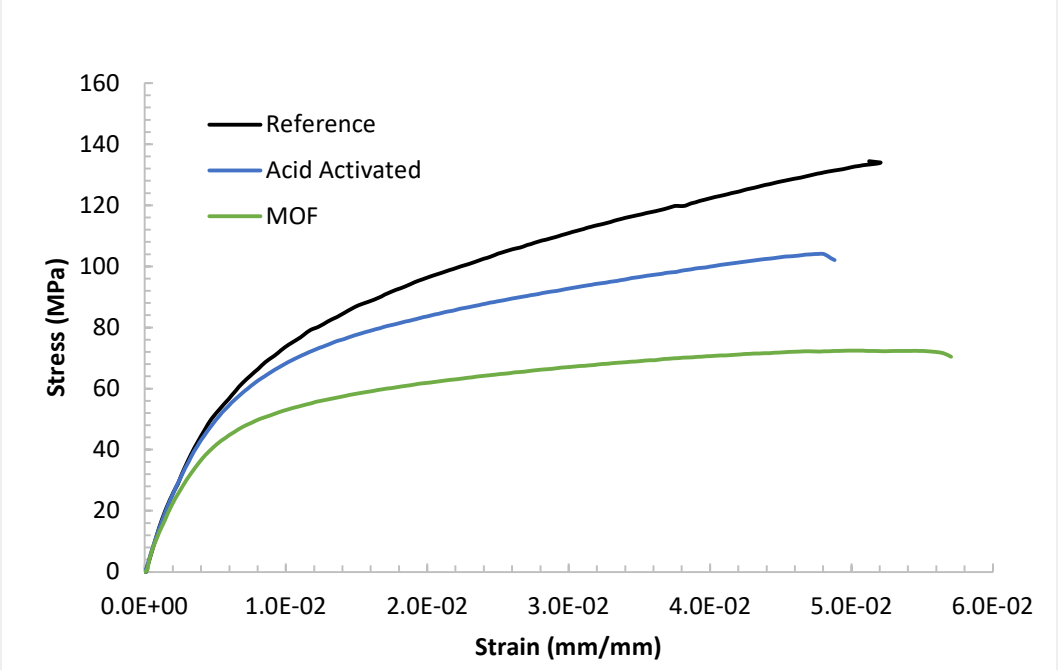

Figure 5.7: Comparison of tenstile test for [45 °/-45 °]$_4$ layout for the different composites

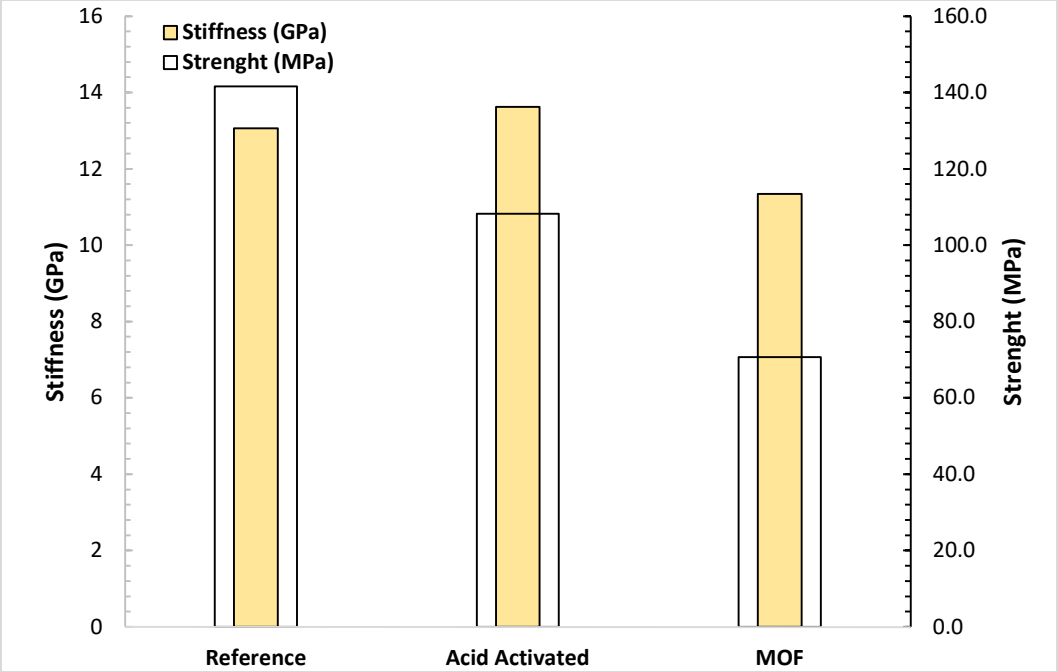

Figure 5.8: Comparison of the stiffness and strenght for [45 °-45 °]$_4$ layout for the different composites

Figure 5.5, and Figure 5.6 show the results from the [0°/90°]$_4$ layout, where all the configurations exhibited a linear elastic behavior. The acid activated configuration attained a small increase in strength and strain of 1% and 9%, respectively. The stiffness was reduced by 7% compared to the reference CFRP. The improvement in strength is attributed to the increase in the surface area generated by the surface oxidation treatment; the increase in performance is also achieved due to the low acid concentration for the oxidation, which prevented significant damage on the carbon fibers. The reduction in the stiffness can be attributed to volumetric changes including insufficient drying or fiber core wakening due to acid absorption. The growth of MOFs on the surface of the carbon fibers to generate HFRP yielded a very significant increase in strength and strain(ductility) of 25% and 40%, respectively. Like the acid activated sample, the major increase in strain generated a reduction of the stiffness by 11%. The strength improvements are

due to the Ni-MOF properties that increase the surface area to reach a better load distribution on the surface of the carbon fibers and generate a better load transition from the matrix to the carbon fibers. Finally, the growth of CNTs using Ni-MOF as a catalyst demonstrated notable damage to the carbon fibers, resulting in a reduction in the strength, strain, and stiffness by 91%, 82%, and 52% respectively. The additional damage due to the prolongated exposure to high temperatures of the carbon fibers to grow CNTs on all surface is responsible for the bad performance of the CNTs composites. The damage generated by the oxidation technique also plays a factor in the decrease in performance of this sample. Furthermore, the dense growth of CNTs on the surface of the carbon fibers also affected the adhesion of the fibers to the matrix by hindering the epoxy impregnation of the carbon fibers.

Figure 5.7, and Figure 5.8 show the average tensile results for the $[45°/-45°]_4$ layout, where all the configurations showed a nonlinear behavior due to the layout of the plies. The stiffness for the three configurations tested was evaluated at 5% of the linear elastic part of the data. The acid activated configuration reached a minimal increase in stiffness and strain of 4% and 6%, respectively; however, the strength decreased by 24%. The MOF configuration showed an increase in strain by 13%; the stiffness and strength were reduced by 13% and 50% respectively.

5.2 Dynamic Mechanic Analysis Results

The DMA three-point bending test was performed on the four composite configurations manufactured with a layout of $[0°/90°]_4$.

The frequency sweep of the storage modulus and tan(δ) evolutions are presented in Figure 5.9, and Figure 5.10, respectively. The storage modulus of the material as an elastic property is independent of the frequency; while the tan(δ) varies with frequency, reaching a maximum peak

at approximately 35 Hz. The acid activated sample showed a decrease in storage modulus and damping by 26% and 5%, respectively; this performance is obtained due to the damage in the core of the carbon fibers because of acid oxidation. The MOF composite experienced a decrease in storage modulus of 14%, which could be attributed to the damage due to the left acid treatment previously performed and the extended exposure to moisture. On the other hand, due to the increase in surface area and aspect ratio created by the Ni-MOF growth in the surface of the carbon fibers. The damping was increased by 64%. The induced surface roughness by the MOFs cells amplifies the frictional and slippage mechanism between the fibers and the matrix, thus, enhancing the damping properties of the material. The composite with CNTs exhibited a significant decrease in the storage modulus by 60% compared to the reference composites. This significant reduction is attributed to the damage to the fibers introduced by the extensive exposure to the high temperatures required to grow CNTs on the carbon fibers. The excessive damage to the fiber countered the improvements due to CNTs allowing a modest improvement in the damping parameter by roughly 10%.

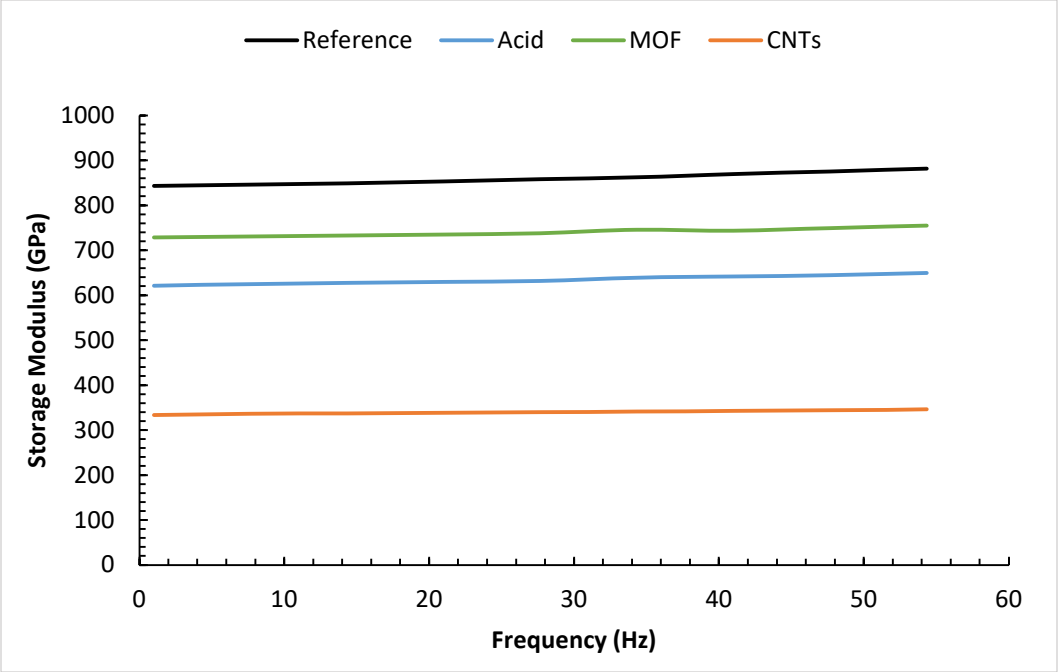

Figure 5.9: Variation of storage modulus with frequency for [0 %90 °]$_4$ layout for the different composites.

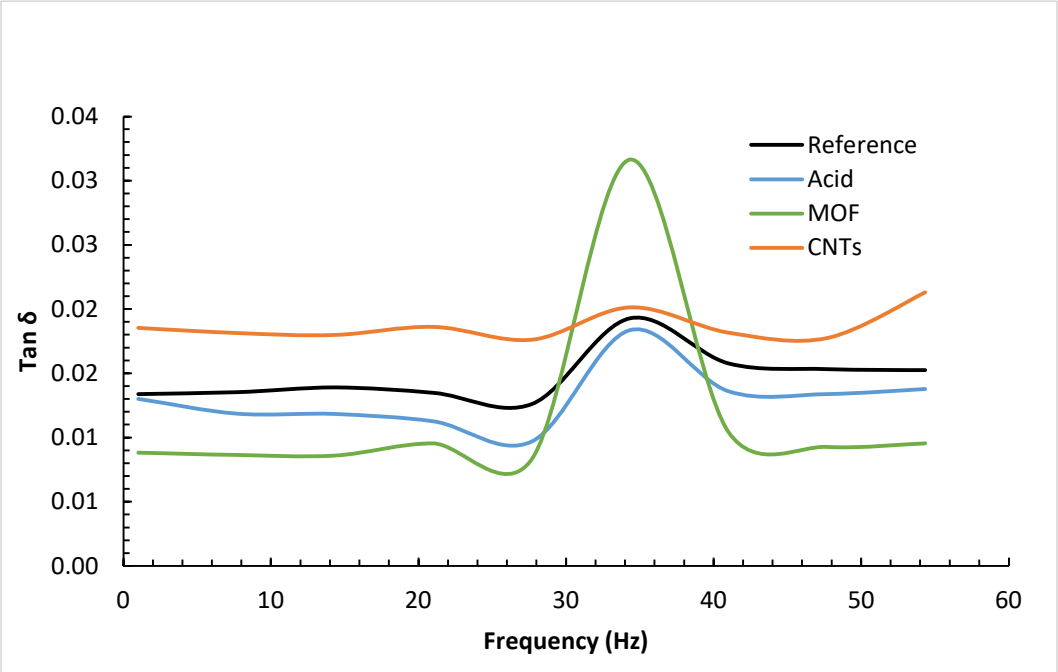

Figure 5.10: Variation of tan (δ) with frequency for [0 %90 °]$_4$ layout of the different composites

The temperature sweeps for the storage modulus and tan(δ) are shown in Figure 5.11, and Figure 5.12., respectively. The storage modulus of each material starts declining after 100 ºC, which can be noticed in Figure 5.8. The location of the peak of the tan(δ) with respect to temperature identifies the glass transition temperature (T_g) for the materials. The CFRP based on the reference fibers showed a T_g of 138.40 ºC; while the acid activated composite showed an increase of T_g to 142.47 ºC due to the etching of the enlarged surface area from the oxidation treatment. Similarly, the MOF composite exhibited an increase of T_g of 142.55 ºC, this result also attributed to the significant increase in surface area that enhanced the interfacial adhesion of the matrix and the fibers. The CNTs-based CFRP also generated an increase in T_g of 142.13 ºC, the difference compared to the other HFRPs could be the result of an excess of CNTs on the surface of the carbon fibers.

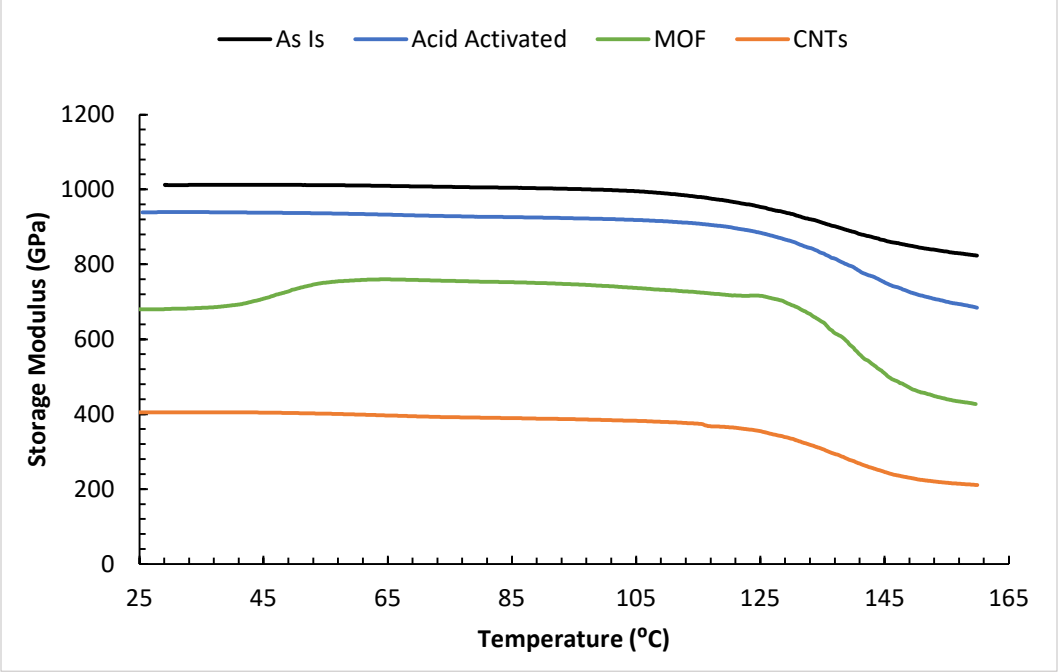

Figure 5.11: Variation of storage modulus with temperature for [0 /90]$_4$ layout of the different composites.

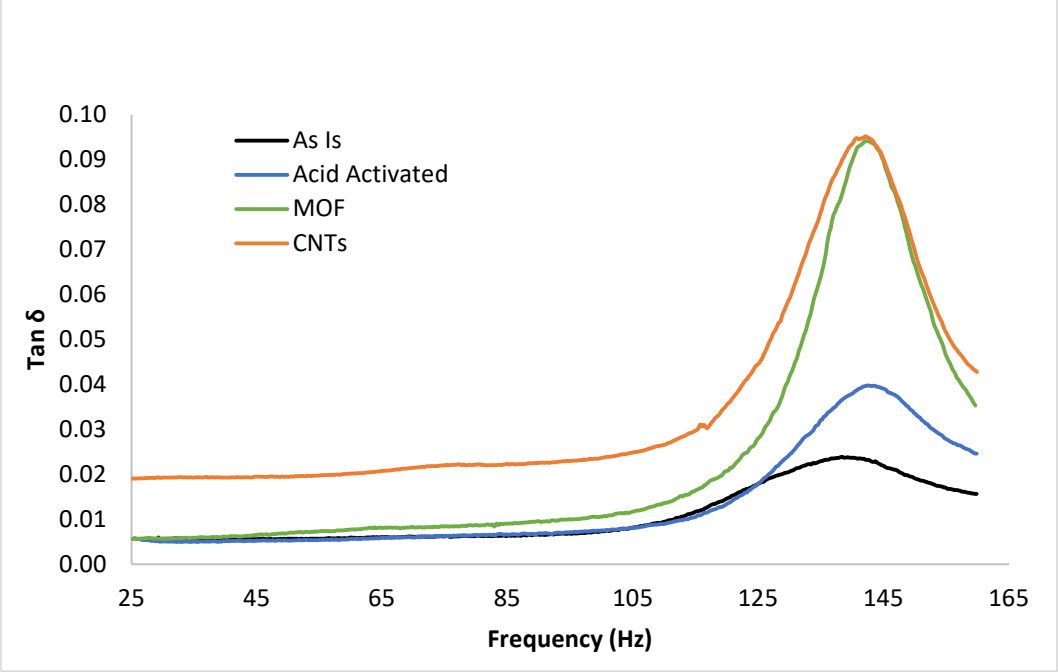

Figure 5.12: Variation of tan δ with temperature for [0 °/90 °]$_4$ layout for the different composites

5.3 Drop Weight Impact Test Results

The data obtained from the drop weight impact test include the maximum load, energy to maximum load, total absorbed energy, and deflection to maximum load. The force-time history is measured from the point of initial contact with the CFRP plate, and as the impactor traverses through the thickness of the plate. The energy is calculated by integrating the force-displacement signal.

The $[0°/90°]_4$ layout for the four configurations were tested by a projectile at terminal velocities of at 3 m/s, 6 m/s, and 9 m/s. The results for the 3 m/s test are shown in Figure 5.13 and Figure 5.14. Results for the 6m/s test are shown in Appendix Figures A.1 and Figure A.2. Table 5.1 summarizes the results for the drop-weight test at terminal velocity of 3m/s for the different composites, while Table 5.2 summarizes the results when the terminal velocity is set to 6 m/s.

The load-time history graphs provide good indication of the progression of damage in the composite. The graphs are mostly asymmetrical indicating the occurrence of cracks. The oscillation in the curves identifies progressive impact damage in the CFRP plate as the impactor penetrates through the thickness. Subsequently all the impactor energy absorbed by the CFRP plate as shown by the plating of energy profile past the peak load. From Fig. 5.13 it is clear that the sample based on MOF treated fiber attained the highest maximum load and maximum total energy absorbed followed by the acid treated sample. The sample with surface grown CNT revealed the least energy due to the significant decrease in strength and stiffness and the increase of the sample brittleness. Higher load peaks indicate better bonding as discussed by Ye et al [58]. The absorbed energy increased by 43.8 % for the MOF sample and 8.7% for the acid activated sample. These results highlight the importance of enhanced bonding due to the increase in the surface area. While CNTs increase the surface area, the fibers were much weaker, and less ductile than the reference yielding a 70.5% decay in the absorbed energy. Other groups reached the same conclusion that adding MWCNTs to fiber does not improve the energy absorption when the sample is tested in a cryogenic environment that induces brittleness [59].

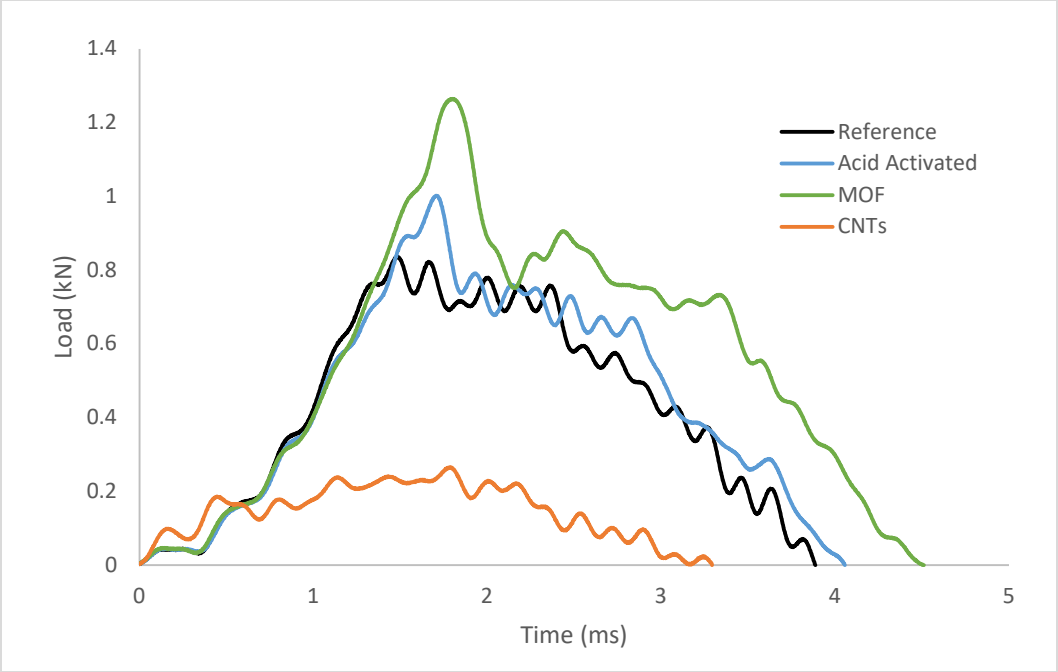

Figure 5.13: Impact load evolution for [0 °/90 °]$_4$ layup of the different CFRPs at 3m/s

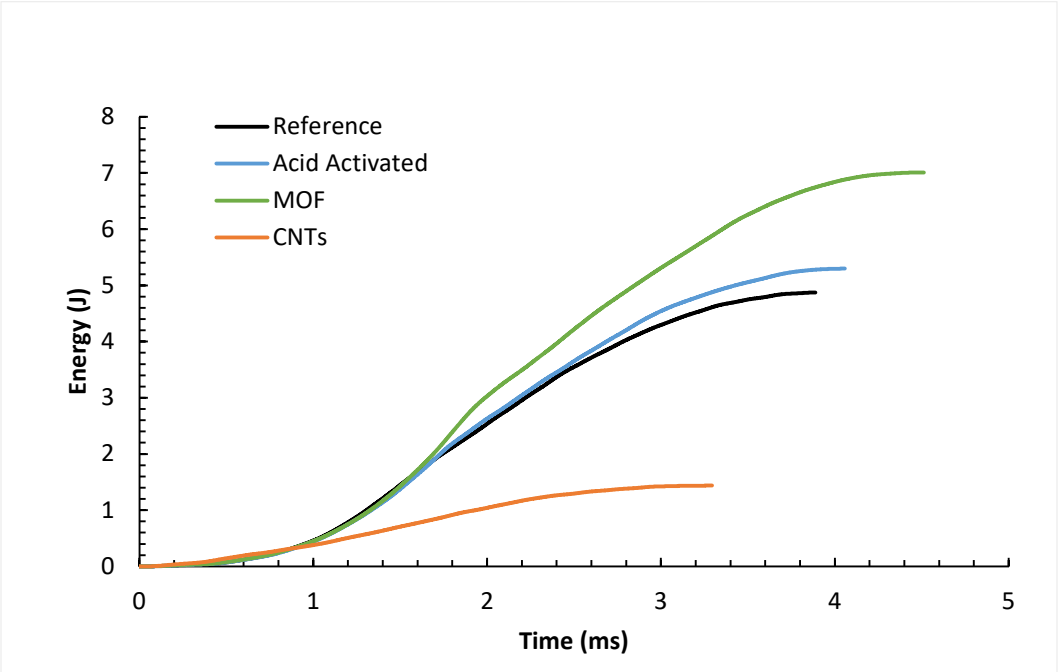

Figure 5.14: Impact Resistance on [0°/90°]$_4$ CFRPs at 3m/s

Table 5.1: Comparison of the $[0°/90°]_4$ CFRPs performance for a weight drop test at terminal velocity of at 3 m/s

Configuration	Maximum Load (N)	Energy to Maximum Load (J)	Total Energy (J)	% Change in Total Energy	Deflection to Maximum Load (mm)
Reference	835.76	1.404	4.876	-	4.414
Acid Activated	1001.84	1.930	5.301	8.7%	5.085
MOF	1264.29	2.365	7.011	43.8%	5.342
CNTs	265.05	0.901	1.441	-70.5%	5.308

By increasing the terminal velocity, the trend was sustained , MOF increased the absorbed energy by 30.7% while the acid treated sample yielded 2.9% in the absorbed energy as shown in Table 5.3.

Table 5.2: Comparison of the $[0°/90°]_4$ CFRPs performance for a weight drop test at terminal velocity of at 6 m/s

Configuration	Maximum Load (N)	Energy to Maximum Load (J)	Total Energy (J)	% Change in Total Energy	Deflection to Maximum Load (mm)
Reference	929.90	1.446	5.397	-	2.850
Acid Activated	1174.65	1.484	5.555	2.9%	4.199
MOF	1254.98	1.962	7.055	30.7%	4.073
CNTs	564.58	0.958	1.889	-65.0%	5.069

To investigate the effect of the thickness (number of plies) a 9 m/s drop weight impact test was performed on the $[0°/90°]_2$, $[0°/90°]_4$, and $[0°/90°]_8$ layouts. The graphical results are shown in Appendix A, and they are summarized in Table 5.3. Both the maximum load and the energy absorbed increase when the number of plies increases.

Table 5.3: Comparison of the $[0°/90°]_2$, $[0°/90°]_4$, and $[0°/90°]_8$ CFRPs performance for a weight drop test at terminal velocity of at 6 m/s

Configuration	Number of layers	Maximum Load (N)	Energy to Maximum Load (J)	Total Energy (J)	% Change in Total Energy	Deflection to Maximum Load (mm)
Reference	2	545.49	0.865	2.472	-	6.816
Acid Activated	2	539.82	0.908	2.693	9.0%	6.779
MOF	2	584.35	0.975	2.834	14.6%	5.962
CNTs	2	157.57	0.463	1.174	-52.5%	4.250
Reference	4	896.37	1.369	5.008	-	4.478
Acid Activated	4	972.09	2.167	5.059	1.0%	5.636
MOF	4	1137.12	2.520	6.576	31.3%	6.002
CNTs	4	235.60	0.153	1.310	-73.8%	1.294
Reference	8	2017.29	4.228	12.428	-	4.855
Acid Activated	8	2080.21	4.278	12.465	0.3%	4.981
MOF	8	2224.68	4.524	16.444	32.3%	5.257

5.4 Non-Destructive Inspection Results

To figure out the internal failure and deformation of the different composites, X-Ray CT-Scan was conducted on the different impacted composite samples .The C-scan images were utilized to determine the failure/deformation area which included delamination.

The maximum crack zone for each configuration was measured as shown in Figure 5.15 - Figure 5.18 for the $[0°/90°]_4$ layout, and Figure 5.19 - Figure 5.21 for the $[0°/90°]_8$ layout, all evaluated for the 9 m/s test. The crack zones for the reference composite of $[0°/90°]_4$, and $[0°/90°]_8$ layouts were 23.4 mm and 26.4 mm, respectively. The acid-treated sample showed a minimal increase in the crack zone of approximately 1% for the $[0°/90°]_4$ layout, while the $[0°/90°]_8$ layout decreased by approximately 7%; these values could be the result of a better interface adhesion for more plies when the carbon fibers experienced an acid treatment. The composites based on MOF carbon fibers exhibited a noticeable decrease in the crack zone of approximately 19% and 14% for the $[0°/90°]_4$, and $[0°/90°]_8$ layouts, respectively. It is shown that the MOF fibers reached an increase of interface adhesion of the fibers and matrix that minimized the crack zone after the

impact, showing local damage on the impacted area. The CNTs composites experienced an increase in crack zone of approximately 9% for the $[0°/90°]_4$ layout. This minimal increase is due to the higher velocity impact; at lower velocities, the CNTs samples experienced a visible higher crack zone compared to the other configurations. For all the configurations inspected, except MOF, it was noticeable that the cracks were propagated along plate planes creating internal delamination on the CFRP. On the other hand, the MOF composites, due to the better load distribution, experienced more local damage without further delamination that could affect other sections of the plates manufactured.

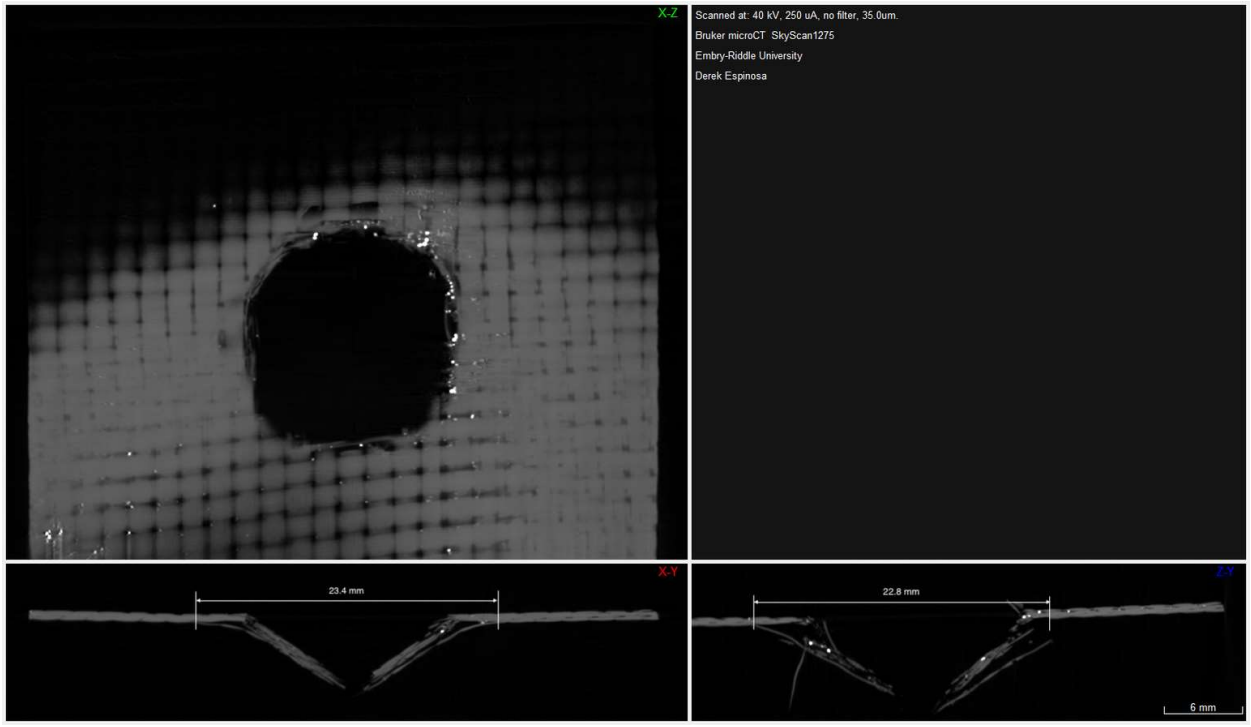

Figure 5.15: X-Ray tomography of Reference composite with [0°/90°]$_4$ layout.

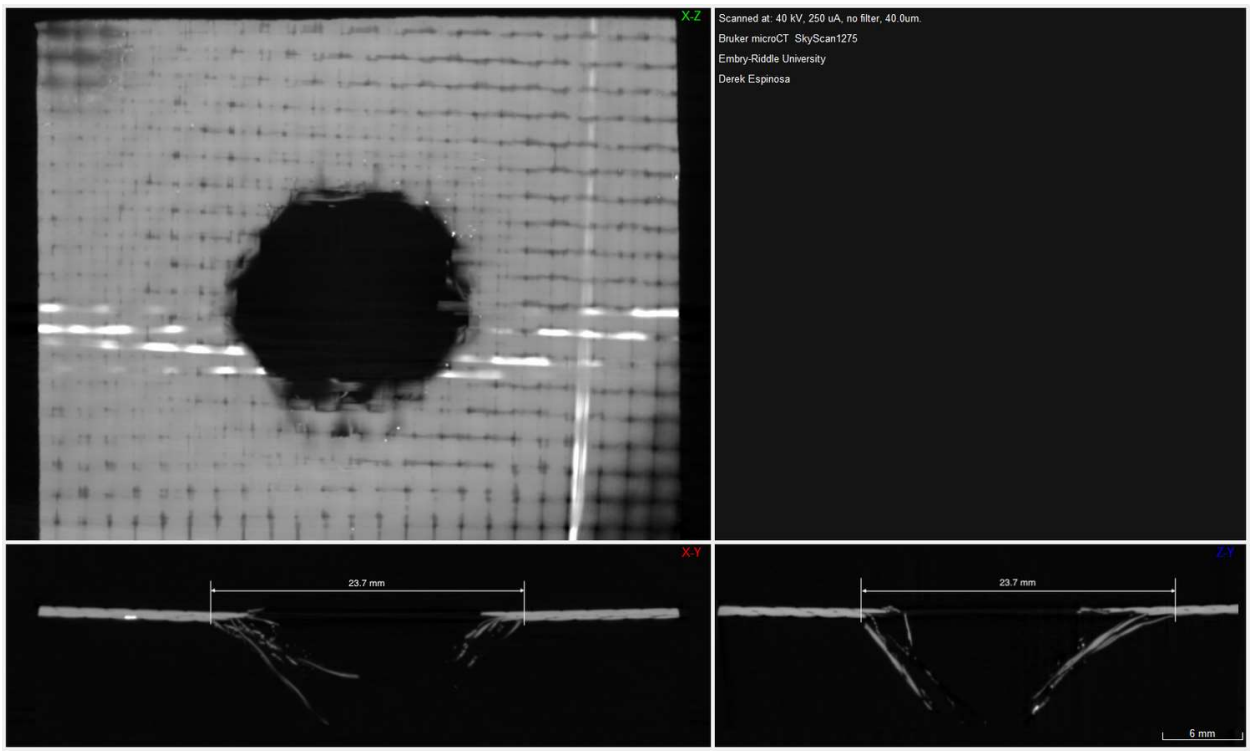

Figure 5.16: X-Ray tomography of Acid Activated composite with $[0\,/90\,]_4$ layout.

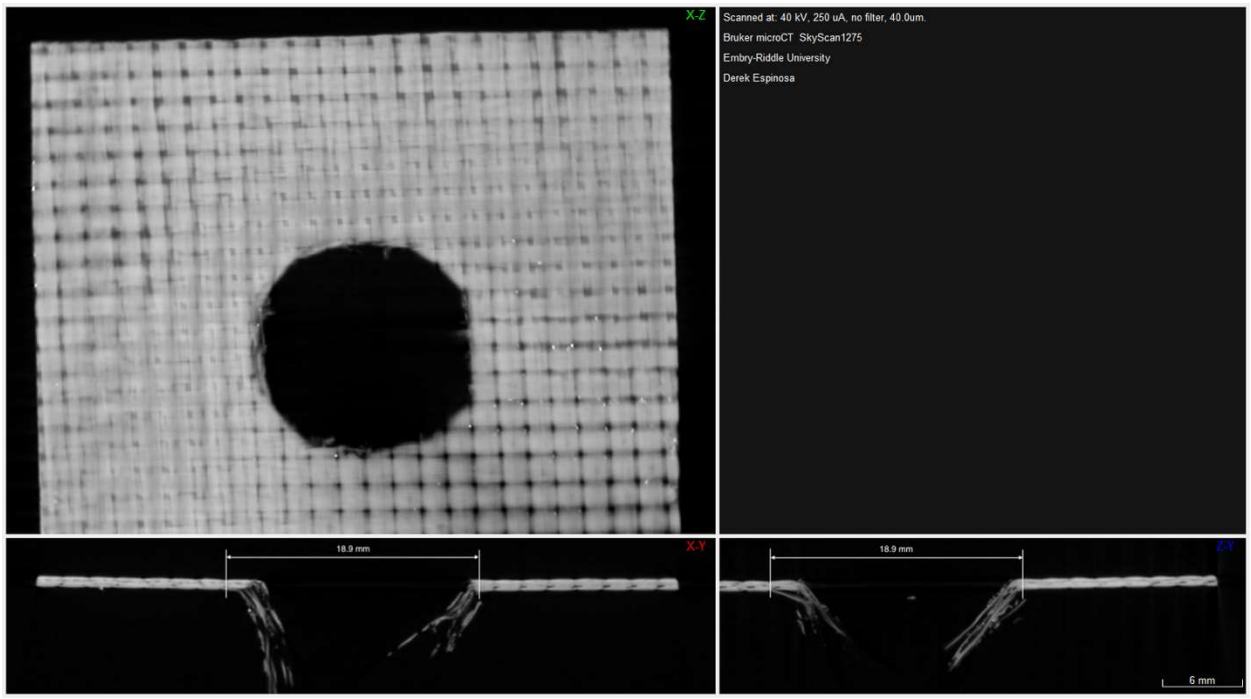

Figure 5.17: X-Ray tomography of MOFs composite with $[0\,/90\,]_4$ layout.

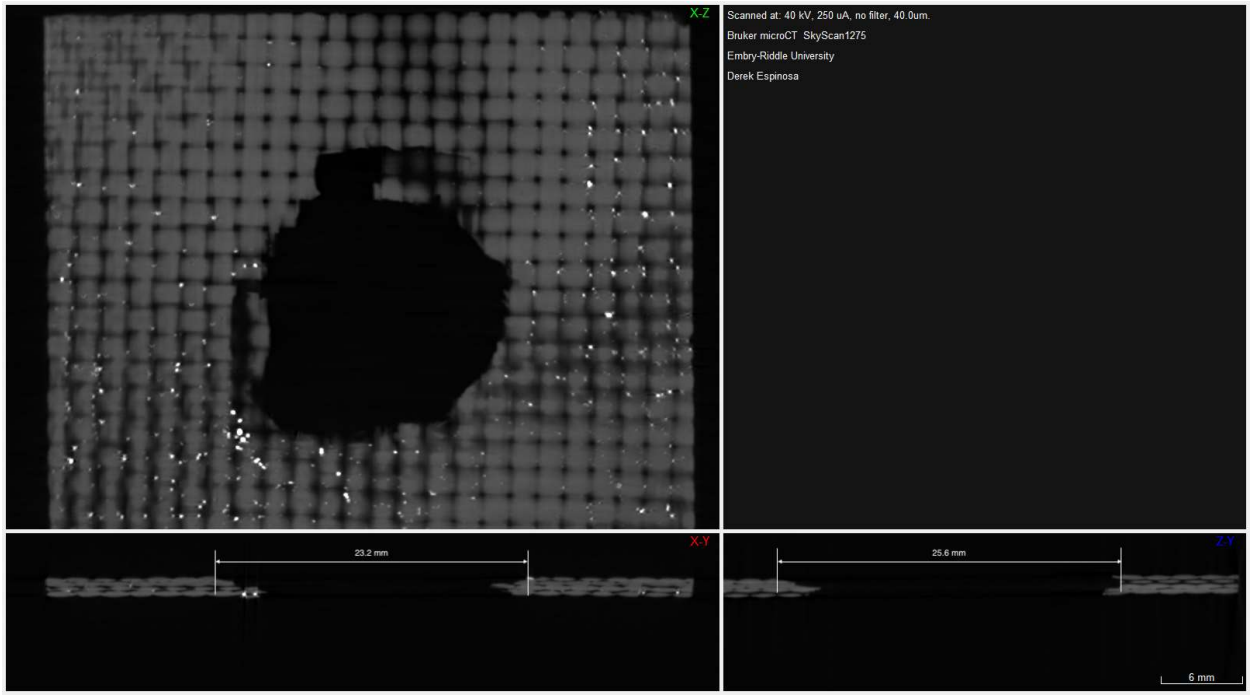

Figure 5.18: X-Ray tomography of CNTs composite with $[0\,/90\,^{\circ}]_4$ layout.

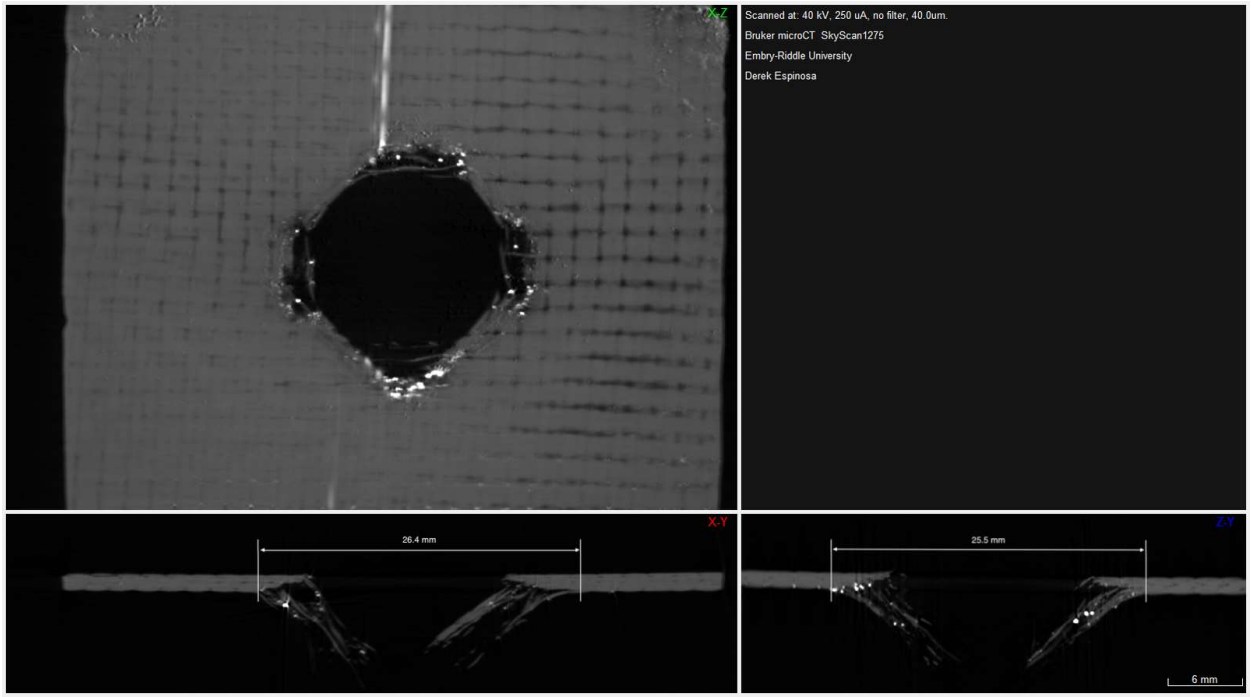

Figure 5.19: X-Ray tomography of Reference composite with $[0\,/90\,^{\circ}]_8$ layout.

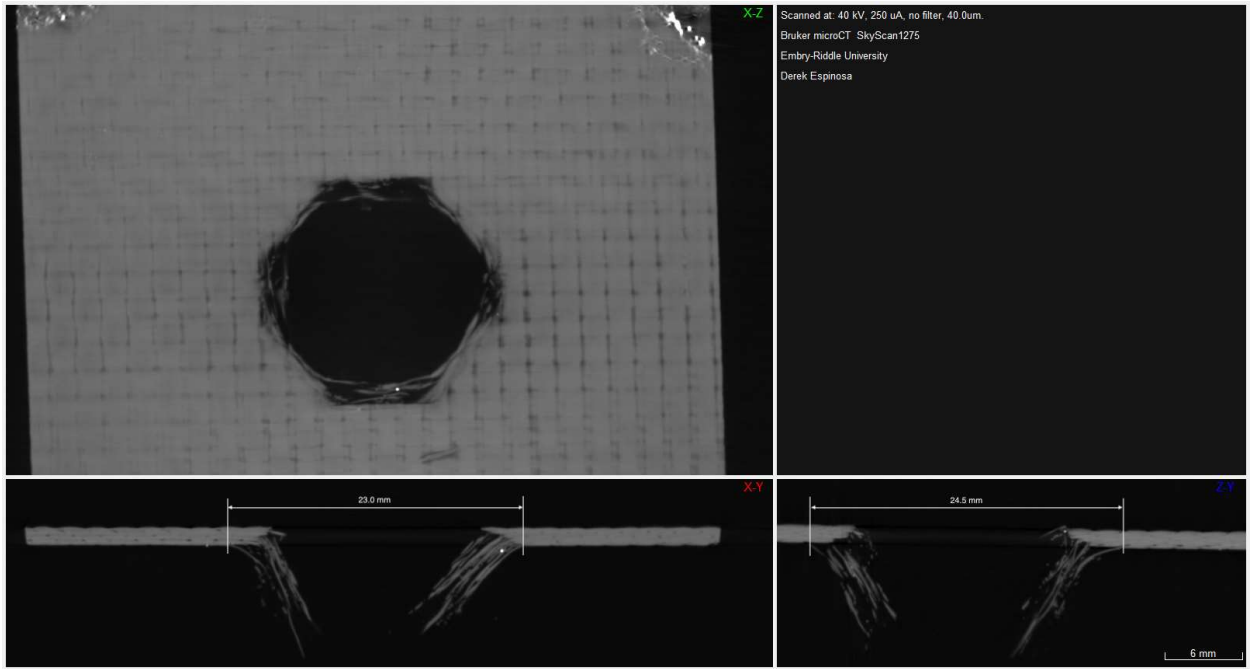

Figure 5.20: X-Ray tomography of Acid Activated composite with $[0\,/90\,]_8$ layout.

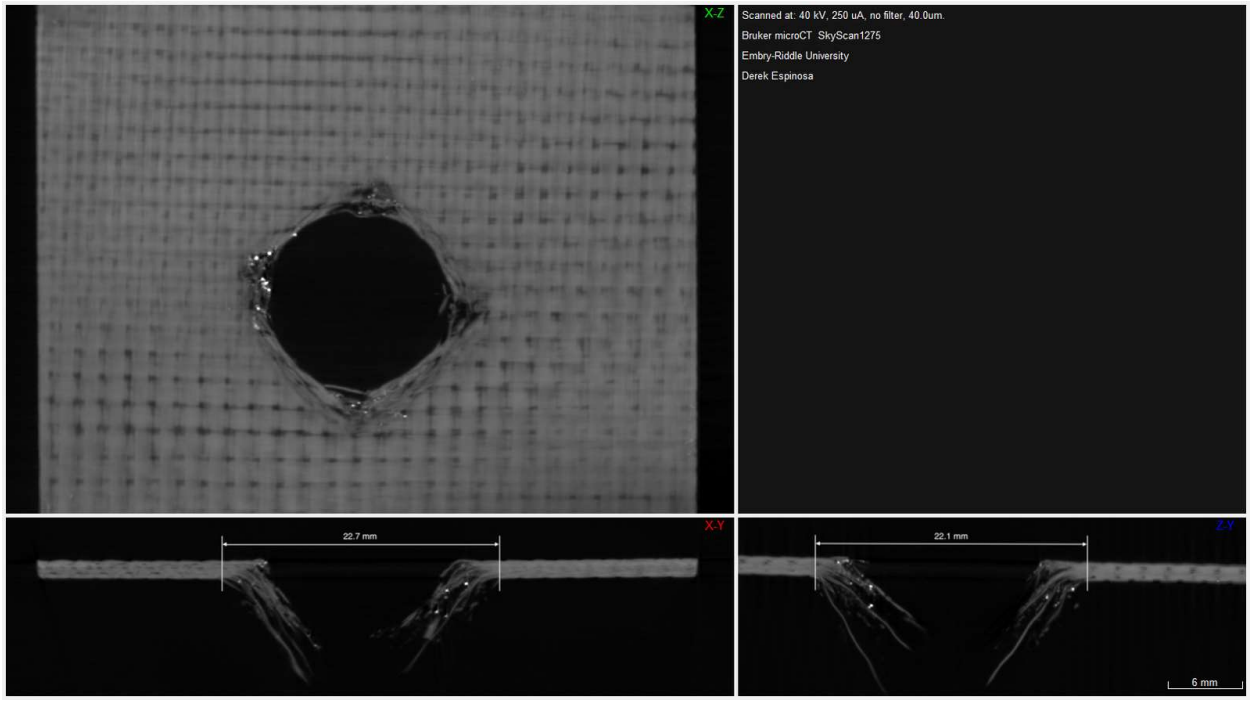

Figure 5.21: X-Ray tomography of MOFs composite with $[0\,/90\,]_8$ layout.

6 Impact Simulation

Computer simulations are usually employed to analyze the behavior of a system or material under different situations, to avoid excessive experimentation. This can be achieved by altering different parameters or the environment of the system to be simulated. Furthermore, these simulations can provide results for conditions that are difficult or costly to replicate due to insufficient experimental setup and prolonged sample preparation.

6.1 Impact Simulation Using LS-DYNA

A model was built to simulate a drop weight impact test with the use of the FEM software LS-Dyna®. The FEM model was based on creating a shell for the composite plate to be analyzed and assigned it MAT-054, also called “Enhanced Composite Damage”, the material properties applied for each configuration were obtained from the mechanical testing performed earlier. The properties used for each composite configuration are indicated in Appendix A, representing the reference, acid activated, and MOF samples respectively. Some properties were not able to be evaluated experimentally due to the absence of the equipment. The missed properties were estimated by different ratios obtained from Wade et al [60]. The impactor or bullet was mimicked by creating a solid in the model and assigning MAT-001, also called “Elastic”, it was assigned to be stainless steel 304 and the material properties were found in the literature [61].

The impactor was placed at a height of 0.01 m on top of the plate to simulate the point where the bullet is about to impact and where the data is obtained in the impact drop weight test. The edges of the plate were constrained to 0 degrees of freedom to simulate the clamping of the sample

to the machine frame. The simulation was set to run for 5.00 ms. and collect data points every 2.00 μs to analyze and compare the results to the experimental test.

The meshing of each FEM part had to be optimized to provide more reliable outcome in the simulation results. The impactor bullet was designed as a sphere solid with 8 mm diameter and a meshing density of 10. The composite plate was designed as a square 4-node shell with dimensions of 120 mm by 120 mm; different meshes were applied to determine which mesh converges to yield accurate and precise results, all the meshes evaluated can be denoted in Figure 6.1. The chosen mesh for the composite plate was a 100 by 100 squared mesh, with a re-mesh of the center of the plate (26.4 mm by 26.4 mm) to triangular mesh to an element size of 0.001; this mesh helps analyze and understand the behavior of the materials in the local zone where the ball is impacting. All the sides of the plate were fixed to simulate the clamping from the experimental test and the impactor was set to a velocity of 9 m/s.

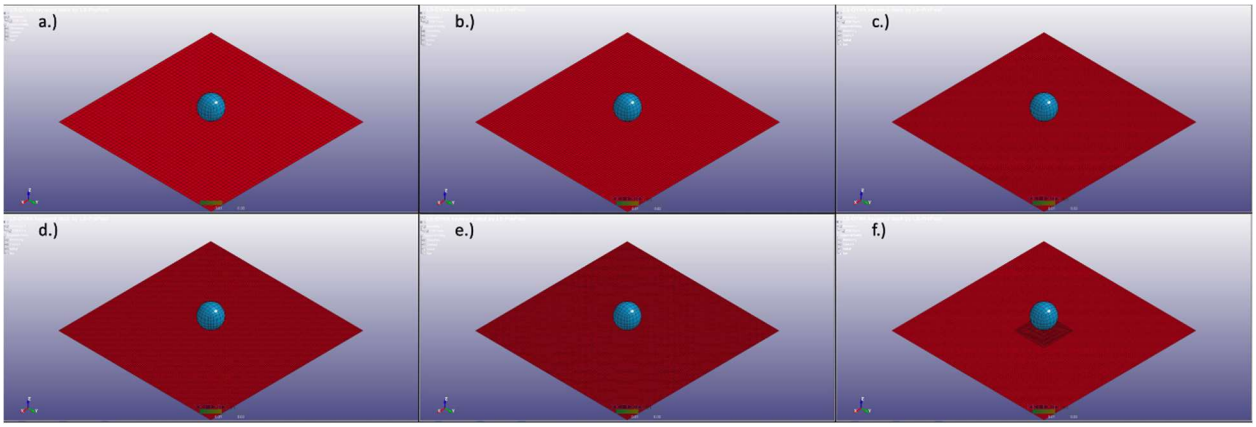

Figure 6.1: a.) 50 by 50 mesh. b.) 75 by 75 mesh. c.) 100 by 100 mesh. d.) 125 by 125 mesh. e.) 150 by 150 mesh. f.) 100 by 100 mesh with center re-meshed to 0.001 element size.

6.2 Impact Simulation Results

The impact model was obtained after several iterations of interpreting how different coefficients, materials, and elements interact in the simulation. Wade et al. [60] provide useful details on how to obtain difference coefficients and material properties for MAT54 on LS-DYNA. It was determined that due to the out-of-plane nature of the experimental impact test performed, the flexural modulus obtained from three-point bending should be used instead of the elastic modulus obtained from tensile testing.

Figure 6.2 shows the difference between the experimental results and the simulation results for the energy resistance of the different configurations. The individual comparison of the loading and energy behaviors for each configuration is shown in Appendix A. The simulation results follow the same trend as the experimental results, showing an enhancement of impact resistivity with the MOF growth on the surface of the carbon fibers. Furthermore, the slopes of the curves are identical, showing good correlation and accuracy from the simulation results. The experimental results revealed a rapid decrease in the loading at the end of the curves, compared to a constant decrease in loading from the simulation results. The different behavior of the unloading sections leads to the maximum energy and time to reach it not correlating. These differences can be attributed to the rebound breaker installed in the drop-weight machine, which does not allow the impactor to fully penetrate the sample. The modeling of a rebound breaker would suggest a more sophisticated model that would drastically increase the running time of the simulation. The maximum loading and maximum energy comparison of the experimental and impact simulation results are shown in Table 6.1.

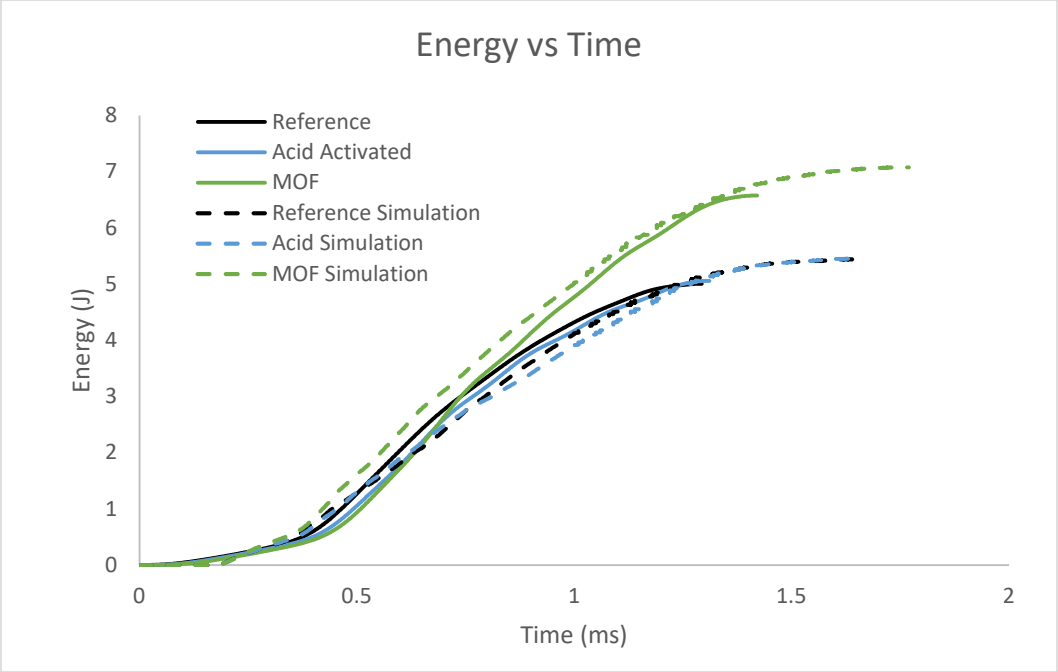

Figure 6.2: Comparison of the experimental results and the LS-DYNA simulation of the different composites energy absorption.

Table 6.1: Comparison of LS-DYNA simulation and the experimental impact test results.

	Reference	Reference Simulation	Acid Act.	Acid Act. Simulation	MOF	MOF Simulation
Max. Load (kN)	0.896	0.893	0.972	0.831	1.137	1.120
Percent Error (%)	-	-0.33%	-	-14.51%	-	-1.50%
Max Energy (J)	5.008	5.457	5.059	5.468	6.576	7.078
Percent Error (%)	-	8.97%	-	8.17%	-	7.63%

7 Conclusions and Future Work

This thesis focused on modifying the surface area of carbon fibers by an acid oxidation technique, MOFs growth, and CNTs growth. The impact resistance of the different configurations of HFRPs were compared to a reference CFRP. A finite element modeling technique using LS-DYNA was also used to correlate the experimental and simulation results of the drop-weight impact test. Furthermore, various mechanical properties were evaluated for the different configurations. The different properties obtained were used in the simulation to define the correct material and obtain accurate results.

7.1 Conclusions

The tensile tests performed on the $[0°/90°]_4$ layout showed a minimal increase in strength and strain of 1% and 9% respectively for the acid activated configuration. The MOFs configuration showed an increase in strength and strain of 25% and 40%, respectively. These enhancements can be related to the significant increase in the surface area due to the MOFs cells which in return yields better bonding. On the other hand, the CNTs configuration significantly decreased the strength and strain by 91% and 82% respectively. This is mainly attributed to the damage of the fibers due to the exposure to elevated temperature. The tensile tests performed on the $[45°/-45°]_4$ layout resulted in an increased strain of 6% but a decrease of strength of 24% for the acid activated configuration. The MOF configuration had similar behavior as the acid activated configuration but more drastic differences with an increase of strain of 13% and a decrease of strength of 50%. All the results from the tensile testing are compared to the reference CFRP with its respective layout.

A three-point bending DMA test was performed to the different CFRPs with $[0°/90°]_4$ layout. A frequency sweep test from 1 Hz. To 50 Hz. at room temperature showed a minimal decrease in the damping of the acid activated sample of 5%. The MOFs and CNTs configurations developed an increase in the damping of 64% and 10%, respectively. A temperature sweep test was evaluated from 25 ºC to 160ºC at 1 Hz. determined the glass transition temperature for each configuration. The reference composite demonstrated a T_g of 138.40 ºC, the acid activated composite obtained a T_g of 142.47 ºC, the MOFs composite exhibited a T_g of 142.55 ºC, and the CNTs composite indicated a T_g of 142.13 ºC. The increase in glass transition indicates that the added surface roughness and nanomaterials hinders the polymer movement, thus requiring higher thermal energy; higher temperature for them to move.

The drop weight impact test was performed on different layouts ($[0°/90°]_2$, $[0°/90°]_4$, and $[0°/90°]_8$) at an impact velocity of 9 m/s. For the $[0°/90°]_4$ layout, the drop weight impact tests were evaluated at impact velocities of 3 m/s, 6 m/s, and 9 m/s. Due to the evaluation at different impact velocities, an average percentage difference of energy resistance was able to be obtained for each configuration with the $[0°/90°]_4$ layout. The acid activated configuration had a minimum increase in the energy resistance of approximately 8.7%. The MOFs configuration enhanced the energy resistance by 43.8%. On the other hand, the CNTs configuration dropped the energy resistance to 70.5%. The maximum crack size; damage zone; was evaluated to determine the damage severity generated in the CFRPs. However, it is not visible to the naked eye, to evaluate the internal damage imparted in the CFRPs due to the impact, a CT scan was performed. For the $[0°/90°]_4$ layout with an impact velocity of 9 m/s, the acid activated and CNTs configurations experienced an increase in the maximum crack zone of 1.28% and 9.40% respectively. On the

other hand, the MOFs configuration developed less internal damage, reducing the maximum crack zone by 19.23%.

An impact modeling was performed on LS-DYNA to correlate the experimental results. Due to the significant reduction in performance of the CNTs, the impact modeling of that configuration was not evaluated. The simulation was based on MAT-54 to model the composite plate, and a spherical impactor was created to model the drop-weight impact machine. The properties for each configuration were obtained from the previous tests performed. The modeling of each configuration followed the same trend and behavior as the experimental test, showing accuracy in the results. The energy resistance of the simulation increased compared to the experimental results, for the reference configuration at 8.97%, for the acid activated configuration at 8.17%, and for the MOFs configuration at 7.63%, respectively. The increases in energy resistance are attributed to the unloading behavior that is different between the simulation and the experimentation and the fact that the model doesn't account for the preexisting defects in the samples. The experimentation counts with a rebound breaker that generates faster unloading toward the end of the test. On the other hand, a rebound breaker would involve a complicated design for drop weight impact modeling, resulting in extensive simulation times.

The results of this thesis show that the growth of MOFs on the carbon fibers improves several mechanical properties without several reductions of other properties. Due to the increase in surface area and uniformity of growth, MOFs improve the interfacial adhesion of the fibers with the matrix, being a good technique to be implemented in industries.

7.2 Future Work

The literature on MOFs growth in carbon fibers and their applications are still limited, it is recommended to keep researching to optimize a technique that could be used in different industries. Based on the results obtained in this thesis, it would be beneficial to evaluate the impact resistivity of MOFs with a different number of layers and different layouts. It also will be beneficial to test at high velocities (greater than 100m/s) to illustrate suitability for several applications. Furthermore, a honeycomb sandwich with MOFs carbon fibers composite would enhance impact resistivity and potentially improve the interfacial adhesion between the fibers and the honeycomb. All these configurations and layouts can be further tested with high-velocity impact devices to evaluate their performance.

8 APPENDIX – A

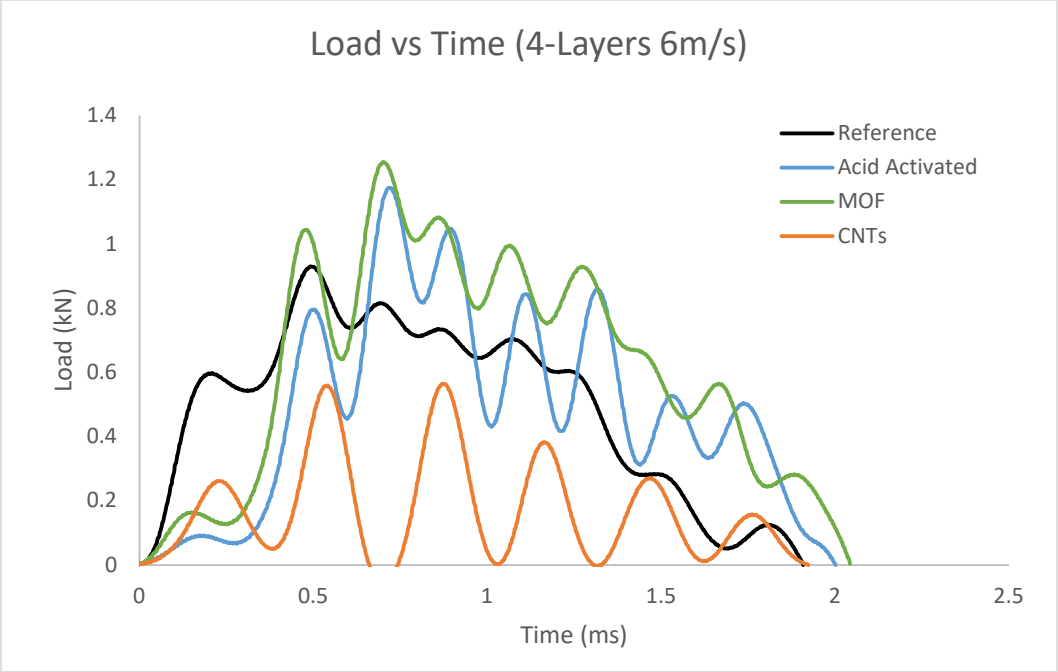

Figure A.1: Impact load evolution for [0 °/90 °]$_4$ layup of the different CFRPs at 6m/s

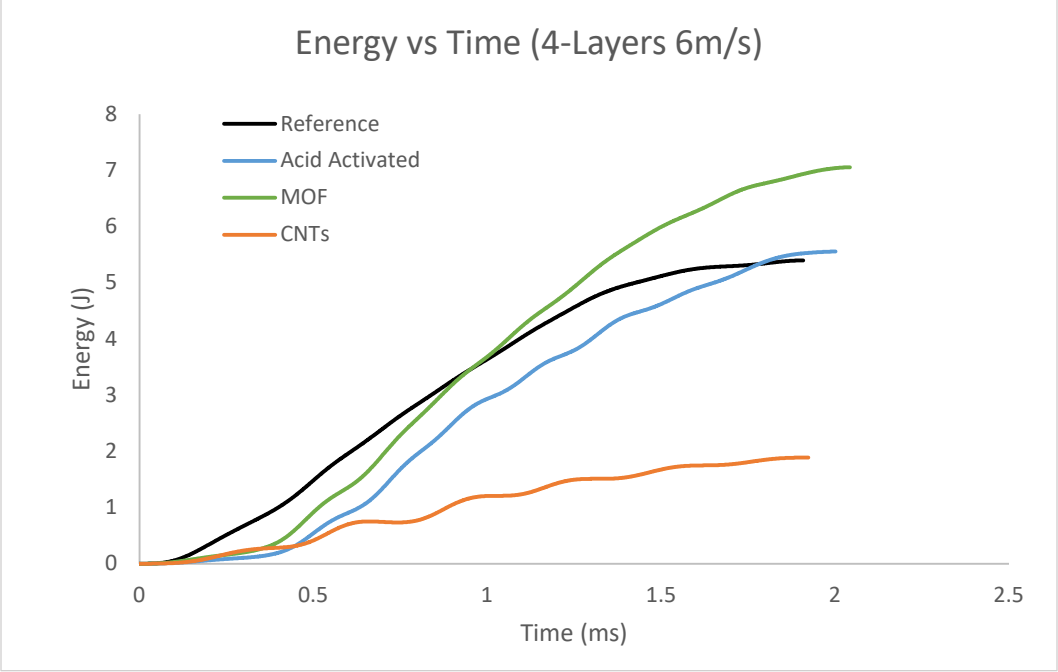

Figure A.2: Impact Resistance on [0°/90°]$_4$ CFRPs at 6m/s

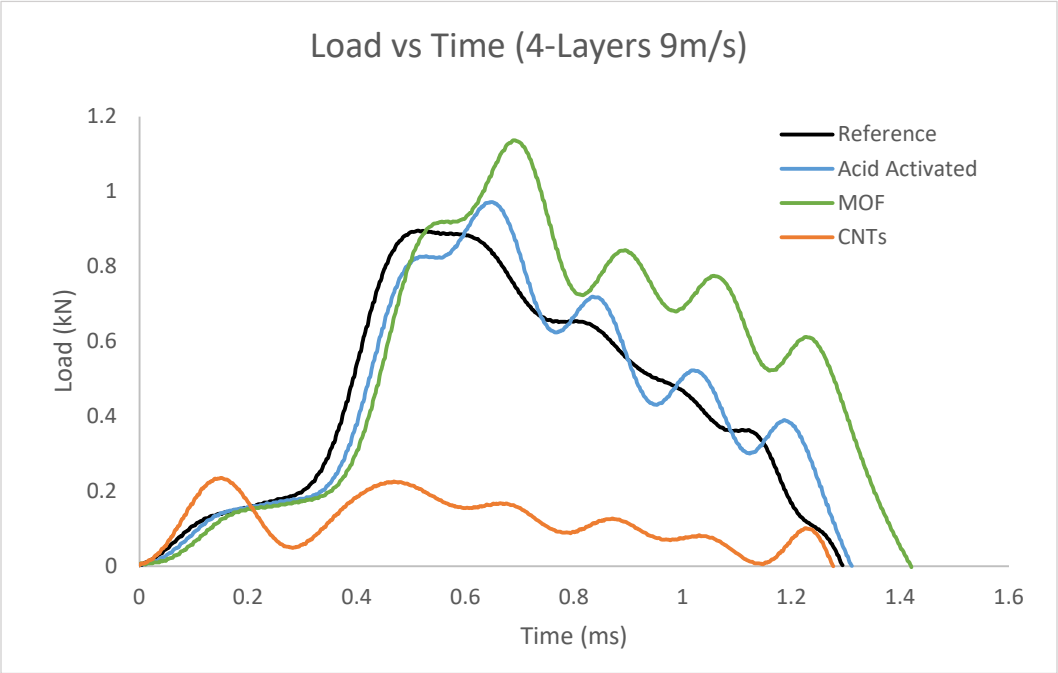

Figure A.3: Impact load evolution for $[0/90]_4$ layup of the different CFRPs at 9m/s

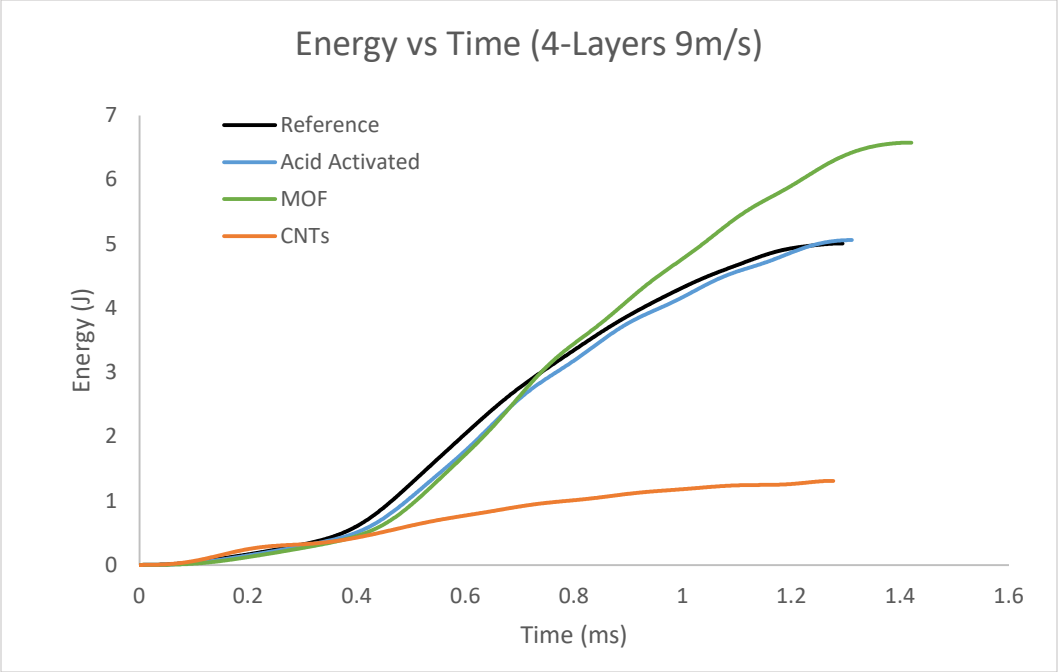

Figure A.4: Impact Resistance on $[0°/90°]_4$ CFRPs at 9m/s

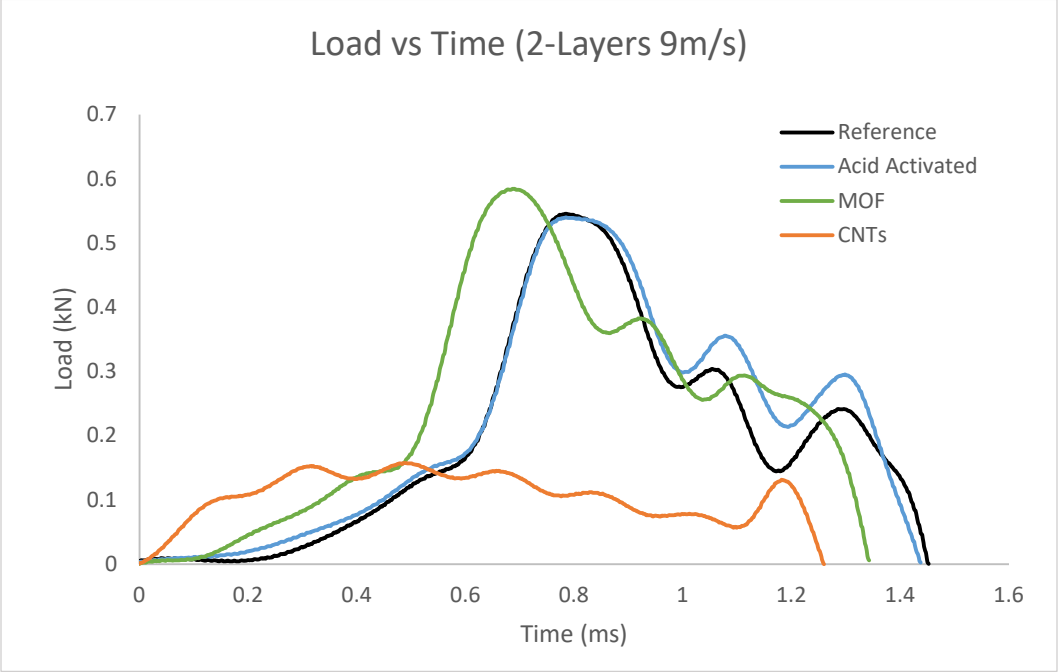

Figure A.5: Impact load evolution for $[0\,°/90\,°]_2$ layup of the different CFRPs at 9m/s

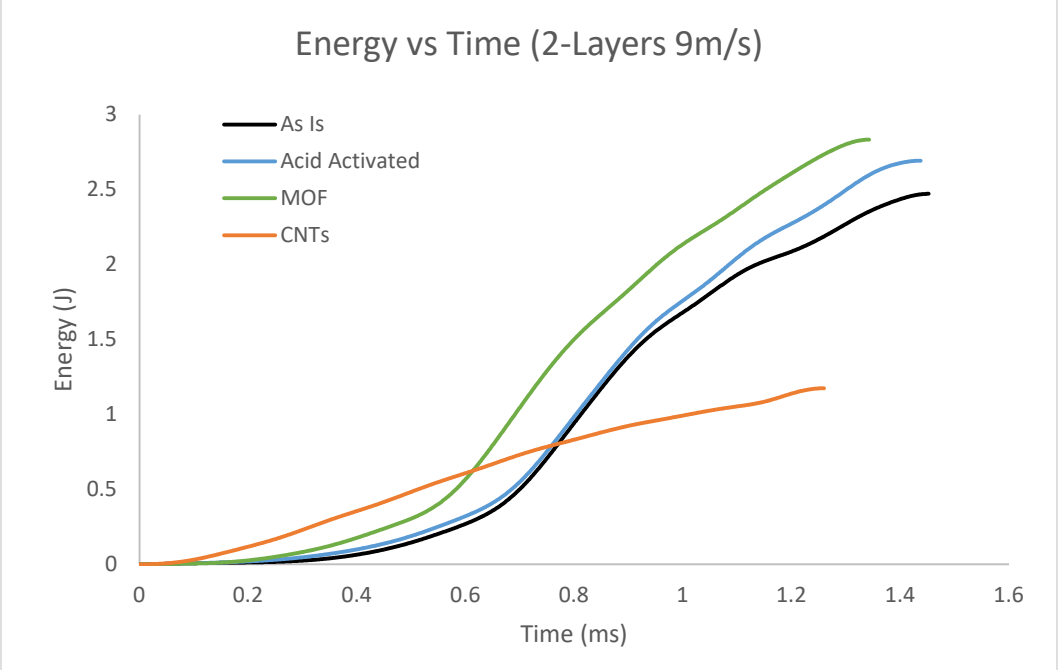

Figure A.6: Impact Resistance on $[0°/90°]_2$ CFRPs at 9m/s

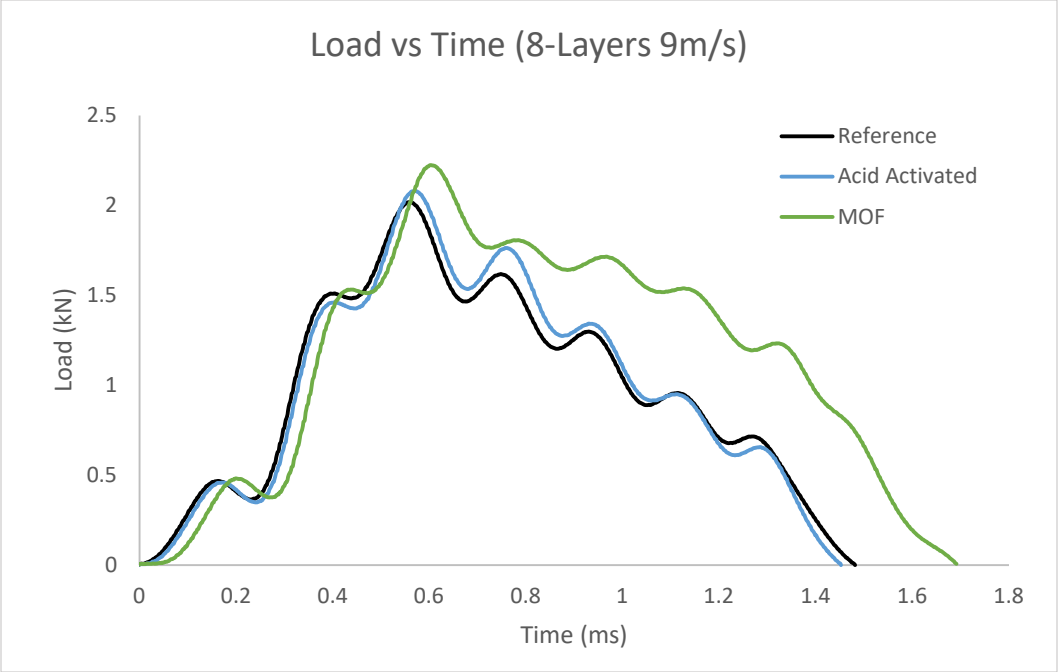

Figure A.7: Impact load evolution for [0 °/90 °]$_8$ layup of the different CFRPs at 9m/s

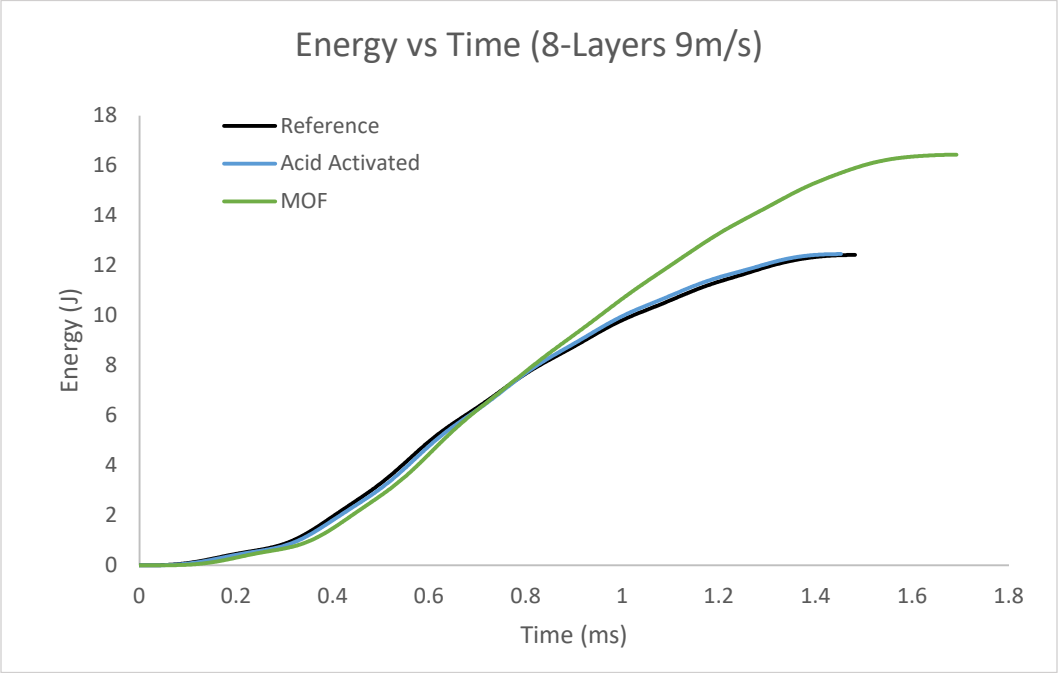

Figure A.8: Impact Resistance on [0°/90°]$_8$ CFRPs at 9m/s

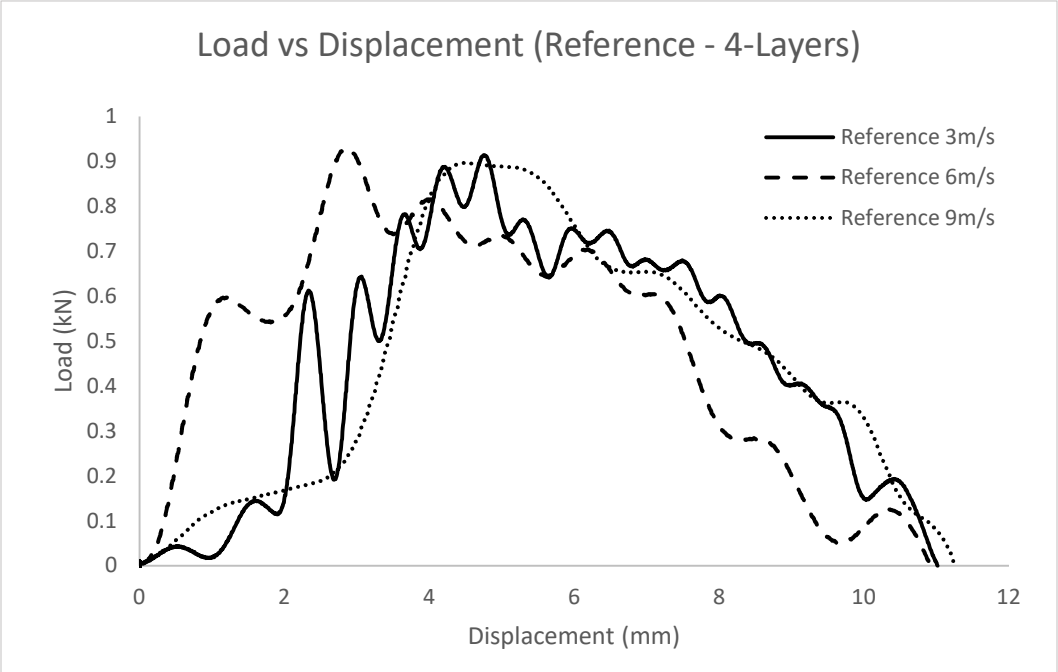

Figure A.9: Impact Load applied on [0°/90°]$_4$ Reference CFRPs at different velocities

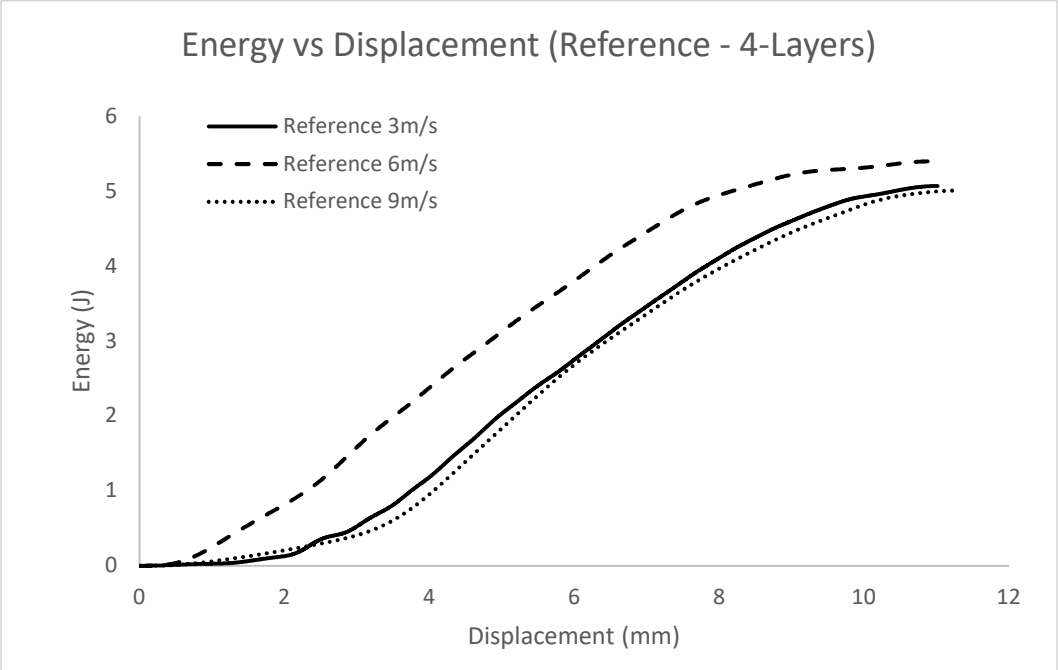

Figure A.10: Impact Resistance on [0°/90°]$_4$ Reference CFRPs at different velocities

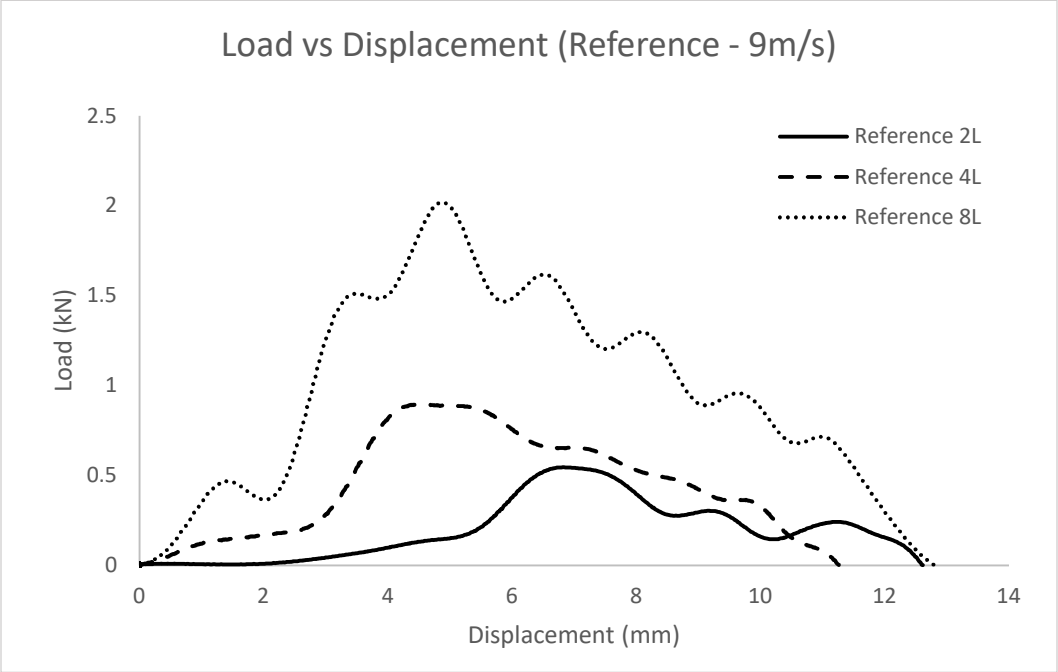

Figure A.11: Impact Load applied on Reference CFRPs at 9m/s with different Layouts

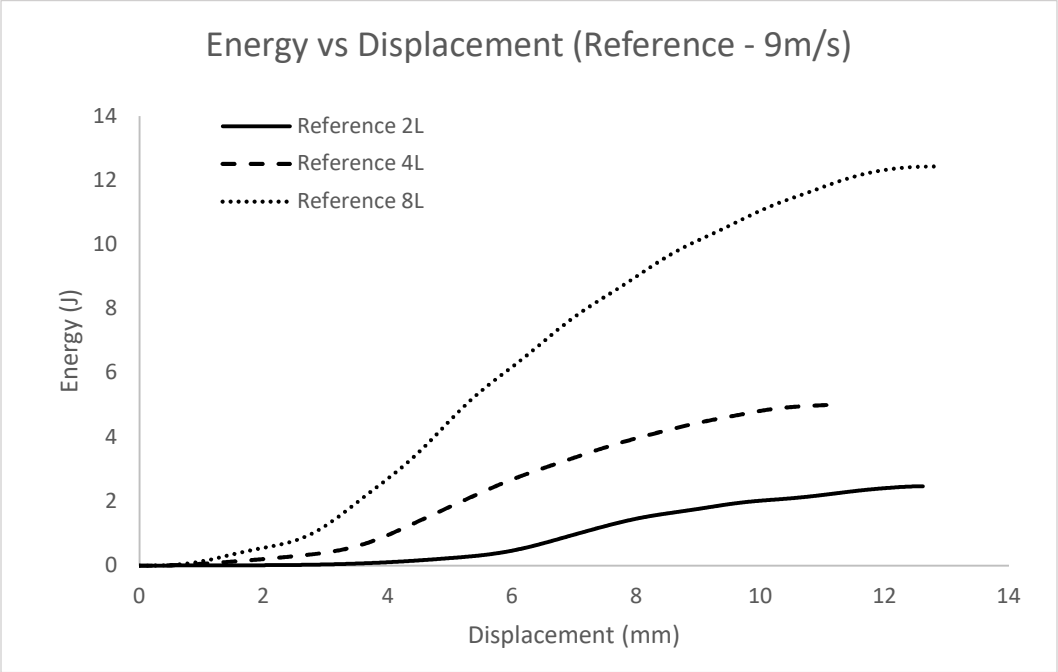

Figure A.12: Impact Resistance on Reference CFRPs at 9m/s with different Layouts

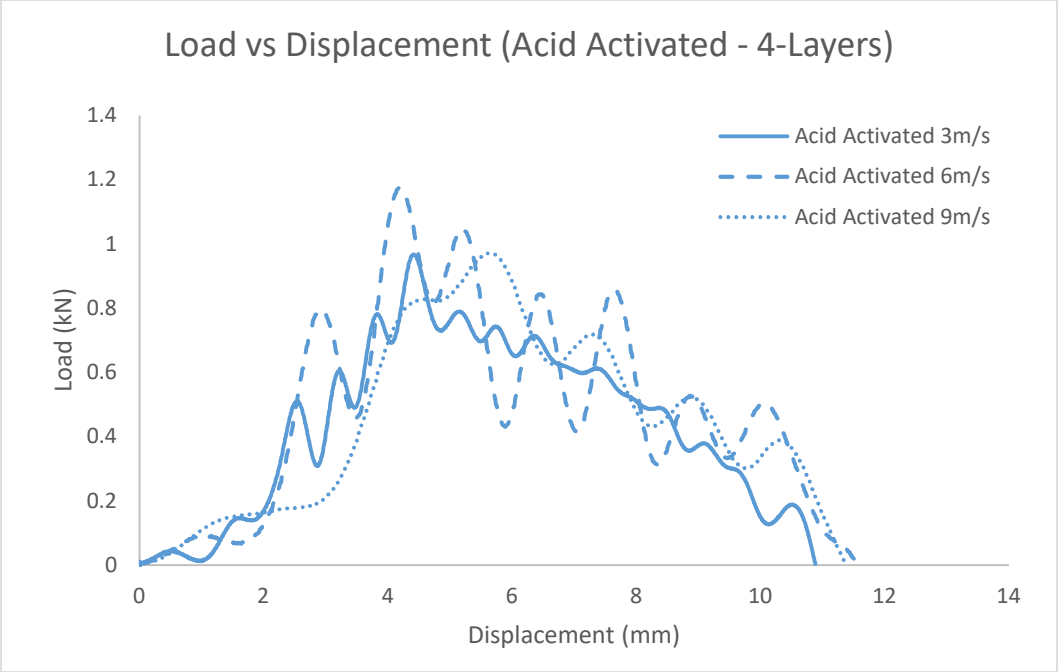

Figure A.13: Impact Load applied on $[0°/90°]_4$ Acid Activated CFRPs at different velocities

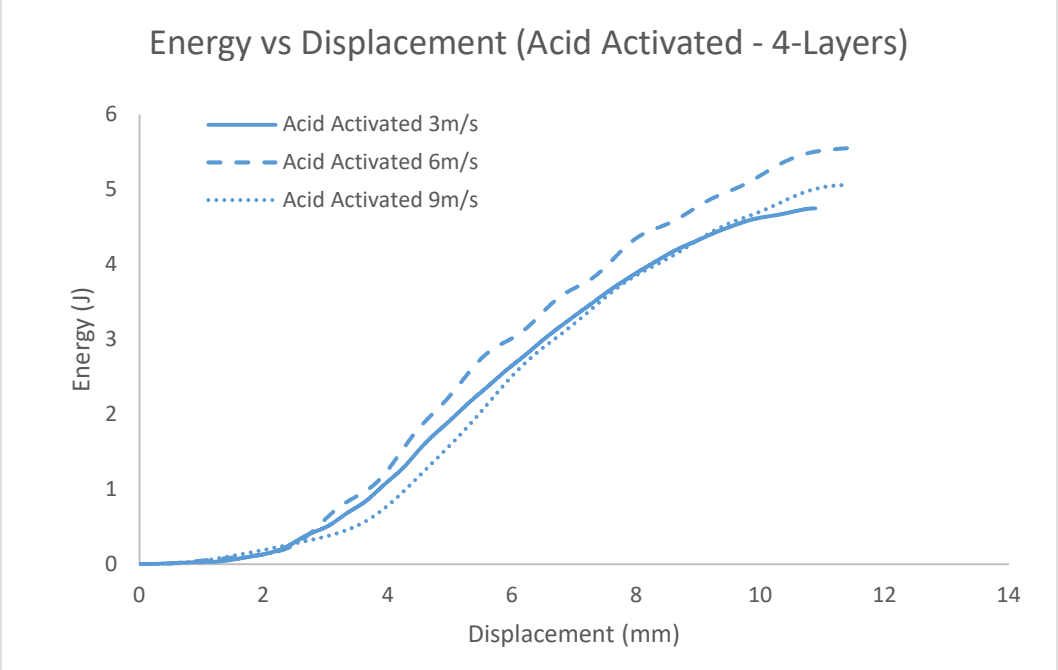

Figure A.14: Impact Resistance on $[0°/90°]_4$ Acid Activated CFRPs at different velocities

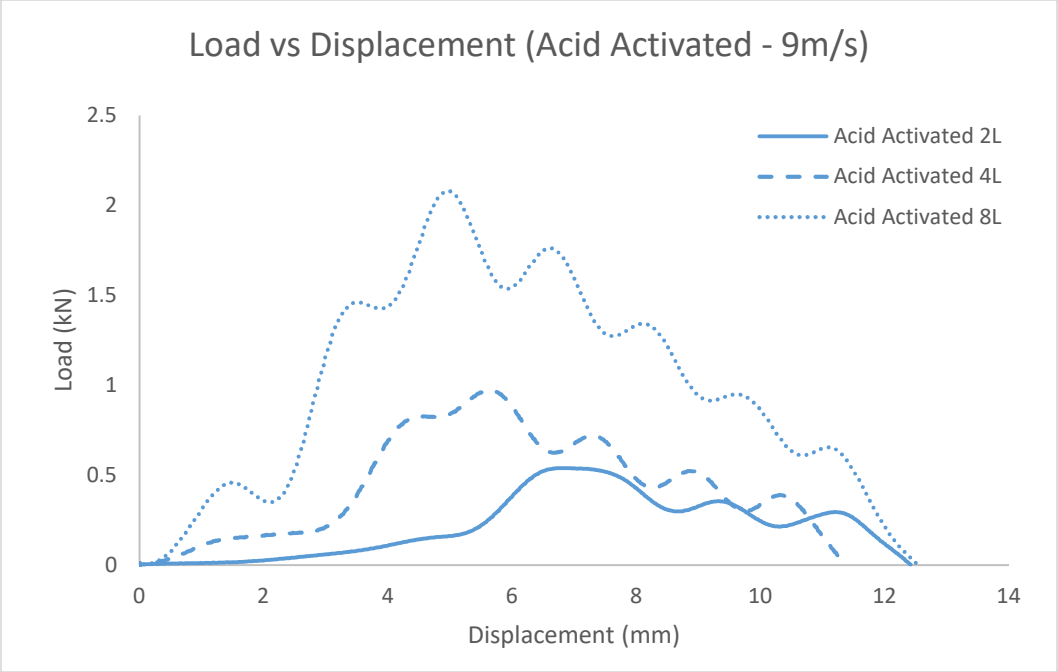

Figure A.15: Impact Load applied on Acid Activated CFRPs at 9m/s with different Layouts

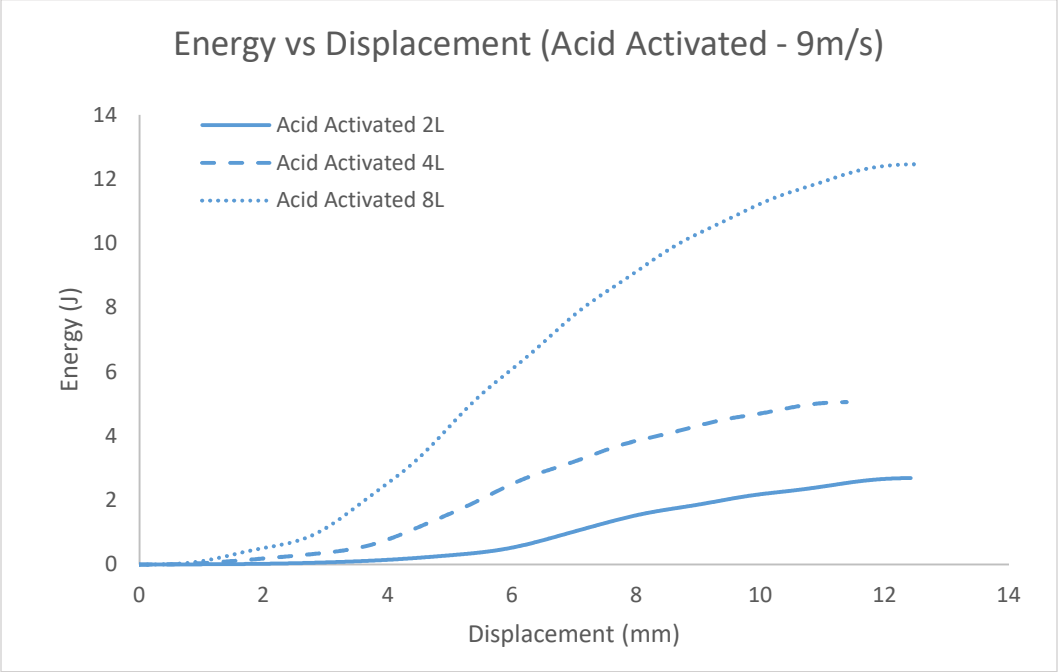

Figure A.16: Impact Resistance on Acid Activated CFRPs at 9m/s with different Layouts

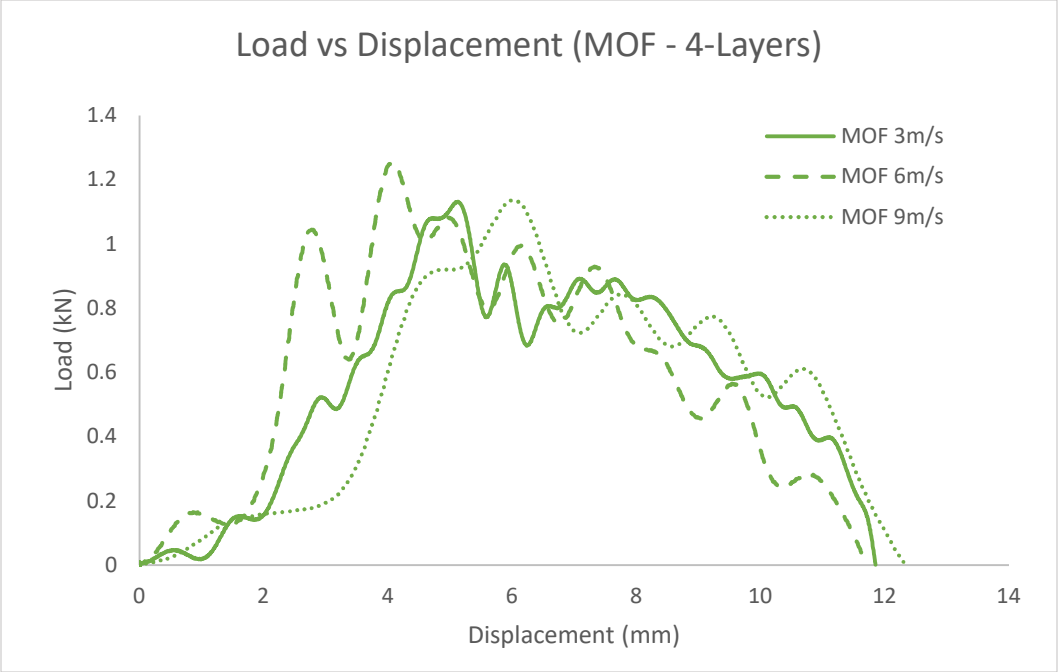

Figure A.17: Impact Load applied on $[0°/90°]_4$ MOF CFRPs at different velocities

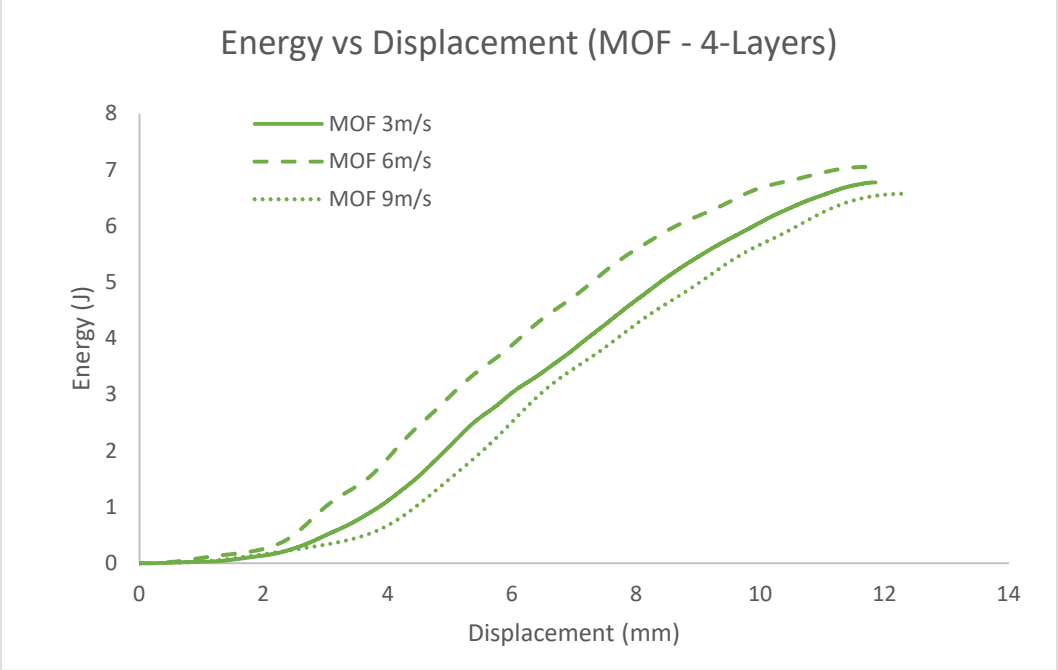

Figure A.18: Impact Resistance on $[0°/90°]_4$ MOF CFRPs at different velocities

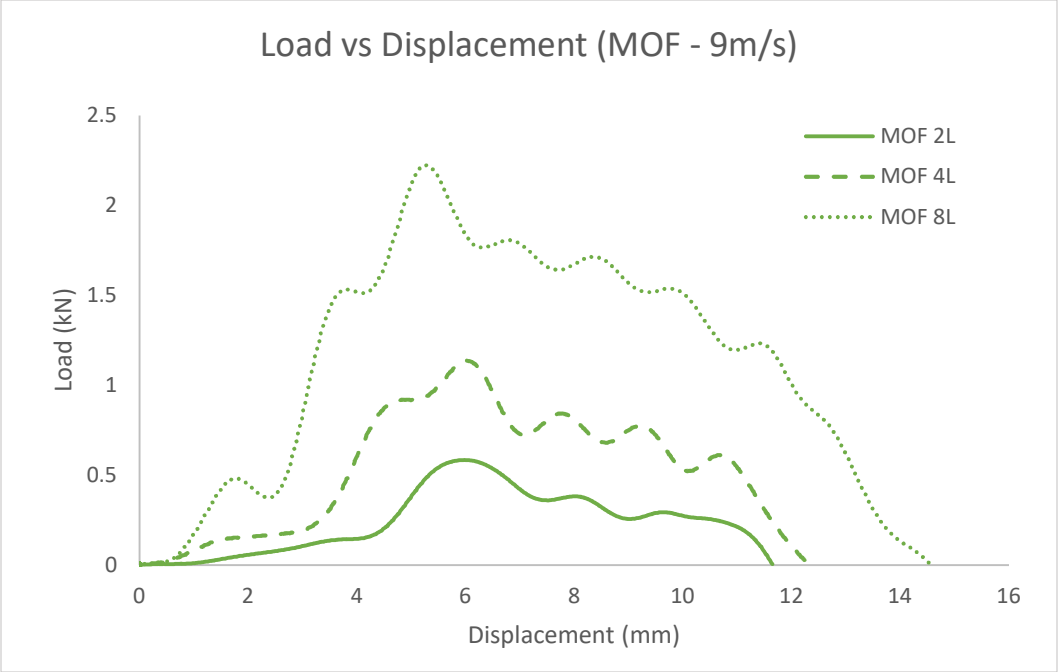

Figure A.19: Impact Load applied on MOF CFRPs at 9m/s with different Layouts

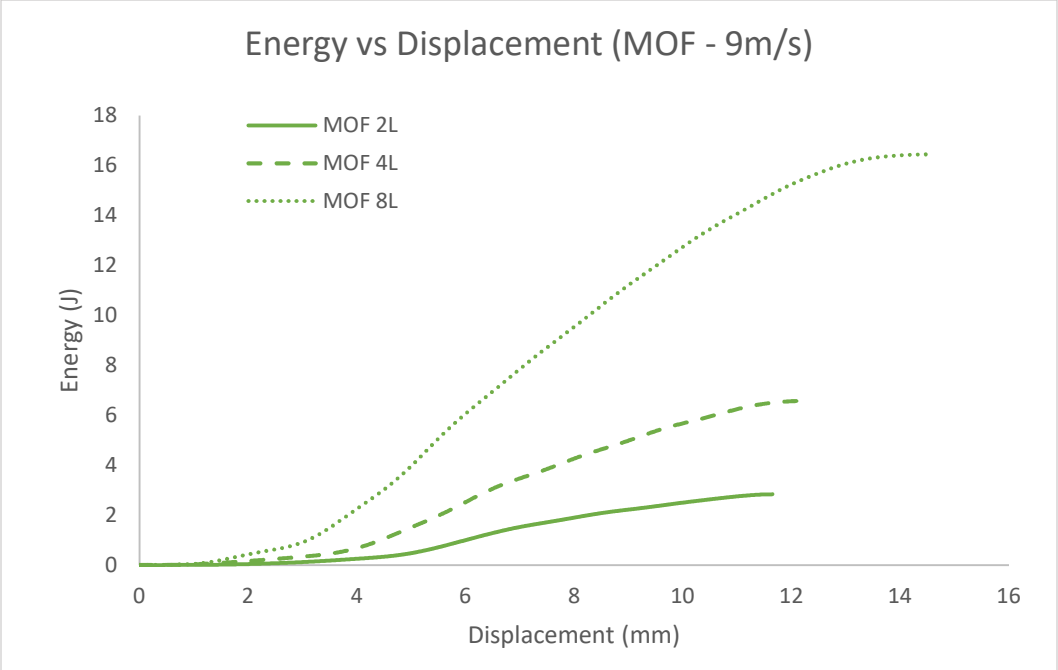

Figure A.20: Impact Resistance on MOF CFRPs at 9m/s with different Layouts

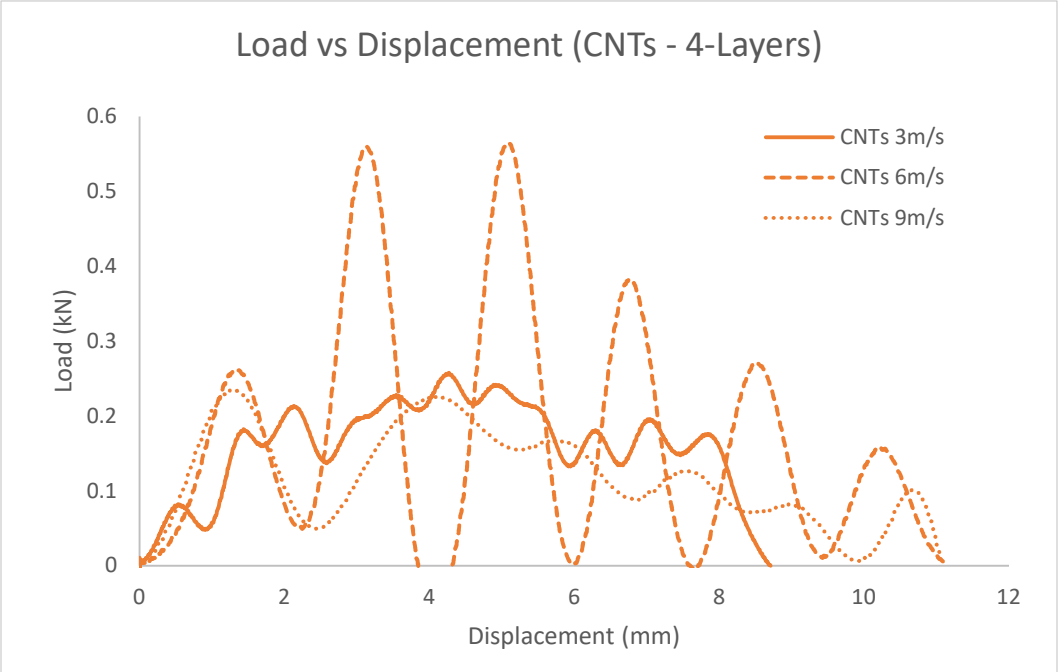

Figure A.21: Impact Load applied on $[0°/90°]_4$ CNTs CFRPs at different velocities

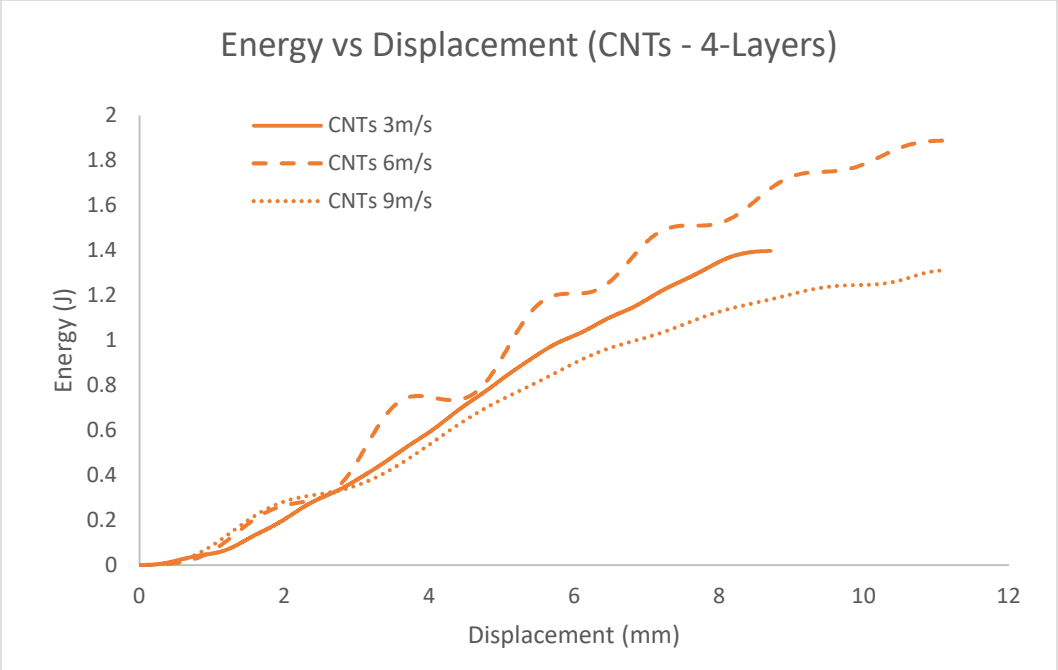

Figure A.22: Impact Resistance on $[0°/90°]_4$ CNTs CFRPs at different velocities

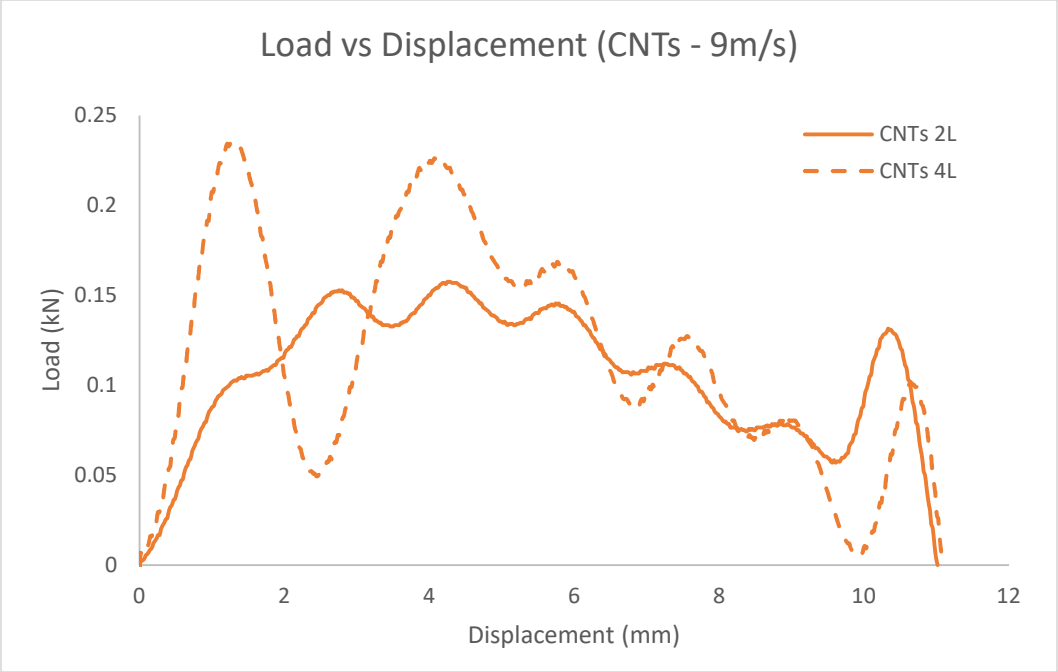

Figure A.23: Impact Load applied on CNTs CFRPs at 9m/s with different Layouts

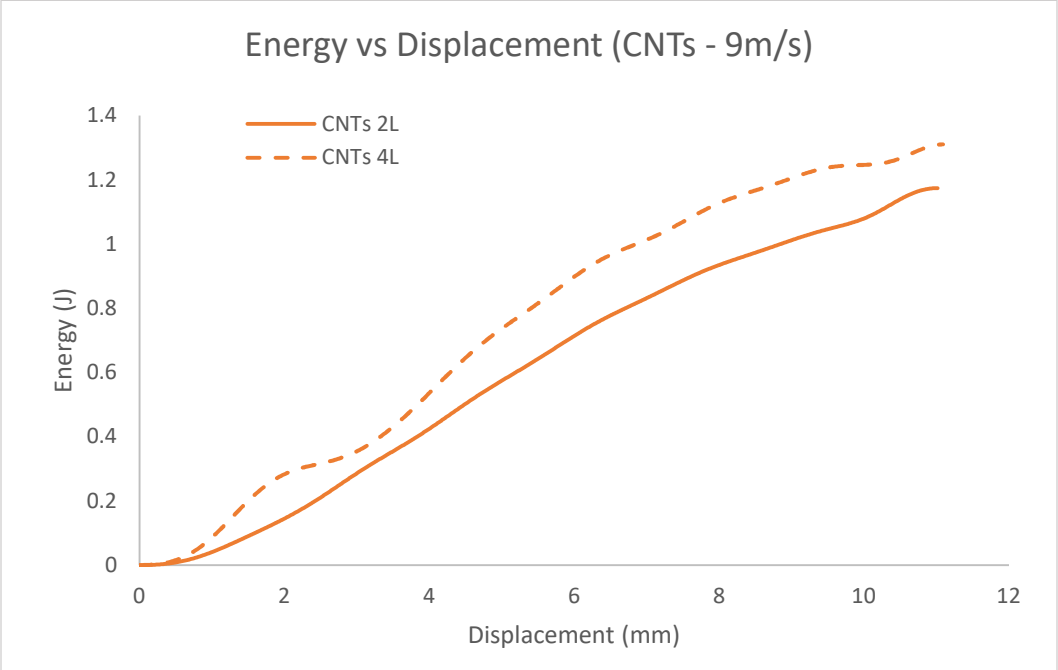

Figure A.24: Impact Resistance on CNTs CFRPs at 9m/s with different Layouts

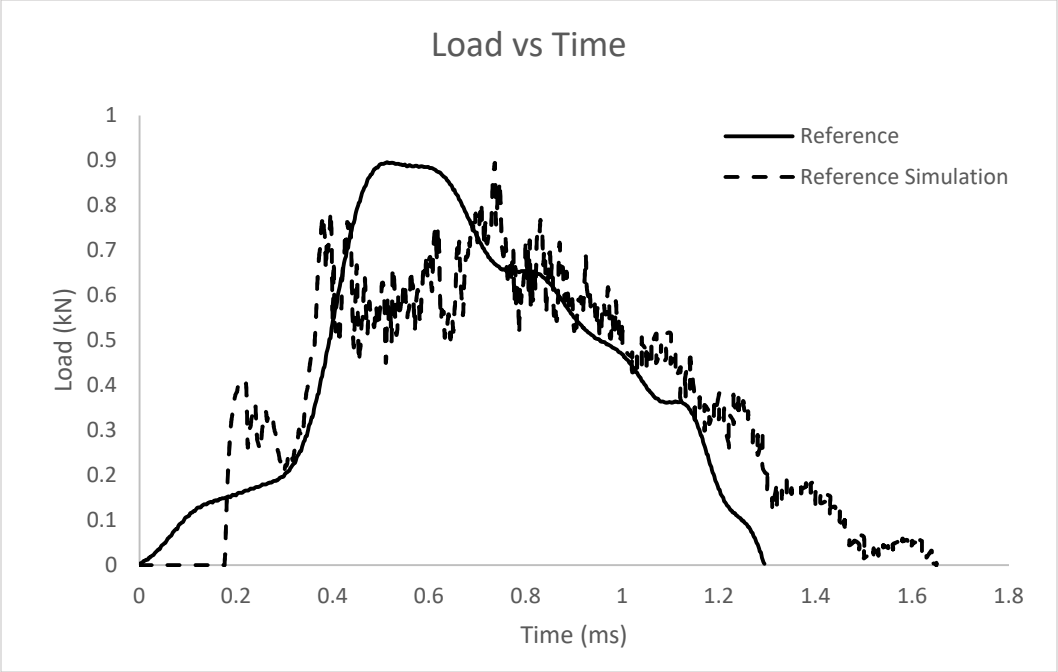

Figure A.25: Impact Load applied comparison between Experimental and Modeling of [0°/90°]$_4$ Reference CFRPs

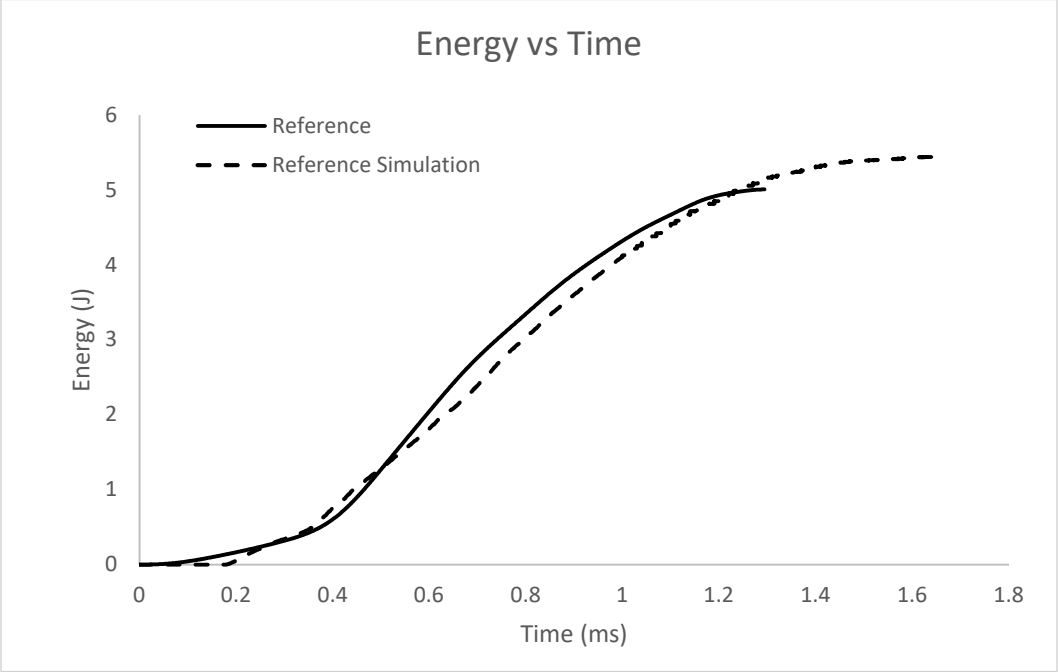

Figure A.26: Impact Resistance comparison between Experimental and Modeling of [0°/90°]$_4$ Reference CFRPs

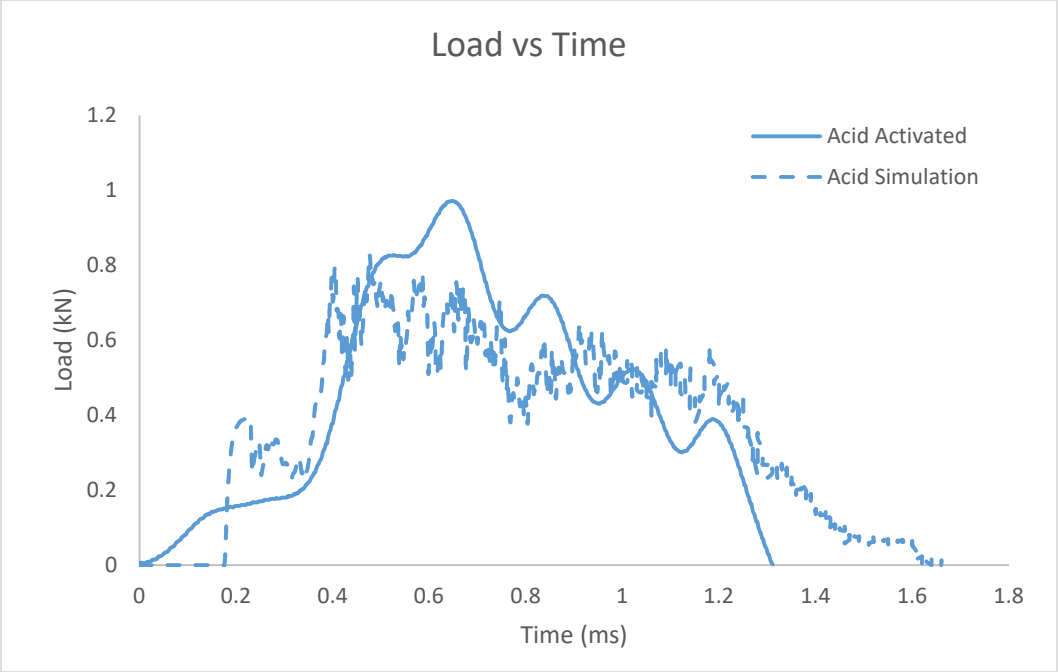

Figure A.27: Impact Load applied comparison between Experimental and Modeling of $[0°/90°]_4$ Acid Activated CFRPs

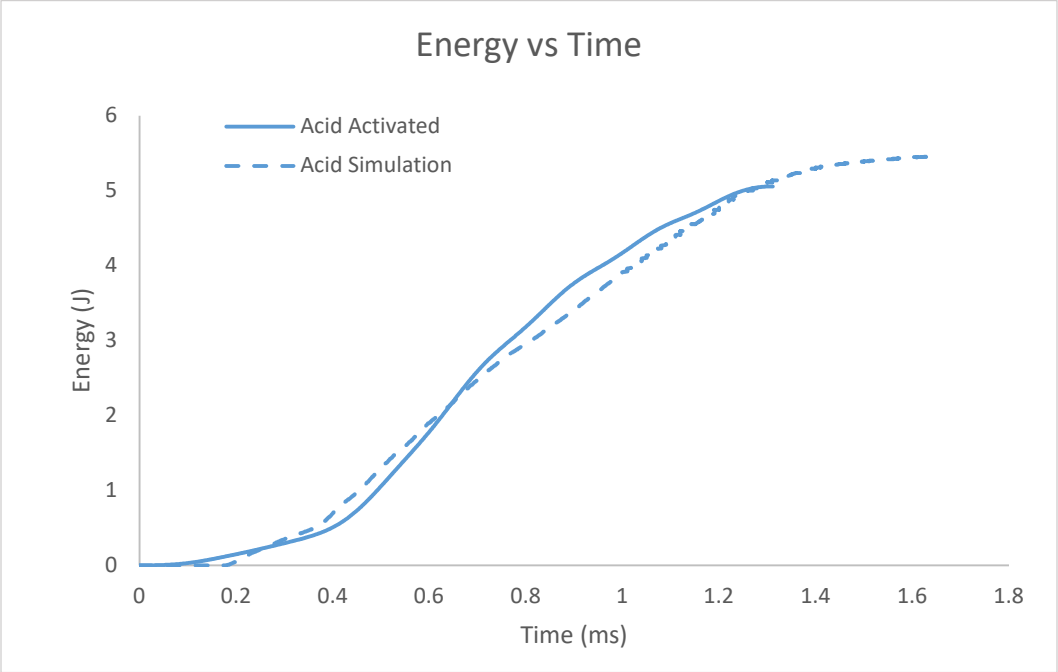

Figure A.28: Impact Resistance comparison between Experimental and Modeling of $[0°/90°]_4$ Acid Activated CFRPs

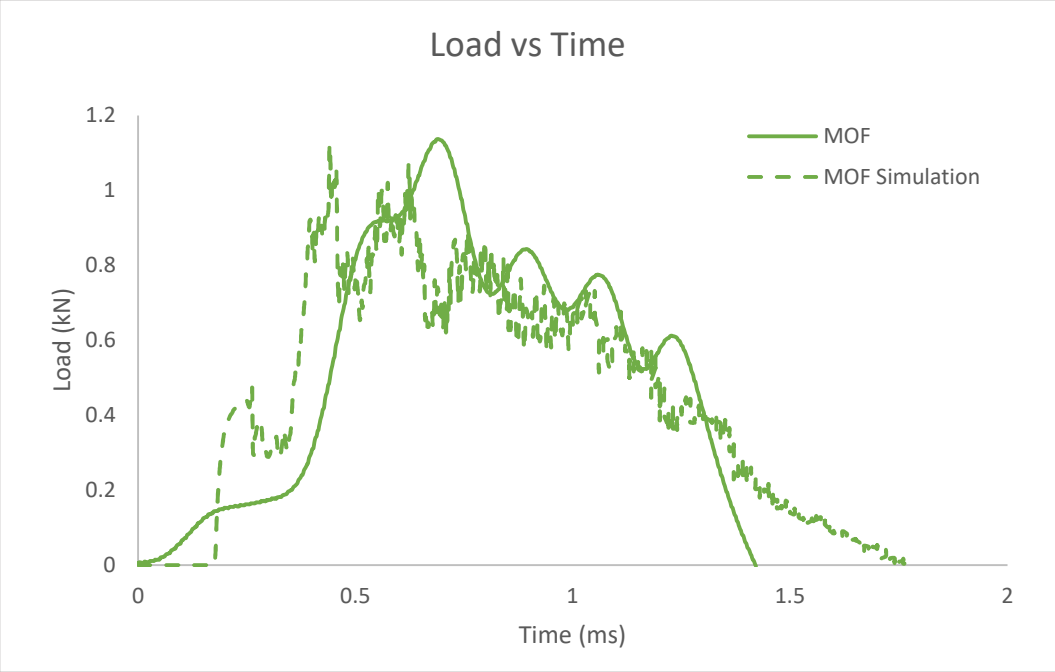

Figure A.29: Impact Load applied comparison between Experimental and Modeling of $[0°/90°]_4$ MOF CFRPs

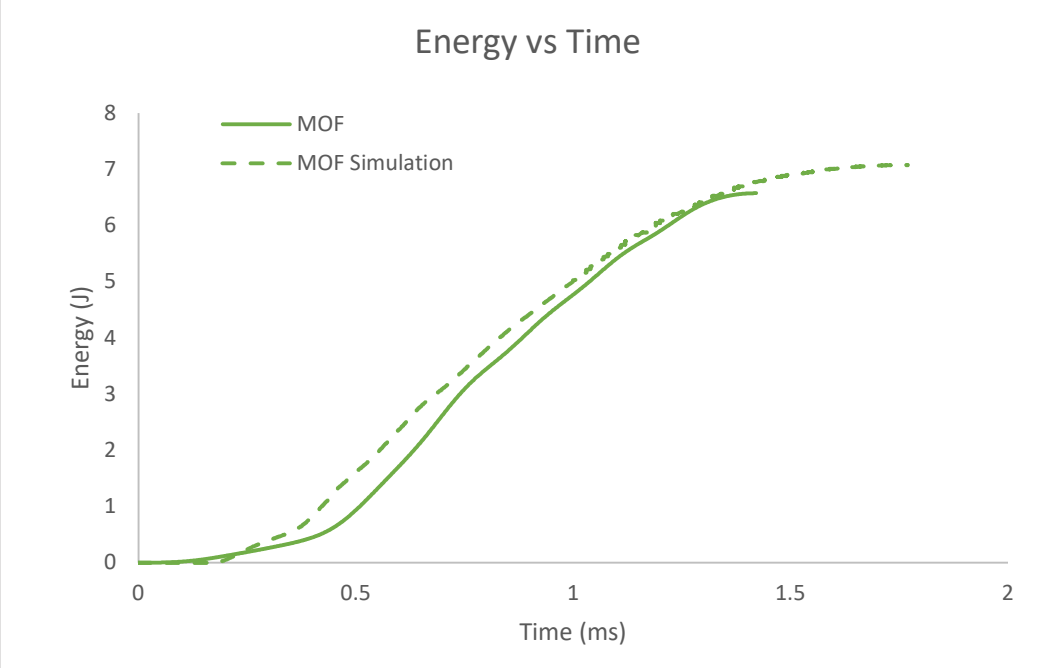

Figure A.30: Impact Resistance comparison between Experimental and Modeling of $[0°/90°]_4$ MOF CFRPs

Table A.1: Material Card used for LS-DYNA modeling of Reference CFRP

***MAT_054 (ENHANCED_COMPOSITE_DAMAGE) – Reference Composite**

MID	RO	EA	EB	(EC)	PRBA	(PRCA)	(PRCB)
1	1086.80	8.220E+11	8.220E+11	0.0	0.3	0.0	0.0
GAB	**GBC**	**GCA**	**(KF)**	**AOPT**	**2WAY**		
3.646E+9	3.646E+9	3.646E+9	0.0	2.00	1.00		
XP	**YP**	**ZP**	**A1**	**A2**	**A3**	**MANGLE**	
0.0	0.0	0.0	1.00	0.0	0.0	0.0	
V1	**V2**	**V3**	**D1**	**D2**	**D3**	**DFAILM**	**DFAILS**
0.0	0.0	0.0	0.0	0.0	0.0	0.01022	0.1180
TFAIL	**ALPH**	**SOFT**	**FBRT**	**YCFAC**	**DFAILT**	**DFAILC**	**EFS**
1.153E-11	1.0	1.0	0.25	0.50	0.01022	-0.009812	0.0
XC	**XT**	**YC**	**YT**	**SC**	**CRIT**	**BETA**	
5.800E+8	6.360E+8	5.800E+8	6.360E+8	3.960E+7	54.00	0.50	

Table A.2: Material Card used for LS-DYNA modeling of Acid Activated CFRP

***MAT_054 (ENHANCED_COMPOSITE_DAMAGE) – Acid Activated Composite**

MID	RO	EA	EB	(EC)	PRBA	(PRCA)	(PRCB)
1	1139.10	6.300E+11	6.300E+11	0.0	0.3	0.0	0.0
GAB	**GBC**	**GCA**	**(KF)**	**AOPT**	**2WAY**		
3.872E+9	3.872E+9	3.872E+9	0.0	2.00	1.00		
XP	**YP**	**ZP**	**A1**	**A2**	**A3**	**MANGLE**	
0.0	0.0	0.0	1.00	0.0	0.0	0.0	
V1	**V2**	**V3**	**D1**	**D2**	**D3**	**DFAILM**	**DFAILS**
0.0	0.0	0.0	0.0	0.0	0.0	0.01110	0.1217
TFAIL	**ALPH**	**SOFT**	**FBRT**	**YCFAC**	**DFAILT**	**DFAILC**	**EFS**
1.153E-11	1.0	1.0	0.25	0.50	0.01110	-0.010659	0.0
XC	**XT**	**YC**	**YT**	**SC**	**CRIT**	**BETA**	
5.670E+8	6.220E+8	5.670E+8	6.220E+8	3.873E+7	54.00	0.50	

Table A.3: Material Card used for LS-DYNA modeling of MOF CFRP

***MAT_054 (ENHANCED_COMPOSITE_DAMAGE) – MOF Composite**

MID	**RO**	**EA**	**EB**	**(EC)**	**PRBA**	**(PRCA)**	**(PRCB)**
1	1078.80	7.130E+11	7.130E+11	0.0	0.3	0.0	0.0
GAB	**GBC**	**GCA**	**(KF)**	**AOPT**	**2WAY**		
3.148E+9	3.148E+9	3.148E+9	0.0	2.00	1.00		
XP	**YP**	**ZP**	**A1**	**A2**	**A3**	**MANGLE**	
0.0	0.0	0.0	1.00	0.0	0.0	0.0	
V1	**V2**	**V3**	**D1**	**D2**	**D3**	**DFAILM**	**DFAILS**
0.0	0.0	0.0	0.0	0.0	0.0	0.01554	0.17194
TFAIL	**ALPH**	**SOFT**	**FBRT**	**YCFAC**	**DFAILT**	**DFAILC**	**EFS**
1.153E-11	1.0	0.75	0.25	0.50	0.01554	-0.014916	0.0
XC	**XT**	**YC**	**YT**	**SC**	**CRIT**	**BETA**	
6.880E+8	7.550E+8	6.880E+8	7.550E+8	4.700E+7	54.00	0.50	

9 REFERENCES

[1] Jones, R. M. *Mechanics of Composite Materials Jones 1999*. 1999.

[2] Trabelsi, W., Michel, L., and Othomene, R. "Effects of Stitching on Delamination of Satin Weave Carbon-Epoxy Laminates under Mode I, Mode II and Mixed-Mode I/II Loadings." *Applied Composite Materials*, Vol. 17, No. 6, 2010. https://doi.org/10.1007/s10443-010-9128-0.

[3] Chung, D. D. L. Structural Composite Materials Tailored for Damping. No. 355, 2003.

[4] Aksoy, A., and Carlsson, L. A. "Interlaminar Shear Fracture of Interleaved Graphite/Epoxy Composites." *Composites Science and Technology*, Vol. 43, No. 1, 1992. https://doi.org/10.1016/0266-3538(92)90133-N.

[5] Zhang, G., Sun, S., Yang, D., Dodelet, J. P., and Sacher, E. "The Surface Analytical Characterization of Carbon Fibers Functionalized by H2SO4/HNO3 Treatment." *Carbon*, Vol. 46, No. 2, 2008. https://doi.org/10.1016/j.carbon.2007.11.002.

[6] Rafiee, R. *Carbon Nanotube-Reinforced Polymers: From Nanoscale to Macroscale*. 2017.

[7] Sager, R. J., Klein, P. J., Lagoudas, D. C., Zhang, Q., Liu, J., Dai, L., and Baur, J. W. "Effect of Carbon Nanotubes on the Interfacial Shear Strength of T650 Carbon Fiber in an Epoxy Matrix." *Composites Science and Technology*, Vol. 69, Nos. 7–8, 2009. https://doi.org/10.1016/j.compscitech.2008.12.021.

[8] Korotcenkov, G. *Nanostructured Zinc Oxide: Synthesis, Properties and Applications*. 2021.

[9] Ayyagari, S., Al-Haik, M., and Rollin, V. "Mechanical and Electrical Characterization of Carbon Fiber/Bucky Paper/Zinc Oxide Hybrid Composites." *C*, Vol. 4, No. 1, 2018. https://doi.org/10.3390/c4010006.

[10] MacGillivray, L. R. *Metal-Organic Frameworks: Design and Application*. 2010.

[11] Tiwari, S., and Bijwe, J. "Surface Treatment of Carbon Fibers - A Review." *Procedia Technology*, Vol. 14, 2014. https://doi.org/10.1016/j.protcy.2014.08.064.

[12] Tang, L. G., and Karoos, J. L. "A Review of Methods for Improving the Interfacial Adhesion between Carbon Fiber and Polymer Matrix." *Polymer Composites*, Vol. 18, No. 1, 1997. https://doi.org/10.1002/pc.10265.

[13] Rahmani, H., Ashori, A., and Varnaseri, N. "Surface Modification of Carbon Fiber for Improving the Interfacial Adhesion between Carbon Fiber and Polymer Matrix." *Polymers for Advanced Technologies*, Vol. 27, No. 6, 2016. https://doi.org/10.1002/pat.3720.

[14] Yuan, B., and Wood, D. A. *Formation Damage during Improved Oil Recovery: Fundamentals and Applications*. 2018.

[15] Rand, B., and Robinson, R. "Surface Characteristics of Carbon Fibres from PAN." *Carbon*, Vol. 15, No. 4, 1977. https://doi.org/10.1016/0008-6223(77)90011-2.

[16] Wu, Z., Pittman, C. U., and Gardner, S. D. "Nitric Acid Oxidation of Carbon Fibers and the Effects of Subsequent Treatment in Refluxing Aqueous NaOH." *Carbon*, Vol. 33, No. 5, 1995. https://doi.org/10.1016/0008-6223(95)00145-4.

[17] Su, F. H., Zhang, Z. Z., Wang, K., Jiang, W., and Liu, W. M. "Tribological and Mechanical Properties of the Composites Made of Carbon Fabrics Modified with Various Methods." *Composites Part A: Applied Science and Manufacturing*, Vol. 36, No. 12, 2005. https://doi.org/10.1016/j.compositesa.2005.04.012.

[18] Nohara, L. B., Filho, G. P., Nohara, E. L., Kleinke, M. U., and Rezende, M. C. "Evaluation of Carbon Fiber Surface Treated by Chemical and Cold Plasma Processes."

Materials Research, Vol. 8, No. 3, 2005. https://doi.org/10.1590/S1516-14392005000300010.

[19] Tran, M. Q., Ho, K. K. C., Kalinka, G., Shaffer, M. S. P., and Bismarck, A. "Carbon Fibre Reinforced Poly(Vinylidene Fluoride): Impact of Matrix Modification on Fibre/Polymer Adhesion." *Composites Science and Technology*, Vol. 68, Nos. 7–8, 2008. https://doi.org/10.1016/j.compscitech.2008.02.021.

[20] Li, J. "The Effect of Surface Modification with Nitric Acid on the Mechanical and Tribological Properties of Carbon Fiber-Reinforced Thermoplastic Polyimide Composite." *Surface and Interface Analysis*, Vol. 41, No. 9, 2009. https://doi.org/10.1002/sia.3089.

[21] Langston, T. A., and Granata, R. D. "Influence of Nitric Acid Treatment Time on the Mechanical and Surface Properties of High-Strength Carbon Fibers." *Journal of Composite Materials*, Vol. 48, No. 3, 2014. https://doi.org/10.1177/0021998312470471.

[22] Hu, Y., and Guo, C. Carbon Nanotubes and Carbon Nanotubes/Metal Oxide Heterostructures: Synthesis, Characterization and Electrochemical Property. In *Carbon Nanotubes - Growth and Applications*, 2011.

[23] Han, C. T., Chi, M., Zheng, Y. Y., Jiang, L. X., Xiong, C. D., and Zhang, L. F. "Mechanical Properties and Bioactivity of High-Performance Poly(Etheretherketone)/Carbon Nanotubes/Bioactive Glass Biomaterials." *Journal of Polymer Research*, Vol. 20, No. 8, 2013. https://doi.org/10.1007/s10965-013-0203-8.

[24] Wu, P., Cheng, S., Yao, M., Yang, L., Zhu, Y., Liu, P., Xing, O., Zhou, J., Wang, M., Luo, H., and Liu, M. "A Low-Cost, Self-Standing NiCo2O4@CNT/CNT Multilayer Electrode for Flexible Asymmetric Solid-State Supercapacitors." *Advanced Functional Materials*, Vol. 27, No. 34, 2017. https://doi.org/10.1002/adfm.201702160.

[25] Sharma, S. P., and Lakkad, S. C. "Effect of CNTs Growth on Carbon Fibers on the Tensile Strength of CNTs Grown Carbon Fiber-Reinforced Polymer Matrix Composites." *Composites Part A: Applied Science and Manufacturing*, Vol. 42, No. 1, 2011. https://doi.org/10.1016/j.compositesa.2010.09.008.

[26] Lee, S. B., Choi, O., Lee, W., Yi, J. W., Kim, B. S., Byun, J. H., Yoon, M. K., Fong, H., Thostenson, E. T., and Chou, T. W. "Processing and Characterization of Multi-Scale Hybrid Composites Reinforced with Nanoscale Carbon Reinforcements and Carbon Fibers." *Composites Part A: Applied Science and Manufacturing*, Vol. 42, No. 4, 2011. https://doi.org/10.1016/j.compositesa.2010.10.016.

[27] Boura, O., Diamanti, E. K., Grammatikos, S. A., Gournis, D., and Paipetis, A. S. "Carbon Nanotube Growth on High Modulus Carbon Fibres: Morphological and Interfacial Characterization." *Surface and Interface Analysis*, Vol. 45, No. 9, 2013. https://doi.org/10.1002/sia.5292.

[28] De Greef, N., Zhang, L., Magrez, A., Forró, L., Locquet, J. P., Verpoest, I., and Seo, J. W. "Direct Growth of Carbon Nanotubes on Carbon Fibers: Effect of the CVD Parameters on the Degradation of Mechanical Properties of Carbon Fibers." *Diamond and Related Materials*, Vol. 51, 2015. https://doi.org/10.1016/j.diamond.2014.11.002.

[29] Fan, W., Wang, Y., Wang, C., Chen, J., Wang, Q., Yuan, Y., and Niu, F. "High Efficient Preparation of Carbon Nanotube-Grafted Carbon Fibers with the Improved Tensile Strength." *Applied Surface Science*, Vol. 364, 2016. https://doi.org/10.1016/j.apsusc.2015.12.189.

[30] Yao, Z. Q., Wang, C. G., and Wang, Y. X. In Situ Growth of CNTs on Carbon Fiber by Chemical Vapor Deposition. No. 354, 2019.

[31] Wang, C., Wang, Y., and Su, S. “Optimization of Process Conditions for Continuous Growth of CNTs on the Surface of Carbon Fibers.” *Journal of Composites Science*, Vol. 5, No. 4, 2021. https://doi.org/10.3390/jcs5040111.
[32] Vigolo, B., and Hrol, C. Processing Carbon Nanotubes. In *Carbon Nanotubes - Synthesis, Characterization, Applications*, 2011.
[33] Roy, K., Alam, M. N., Mandal, S. K., and Debnath, S. C. “Sol-Gel Derived Nano Zinc Oxide for the Reduction of Zinc Oxide Level in Natural Rubber Compounds.” *Journal of Sol-Gel Science and Technology*, Vol. 70, No. 3, 2014. https://doi.org/10.1007/s10971-014-3293-9.
[34] Cherumannil Karumuthil, S., Singh, K., Valiyaneerilakkal, U., Akhtar, J., and Varghese, S. “Fabrication of Poly (Vinylidene Fluoride-Trifluoroethylene) – Zinc Oxide Based Piezoelectric Pressure Sensor.” *Sensors and Actuators, A: Physical*, Vol. 303, 2020. https://doi.org/10.1016/j.sna.2019.111677.
[35] Stanković, A., Sezen, M., Milenković, M., Kaišarević, S., Andrić, N., and Stevanović, M. “PLGA/Nano-ZnO Composite Particles for Use in Biomedical Applications: Preparation, Characterization, and Antimicrobial Activity.” *Journal of Nanomaterials*, Vol. 2016, 2016. https://doi.org/10.1155/2016/9425289.
[36] Sharma, S. P., Chang, C. K., and Ting, J. M. “Surface Modification of Carbon Fiber by Direct Growth of Zinc Oxide Nanowalls Using a Radio-Frequency Magnetron Sputtering Technique.” *Thin Solid Films*, Vol. 570, No. PB, 2014. https://doi.org/10.1016/j.tsf.2014.02.112.
[37] Kolodziejczak-Radzimska, A., and Jesionowski, T. Zinc Oxide-from Synthesis to Application: A Review. *Materials*. 4. Volume 7.
[38] Masghouni, N., and Al-Haik, M. “Quasistatic and Dynamic Mechanical Characterization of a Woven Carbon Fiber-Zinc Oxide Nanowires-Epoxy Composite.” *Polymer Composites*, Vol. 36, No. 12, 2015. https://doi.org/10.1002/pc.23129.
[39] Groo, L. A., Inman, D. J., and Sodano, H. A. “In Situ Damage Detection for Fiber-Reinforced Composites Using Integrated Zinc Oxide Nanowires.” *Advanced Functional Materials*, Vol. 28, No. 35, 2018. https://doi.org/10.1002/adfm.201802846.
[40] Tunç, I. D., Erol, M., Güneş, F., and Sütçü, M. “Growth of ZnO Nanowires on Carbon Fibers for Photocatalytic Degradation of Methylene Blue Aqueous Solutions: An Investigation on the Optimization of Processing Parameters through Response Surface Methodology/Central Composite Design.” *Ceramics International*, Vol. 46, No. 6, 2020. https://doi.org/10.1016/j.ceramint.2019.11.244.
[41] Albiss, B., and Abu-Dalo, M. “Photocatalytic Degradation of Methylene Blue Using Zinc Oxide Nanorods Grown on Activated Carbon Fibers.” *Sustainability (Switzerland)*, Vol. 13, No. 9, 2021. https://doi.org/10.3390/su13094729.
[42] Zhong, Z., Wang, C., Han, R., Gao, M., Huang, Y., and Ramakrishna, S. “Synthesis of Zinc Oxide/Carbon Fiber Composites with Improved Piezoelectric Response by Plasma-Liquid Interaction.” *Composites Communications*, Vol. 38, 2023, p. 101495. https://doi.org/10.1016/j.coco.2023.101495.
[43] Bradshaw, D., Garai, A., and Huo, J. “ChemInform Abstract: Metal-Organic Framework Growth at Functional Interfaces: Thin Films and Composites for Diverse Applications.” *ChemInform*, Vol. 43, No. 24, 2012. https://doi.org/10.1002/chin.201224278.
[44] Ni, Z., and Masel, R. I. “Rapid Production of Metal-Organic Frameworks via Microwave-Assisted Solvothermal Synthesis.” *Journal of the American Chemical Society*, Vol. 128,

No. 38, 2006. https://doi.org/10.1021/ja0635231.
[45] Meng, J., Niu, C., Xu, L., Li, J., Liu, X., Wang, X., Wu, Y., Xu, X., Chen, W., Li, Q., Zhu, Z., Zhao, D., and Mai, L. "General Oriented Formation of Carbon Nanotubes from Metal-Organic Frameworks." *Journal of the American Chemical Society*, Vol. 139, No. 24, 2017. https://doi.org/10.1021/jacs.7b01942.
[46] Tran, T. Q. N., Das, G., and Yoon, H. H. "Nickel-Metal Organic Framework/MWCNT Composite Electrode for Non-Enzymatic Urea Detection." *Sensors and Actuators, B: Chemical*, Vol. 243, 2017. https://doi.org/10.1016/j.snb.2016.11.126.
[47] Liu, W., Shao, Q., Ji, G., Liang, X., Cheng, Y., Quan, B., and Du, Y. "Metal–Organic-Frameworks Derived Porous Carbon-Wrapped Ni Composites with Optimized Impedance Matching as Excellent Lightweight Electromagnetic Wave Absorber." *Chemical Engineering Journal*, Vol. 313, 2017. https://doi.org/10.1016/j.cej.2016.12.117.
[48] Lei, C., Gao, J., Ren, W., Xie, Y., Abdalkarim, S. Y. H., Wang, S., Ni, Q., and Yao, J. "Fabrication of Metal-Organic Frameworks@cellulose Aerogels Composite Materials for Removal of Heavy Metal Ions in Water." *Carbohydrate Polymers*, Vol. 205, 2019. https://doi.org/10.1016/j.carbpol.2018.10.029.
[49] Zhang, L., Chen, S., Pan, Y. T., Zhang, S., Nie, S., Wei, P., Zhang, X., Wang, R., and Wang, D. Y. "Nickel Metal-Organic Framework Derived Hierarchically Mesoporous Nickel Phosphate toward Smoke Suppression and Mechanical Enhancement of Intumescent Flame Retardant Wood Fiber/Poly(Lactic Acid) Composites." *ACS Sustainable Chemistry and Engineering*, Vol. 7, No. 10, 2019. https://doi.org/10.1021/acssuschemeng.9b00174.
[50] Xue, Y., Zheng, S., Xue, H., and Pang, H. Metal-Organic Framework Composites and Their Electrochemical Applications. *Journal of Materials Chemistry A*. 13. Volume 7.
[51] Liu, X. W., Sun, T. J., Hu, J. L., and Wang, S. D. Composites of Metal-Organic Frameworks and Carbon-Based Materials: Preparations, Functionalities and Applications. *Journal of Materials Chemistry A*. 10. Volume 4.
[52] Yang, X., Jiang, X., Huang, Y., Guo, Z., and Shao, L. "Building Nanoporous Metal-Organic Frameworks 'Armor' on Fibers for High-Performance Composite Materials." *ACS Applied Materials and Interfaces*, Vol. 9, No. 6, 2017. https://doi.org/10.1021/acsami.6b15098.
[53] Fu, Y., Hu, J., Wang, Q., lin, D., Li, K., and Zhou, L. "Thermally Etched Porous Carbon Cloth Catalyzed by Metal Organic Frameworks as Sulfur Hosts for Lithium–Sulfur Batteries." *Carbon*, Vol. 150, 2019. https://doi.org/10.1016/j.carbon.2019.05.008.
[54] Li, Y., Jiang, B., and Huang, Y. "Constructing Nanosheet-like MOF on the Carbon Fiber Surfaces for Improving the Interfacial Properties of Carbo Fiber /Epoxy Composites." *Applied Surface Science*, Vol. 514, 2020. https://doi.org/10.1016/j.apsusc.2020.145870.
[55] Ayyagari, S., Al-Haik, M., Ren, Y., Abbott, A., Trigg, E. B., Zheng, B., and Koerner, H. "Metal Organic Frameworks Modification of Carbon Fiber Composite Interface." *Composites Part B: Engineering*, Vol. 224, 2021. https://doi.org/10.1016/j.compositesb.2021.109197.
[56] Moosburger-Will, J., Bauer, M., Laukmanis, E., Horny, R., Wetjen, D., Manske, T., Schmidt-Stein, F., Töpker, J., and Horn, S. "Interaction between Carbon Fibers and Polymer Sizing: Influence of Fiber Surface Chemistry and Sizing Reactivity." *Applied Surface Science*, Vol. 439, 2018. https://doi.org/10.1016/j.apsusc.2017.12.251.
[57] D7136/D7136M - 20, A. I. "D7136: Standard Test Method for Measuring the Damage

Resistance of a Fiber-Reinforced Polymer Matrix Composite to a Drop-Weight Impact Event." *Annual Book of ASTM Standards*, Vol. i, No. C, 2012.
[58] Ye, J., Gao, Y., Wu, Y., Liu, C., Dong, J., Wang, H., Su, B., and Peng, H.-X. "Low Velocity Impact Response of Fiber Metal Laminates with Nano-Patterned Metal Surfaces." *Composites Science and Technology*, Vol. 228, 2022, p. 109641. https://doi.org/10.1016/j.compscitech.2022.109641.
[59] Kara, M., Kırıcı, M., Tatar, A. C., and Avcı, A. "Impact Behavior of Carbon Fiber/Epoxy Composite Tubes Reinforced with Multi-Walled Carbon Nanotubes at Cryogenic Environment." *Composites Part B: Engineering*, Vol. 145, 2018. https://doi.org/10.1016/j.compositesb.2018.03.027.
[60] Wade, B., Feraboli, P., and Osborne, M. "Simulating Laminated Composites Using LS-DYNA Material Model MAT54 Part I : [0] and [90] Ply Single-Element Investigation." *FAA Joint Advanced Materials and Structures (JAMS) Centre of Excellence, Technical Review Meeting*, 2012.
[61] ASM International. *Properties and Selection: Irons, Steels, and High-Performance Alloys*. ASM International, 1990.
[62] Khagendra, K., Yadav, S., and Lohchab, D. "Influence of Aviation Fuel on Mechanical Properties of Glass Fiber-Reinforced Plastic Composite." *International Advanced Research Journal in Science, Engineering and Technology*, Vol. 3, No. 4, 2016.
[63] Zhang, Y., Zhu, S., Liu, Y., Yang, B., and Wang, X. "The Mechanical and Tribological Properties of Nitric Acid-Treated Carbon Fiber-Reinforced Polyoxymethylene Composites." *Journal of Applied Polymer Science*, Vol. 132, No. 15, 2015. https://doi.org/10.1002/app.41812.
[64] Wang, Z. L. "Nanostructures of Zinc Oxide." *Materials Today*, Vol. 7, No. 6, 2004. https://doi.org/10.1016/S1369-7021(04)00286-X.
[65] Bell, D. S. "The Promise of Metal-Organic Frameworks for Use in Liquid Chromatography." *LC-GC North America*, Vol. 36, No. 6, 2018.